TECHNISCHE UNIVERSITÄT MÜNCHEN

FAKULTÄT FÜR CHEMIE

PROTEINCHEMIE

Manipulation of small GTPases by bacterial proteases

and GTPase activating proteins

Sergey Savitskiy

Vollständiger Abdruck der von der Fakultät für Chemie der Technischen Universität München zur Erlangung des akademischen Grades eines

Doktors der Naturwissenschaften (Dr. rer. nat.)

genehmigten Dissertation.

Vorsitzender: Prof. Dr. Bernd Reif

Prüfer der Dissertation:

                1. Prof. Dr. Aymelt Itzen

                2. Prof. Dr. Matthias Feige

Die Dissertation wurde am 04.11.2020 bei der Technischen Universität München eingereicht und durch die Fakultät für Chemie am 10.12.2020 angenommen.

Im Oktober 2020 vorgelegt von

Sergey Savitskiy
aus Potsdam
geboren am 17.02.1991

Die vorliegende Arbeit wurde im Zeitraum von Dezember 2016 bis Oktober 2020 an der Fakultät für Chemie der Technischen Universität München und am Institut für Biochemie und Signaltransduktion am Universitätsklinikum Hamburg-Eppendorf unter der Anleitung von Prof. Dr. Aymelt Itzen durchgeführt.

Im Rahmen dieser Arbeit ist folgende Veröffentlichung erschienen:

Fauser J., Savitskiy S., Fottner M., Trauschke V. and Gulen B. (2020) **Sortase-Mediated Quantifiable Enzyme Immobilization on Magnetic Nanoparticles.** *Bioconjugate chemistry* https://doi.org/10.1021/acs.bioconjchem.0c00322

Folgendes Manuskript befindet sich "under review":

Sergey Savitskiy, Rudolf Wachtel, Danial Pourjafar-Dehkordi, Hyun-Seo Kang, Vanessa Trauschke, Don C. Lamb, Michael Sattler, Martin Zacharias, Aymelt Itzen (2020) **Proteolysis of Rab32 by *Salmonella* GtgE induces an inactive GTPase Conformation.** *iScience*

Weiteres Manuskript ist bereit zum Einreichen:

Sergey Savitskiy, Aymelt Itzen (2020) **SopD from *Salmonella* specifically inactivates Rab8.**

TABLE OF CONTENTS

ABBREVIATIONS

Amino acids	
Ala/A	alanine
Arg/R	arginine
Asn/N	asparagine
Asp/D	aspartic acid
Cys/C	cysteine
Gln/Q	glutamine
Glu/E	glutamic acid
Gly/G	glycine
His/H	histidine
Ile/I	isoleucine
Leu/L	leucine
Lys/K	lysine
Met/M	methionine
Phe/F	phenylalanine
Pro/P	proline
Ser/S	serine
Thr/T	threonine
Trp/W	tryptophan
Tyr/Y	tyrosine
Val/V	valine

°C	degree Celsius
aa	amino acids
cAMP	cyclic adenosine monophosphate
Fbx8	F-box protein bearing the Sec7 domain
FTase	farnesyl transferase
GAP	GTPase-activating protein
GDI	GDP-dissociation inhibitor
GDF	GDI displacement factor
GDP	guanosine-5'-diphosphate
GEF	guanosine nucleotide exchange factor
GGTase II	geranylgeranyl transferase II or Rab geranylgeranyl transferase
GTP	guanosine-5'-triphosphate
h	hours

ABBREVIATIONS

ICMT	isoprenylcysteine carboxylmethyltransferase
IPTG	isopropylthiogalactopyranosid
LRO	lysosome-related organelles
MAPK	Ras–mitogen-activated protein kinase
MNP	magnetic nanoparticle
MBP	maltose-binding protein
min	minutes
PAT	palmitoyl acyltransferase
PD	Parkinson's disease
PCR	polymerase chain reaction
PI3K	phospho-inositide 3-kinase
PI3P	phosphatidylinositol-3-phosphate
PKA	cAMP-dependent protein kinase
PTM	post-translational modification
Rab	Ras-related in brain
RalGDS	Ral guanine nucleotide dissociation stimulator
Ras	rat sarcoma
REP	Rab escort protein
RRSP	Ras/Rap1 site-specific endopeptidase
s	seconds
SCV	*Salmonella*-containing vacuoles
SDS-PAGE	sodium dodecyl sulfate polyacrylamide gel electrophoresis
SPI	*Salmonella*-pathogenicity island
SUMO	small ubiquitin-like modifier
TBC	Tre-2/Bub2/Cdc16
TBK1	TANK-binding kinase
T1SS	type 1 secretion system
T3SS	type 3 secretion system
Tyrp1	tyrosinase-related protein 1
Tyrp2	tyrosinase-related protein 2
Varp	VPS9-ankyrin-repeat protein
VPS	vacuolar protein sorting
Y2H	yeast two-hybrid
YpkA	*Yersinia* protein kinase A

ABSTRACT

Rab GTPases are central regulators of intracellular vesicular trafficking. They are frequently targeted by bacterial pathogens through post-translational modifications. *Salmonella* Typhimurium secretes the cysteine protease GtgE during infection, leading to a regioselective proteolytic cleavage of the regulatory switch I loop in the inactive small GTPases of the Rab32 subfamily. Results of this work – produced by using a combination of biochemical methods, molecular dynamics simulations, NMR spectroscopy, and single-pair FRET – demonstrate that the cleavage of Rab32 causes a local increase of conformational flexibility in the switch regions. Cleaved Rab32 maintains its ability to interact with the GDP dissociation inhibitor (GDI). Interestingly, the Rab32 cleavage also enables GDI binding with an active GTP-bound Rab32 in vitro. Furthermore, the Rab32 proteolysis provokes disturbances in the interaction with its downstream effector VARP. Additionally, the proteolytic cleavage of Ras by the RRSP protease from *Vibrio vulnificus* was investigated. Like GtgE, RRSP protease also cleaves the switch I in Ras isoforms, disabling the binding of Ras to its effector RalGDS. However, NMR experiments showed, that RRSP-mediated cleavage provokes stronger structural changes in Ras than GtgE in Rab32.

In the context of this work, a sortase-mediated protein immobilization method on magnetic nanoparticles was developed to produce suitable samples for single-pair FRET. Furthermore, the developed method includes a sensitive GFP-based quantification system for immobilized proteins. Using this method, GtgE protease was successfully immobilized, and the amount of coupled enzyme was quantified by fluorescence spectroscopy. The activity of soluble and immobilized GtgE assessed via kinetic measurements revealed comparable enzymatic activities. Noteworthy, the magnetic nanoparticles permit easy addition and removal of coupled enzymes to and from a reaction mixture. Thus, the sortase-mediated coupling of enzymes combined with the versatility of magnetic nanoparticles enables the preparation of biological samples with a high demand for purity as demonstrated by single-pair FRET experiments.

During the first stages of the *Salmonella* infection, *Salmonella* outer protein D (SopD) is secreted into a host contributing to the systemic virulence of the bacterium. SopD2 is a SopD homolog and possesses GTPase activating protein (GAP) activity towards Rab32. Here, Rab-proteins were identified as putative SopD-targets by yeast two-hybrid approach. *In vitro* investigations, subsequently, revealed Rab8a as an exclusive SopD substrate. Moreover, mutagenesis studies suggest that SopD and SopD2 may utilize a GAP-mechanism requiring a dual catalytic finger provided by the GAP as well as the catalytic Gln located in the G3 motif of Rab proteins, thereby representing a combination of human and bacterial GAP mechanisms. Additionally, the catalytic efficiencies of SopD and SopD2 towards their physiologically relevant substrates were determined. In conclusion, SopDs from *Salmonella* act as RabGAPs and could inactivate Rab signaling.

ZUSAMMENFASSUNG

Rab GTPasen sind zentrale Regulatoren des intrazellulären vesikulären Transports. Sie werden häufig durch die bakteriellen Krankheitserreger posttranslational modifiziert. *Salmonella* Typhimurium sezerniert während der Infektion die Cysteinprotease GtgE, was zu einer regioselektiven proteolytischen Spaltung des regulatorischen switch I in den inaktiven kleinen GTPasen der Rab32-Unterfamilie führt. Die Ergebnisse dieser Arbeit - die unter Verwendung einer Kombination von biochemischen Methoden, Molekulardynamik-Simulationen, NMR-Spektroskopie und Einzelpaar-FRET erzielt wurden - zeigen, dass die Spaltung von Rab32 eine lokale Erhöhung der konformationellen Flexibilität in beiden switch Regionen bewirkt. Gespaltenes Rab32 behält seine Fähigkeit, mit dem GDP-Dissoziationsinhibitor (GDI) zu interagieren. Interessanterweise ermöglicht die Rab32-Spaltung auch die GDI-Bindung mit einem aktiven, GTP-gebundenen, Rab32 *in vitro*. Darüber hinaus unterbindet die Rab32-Proteolyse seine Interaktion mit dem nachgeschalteten Effektor VARP. In ähnlicher Weise spaltet die RRSP-Protease aus *Vibrio vulnificus* auch den switch I in Ras-Isoformen, wodurch die Bindung von Ras an seinen Effektor RalGDS verhindert wird. NMR-Experimente zeigten jedoch, dass die RRSP-vermittelte Spaltung stärkere strukturelle Veränderungen in Ras als GtgE in Rab32 hervorruft. Zusätzlich veranlassten die Schwierigkeiten bei der Herstellung von FRET-geeigneten Proben die Entwicklung einer Sortase-vermittelten Protein-Immobilisierungsmethode auf magnetischen Nanopartikeln. Darüber hinaus bietet die entwickelte Methode ein empfindliches GFP-basiertes Quantifizierungssystem für immobilisierte Proteine. Mit dieser Methode wurde GtgE erfolgreich immobilisiert, und die Menge des gekoppelten Enzyms wurde mittels Fluoreszenzspektroskopie quantifiziert. Lösliches und immobilisiertes GtgEs zeigten vergleichbare enzymatische Aktivität. Bemerkenswert ist, dass die magnetischen Nanopartikel eine einfache Zugabe und Entfernung der gekoppelten Enzyme zu und von einem Reaktionsgemisch ermöglichen. Somit bietet die Sortase-vermittelte Kopplung von Enzymen in Kombination mit den vielseitigen Einsatzmöglichkeiten der magnetischen Nanopartikel die Möglichkeit für die Präparation biologischer Proben mit einem hohen Reinheitsanspruch, wie durch Einzelpaar-FRET-Experimente nachgewiesen wurde.

Das äußere *Salmonella*-Protein D (SopD) wird in den ersten Stadien der *Salmonella*-Infektion in den Wirt sezerniert und trägt zur systemischen Virulenz des Bakteriums bei. SopD2 ist ein SopD-Homolog und besitzt eine Aktivität des GTPase aktivierenden Proteins (GAP) gegenüber Rab32. Hier wurden Rab-Proteine als mutmaßliche SopD-Ziele durch einen Hefe-Zwei-Hybrid-Ansatz identifiziert. *In vitro* Untersuchungen ergaben, dass Rab8a das exklusive SopD-Substrat darstellt. Außerdem deuten Mutagenesestudien darauf hin, dass SopD und SopD2 einen GAP-Mechanismus nutzen könnten, der sowohl einen doppelten katalytischen Finger vom GAP als auch das katalytische Gln, das sich im G3-Motiv des Rab-Proteins befindet, benötigt und somit eine Kombination aus humanen und bakteriellen GAP-Mechanismen darstellt. Zusätzlich wurden die

9

katalytischen Effizienzen von SopD und SopD2 gegenüber ihren physiologisch relevanten Substraten bestimmt. Zusammenfassend lässt sich sagen, dass SopDs aus *Salmonellen* als RabGAPs fungieren und Rab-Signalwege inaktivieren können.

1. INTRODUCTION

In the following four sections of the introduction, the reader will be able to gain the background information necessary to better understand the focus of the work and the results presented in it. Since the scope of the work was mainly on small GTPases, first, the reader will be provided with information concerning their structure, functions in the cell, as well as the ways of their regulation. Noteworthy, small GTPases are subject to regulation by not only the host but also by pathogens during infection. Therefore, essential information about two bacteria, *Salmonella* Typhimurium and *Vibrio vulnificus*, and their means of manipulation of small GTPases will support the understanding of the second part of this thesis – impact of bacterial effectors from Salmonella and *V. vulnificus* on small GTPases. Lastly, sortase A – a transpeptidase from Gram positive bacteria enabling the anchoring of proteins to the bacterial cell wall – will be briefly presented, since it was used as a tool to generate a set of samples for the single-pair FRET measurements presented in results of the thesis.

1.1 Small GTPases as intracellular molecular switches

During the past 40 years, scientists discovered and elaborated on the field of small GTPases [3]. Proteins of the Ras superfamily of small GTPases are present in eukaryotes from yeast to human and are essential regulators in a large number of intracellular signaling processes [4–8]. The members of the Ras superfamily are monomeric proteins with a molecular weight of 20-40 kDa, which can be divided into five functionally different families (Table 1) [5]. The biggest family consists of approximately 70 members belonging to the Rab (Ras-related in brain) GTPases [8,9].

Table 1 | The Ras superfamily of small GTPases is represented by over 150 members with different functions in humans.

Family	Members	Function
Ras	39	Gene expression, cell cycle
Rho/Rac/Cdc42	22	Cytoskeleton reorganization
Rab	appr. 70	Intracellular vesicular transport
Sar1/Arf	30	Intracellular vesicular transport
Ran	1	Nucleocytoplasmic transport, microtubule organization

Despite the functional variety of small GTPases, they all bind guanosine-5'-triphosphate (GTP) that is crucial for their activity and functionality. The ability to bind and to hydrolyze GTP is also responsible for the common names of these proteins – GTPases, GTP hydrolases, G proteins. The

nucleotide-binding mode is also directly connected to the activity of the G proteins. Small GTPases exist in two different activity states: the inactive state where they bind guanosine diphosphate (GDP) and the active state where GTP is bound. Since they have a low intrinsic GTP hydrolytic activity they depend on regulatory proteins in order to acquire a defined activity state [3]. This property makes G proteins ideal biological molecular switches and central elements of intracellular signaling networks. Based on the bound G nucleotide (GDP/GTP), GTPases recruit specific effectors via protein-protein interactions, thereby controlling downstream effects.

Due to the central role of small GTPases in the signal transduction and regulation of complex cellular processes, they are frequently manipulated by bacterial pathogens, to exploit them for their own dissemination. Intracellularly and extracellularly replicating pathogens have developed strategies for interfering with the regulation of small GTPases. Such manipulations often occur by introducing bacterial proteins into the host cell, which - in turn - act as binding partners, regulators, or modifying enzymes [10–13].

1.1.1 Architecture of small GTPases

Small GTPases share a conserved G domain, which determines the activity state of the GTPase by binding GDP or GTP. This domain consists of six-stranded β-sheets and five surrounding α-helices containing conserved sequence motifs, which form the nucleotide-binding region (Figure 1).
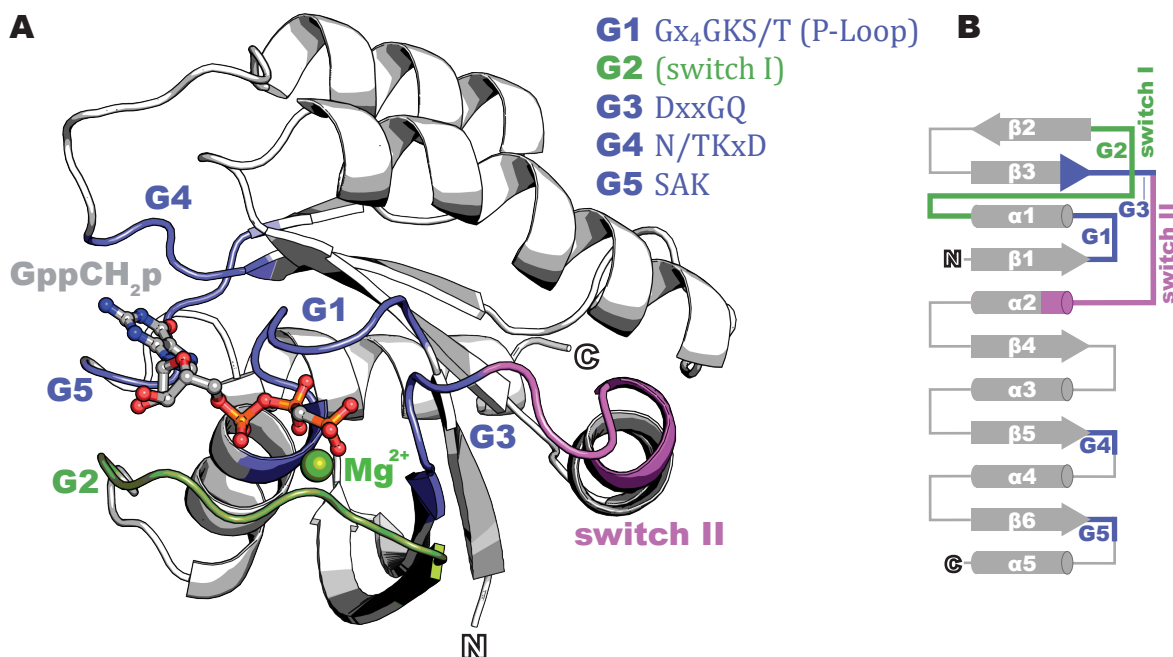
Figure 1 | Schematic representation of conserved sequence motifs of small GTPases. (A) *Small GTPases contain five conserved sequence motifs G1-G5, which are essential for their activity. Balls with sticks: GppCH$_2$p; green sphere: Mg^{2+} ion. PDB ID: 121P [14]. **(B)** The topology diagram represents a typical structural architecture of small GTPases with numbered α-helices (barrels) and β-sheets (arrows). G motifs (blue), N- and C-termini as well as switch regions (green and purple) are indicated.*

Among these conserved motifs, five can be distinguished: G1 - G5 (Figure 1B). The first, a sequentially and structurally conserved region is the P-Loop (G1), originally termed the Walker A motif [15]. The G1 motif coordinates not only the Mg^{2+} ion that is essential for the nucleotide binding, but also an α, β, and γ-phosphates of the bound nucleotide [16]. The next two regulatory vital motifs of small GTPases are the G2 and the G3 motifs. G2 is also designated as the switch I, while G3 is located just prior the beginning of the switch II. The switch regions of small GTPases are crucial for the binding of the effector proteins [17]. The conformations of the switch regions differ significantly depending on the GDP- and GTP-bound states as evident in several crystal structures and nuclear magnetic resonance (NMR) experiments [18,19]. In the GDP-bound inactive state, the switch regions are disordered, while GTP binding leads to a structural rigidification of these regions (Figure 2).
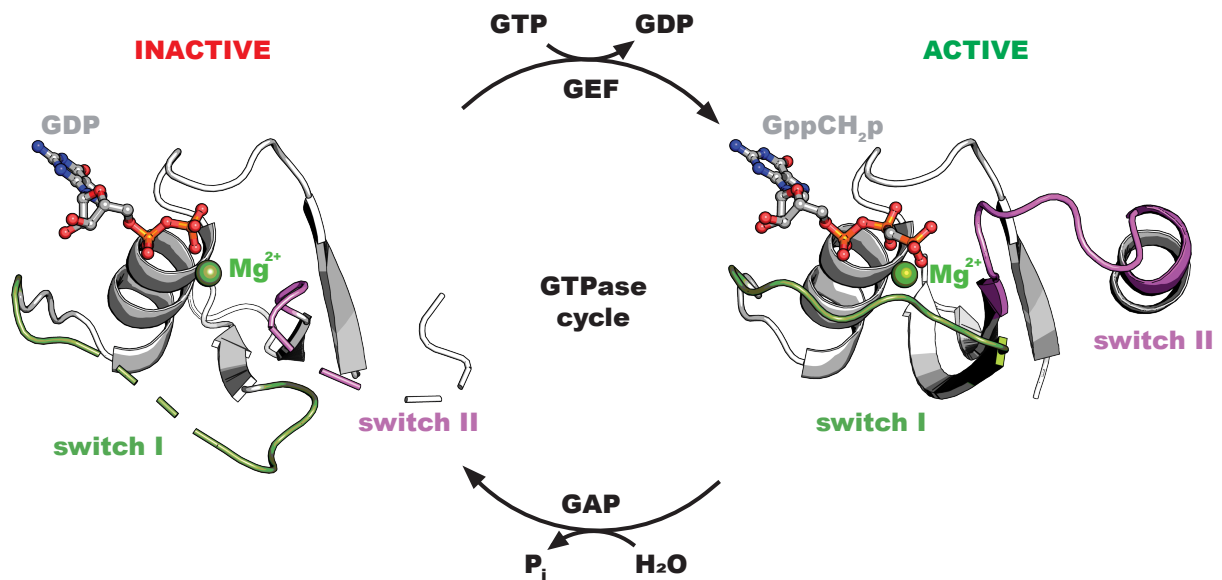
Figure 2 | Crystal structures of GDP- and GppCH₂p-bound GTPases. *The switch regions are disordered in the inactive GTPase state, whereas in the active state they adopt a highly ordered structure. Cycling between both activity states is mediated by guanosine nucleotide exchange factors (GEFs) and GTPase activating proteins (GAPs). Green: switch I; purple: switch II; balls with sticks: nucleotide; green sphere: Mg^{2+} ion. PDB IDs: 1KY3 [20]; 121P [14].*

This structural change is caused by the loss of the γ-phosphate of the G nucleotide that is coordinated via several hydrogen bonds by the conserved Thr and Gly from the G2 and G3 motif, respectively. Upon GTP hydrolysis, these hydrogen bonds are released, thereby leading to the conformational changes in the switch regions. The structural alterations following the loss of γ-phosphate have been termed the loaded-spring mechanism (Figure 3A). The G3 Asp establishes water-mediated contact with the Mg^{2+} ion, which is vital not only for the tight binding of the nucleotide but also for the GTP hydrolysis in multiple G proteins [16]. The Mg^{2+} ion is also coordinated by the Thr of the G2 motif [16]. The G3 Gln is crucial for the activation of the in-line water molecule required for the nucleophilic attack of the γ-phosphate of GTP, thus enabling GTP hydrolysis and efficient GTPase inactivation (Figure 3B) [21]. Another structural element of small GTPases important for their interactions with the effectors is the interswitch region (composed

by β2 and β3), which connects the switch regions [22]. The last two motifs, namely G4 (N/TKxD) and G5 (SAK) form the specific guanine binding pocket. The G4 Asp and the G5 Ala coordinate the nucleobase, hence, enabling the nucleobase specificity of the small GTPases. The conserved described elements contribute to the high affinity toward the nucleotide and establish the conformational switching mechanism at the molecular level [16].

1.1.2 Cellular regulation of small GTPases via GEFs, GAPs, and GDIs

As previously mentioned, G proteins rely on their regulatory proteins which enable the cycling between the active and inactive states (Figure 2). The activation of small G protein is mediated by guanosine nucleotide exchange factors (GEFs). GEFs activate them by stimulating GDP release and thereby facilitate the exchange with GTP. GEFs represent a heterogeneous group of proteins in terms of their secondary and tertiary structure [23]. However, many characterized GEF:GTPase complexes show several mechanistic analogies which are important for nucleotide exchange. First, a low-affinity ternary GTPase:GDP:GEF complex is formed. The GEF interaction with the nucleotide-binding motifs (G1-G3) initially reduces the affinity to the centrally coordinated magnesium ion. Second, further specific interactions of the GEF with both switch regions of the GTPase ensure the shielding and relaxation of the nucleotide-binding pocket. Consequently, the affinity to the bound nucleotide decreases and facilitates its dissociation, forming a high-affinity binary GTPase:GEF complex. Due to the high intracellular GTP concentration ($\sim$ 0.5 – 1.0 mM) in contrast to GDP, the binary protein complex is dissolved leaving a GTP-bound G protein. This process is independent of the bound nucleotide and the loading of the GTPase depends on the intracellular GDP/GTP ratio [24,25]. Once G proteins become active, they can interact with their downstream effectors affecting diverse cellular events [7].

After fulfilling its cellular function, the small GTPase can be deactivated. GTPase-activating proteins (GAPs) catalyze the conversion of GTPases back to the inactive GDP-bound state. GAPs stimulate the intrinsic GTP hydrolysis of GTPases. In contrast to GEFs, GAPs of a given GTPase family are far less diverse in terms of sequence and structure, therefore they may target multiple GTPases [3]. Two main variants have so far been described for Rab GTPases, explaining the mechanisms responsible for the stimulation of GTP hydrolysis by small GTPases. In the first case, the intrinsic G3 Gln (Gln$_G$) activates a water molecule for in-line attack of the γ-phosphate. The GAP, in turn, provides an Arg residue placed in the proximity of the β- and γ-phosphates of the bound nucleotide, that stabilizes the transition state and neutralizes the developing negative charge during the hydrolysis (Figure 3C). The second mechanism is represented by GAPs containing TBC (Tre-2/Bub2/Cdc16) - domain (TBC-GAPs). TBC-domains can be distinguished by their conserved motifs: RxxxW, IxxDxxR, and YxQ, two of which (IxxDxx<u>R</u> and Yx<u>Q</u>) are crucial for the hydrolytic mechanism [26]. TBC-GAPs utilize a dual catalytic finger composed of Arg and Gln residues located in two of three conserved motifs (Figure 3D). Upon interaction of small GTPases

with TBC-GAPs the intrinsic Gln_G is dislocated and reoriented toward the amino acids from the GAP's backbone located next to its catalytic Gln (Gln_{GAP}). The rearrangement of the Gln_G provides space for the Gln_{GAP}, thus the Gln_{GAP} can take over the position and function of the intrinsic Gln_G. The Arg residue plays the same role here as in the first GAP mechanism and functions as a transition state stabilizer and a neutralizer of developing charge during the hydrolysis. Noteworthy, multiple crystal structures of GTPase:GDP:GAP complexes were derived by the co-crystallization of both proteins in presence of BeF_3^- or AlF_4^-, which mimic the γ-phosphate position of GTP or the transition state of the GTP hydrolysis, respectively [27].
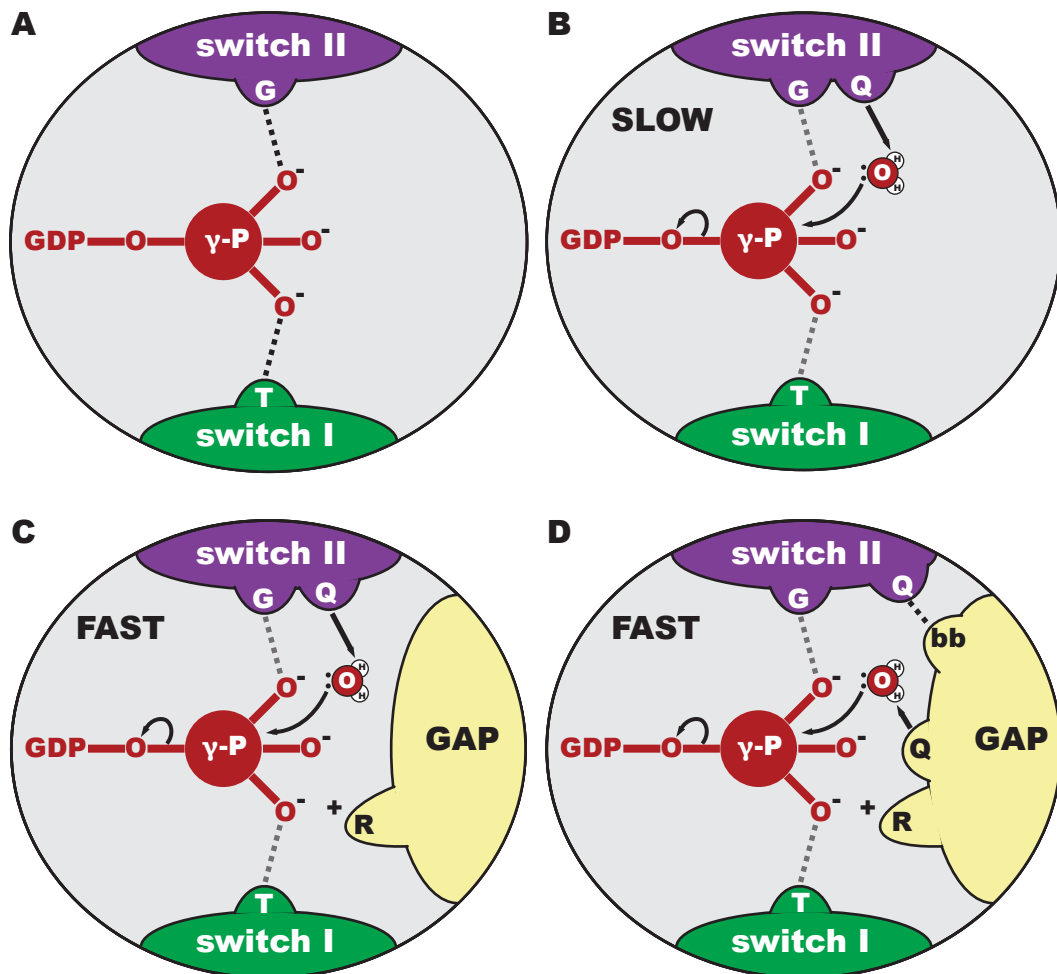
Figure 3 | Schematic representation of loaded-spring and (GAP-mediated) GTP hydrolysis mechanisms. (A) The canonical switch mechanism involves the interaction of the γ-phosphate with Thr (T) and Gly (G) of switch I and II via hydrogen bonds, which are released upon GTP hydrolysis in what has been called the loaded-spring mechanism. (B) Schematic representation of typical intrinsic GTP hydrolysis by G proteins via intrinsic Gln (Q). Depending on the GTPase the reaction rate varies; however, it tends to be slow in terms of biological time scale. (C) One class of GAPs facilitate the GTP hydrolysis by virtue of a single Arg (R) finger placed directly into the active site of the G protein. (D) Another, TBC-domain containing GAPs utilize the dual catalytic finger composed of Arg (R) and Gln (Q) residues; simultaneously, intrinsic Gln (Q) of the G protein is pulled to the site by the interactions with the backbone (bb) of the GAP. Switch regions, GAP, and structural parts relevant to mechanisms are indicated.

The members of the Ras superfamily (except Ran) transit in a cyclic fashion not only between GDP and GTP activity states, but also between cytosolic and membrane-bound pools. Cytosolic and membrane-bound forms depend on the bound nucleotide, thus GDP-bound GTPases are present

in the cytosol, and GTP-bound are attached to the membranes [28]. The prerequisite for the membrane anchoring of G proteins is the post-translationally attached lipid moiety on their C-terminus [29]. Since the membrane localization is crucial for signaling processes regulated by the small GTPases, its reversibility allows for the spatial and temporal control of GTPase activity. However, there is a serious hindrance for small GTPases of the Rab and Rho families on the way to the cytosolic pool. In comparison to the moderate hydrophobicity of other lipidated GTPases, the highly hydrophobic geranylgeranyl moieties of Rab and Rho proteins tremendously reduce their solubility, thereby locking them on the membrane [30]. In order to ensure the proper transition from the membrane to the cytosol, the small GTPases require another regulatory unit called GDP-dissociation inhibitor (GDI) – RabGDI (3 isoforms) and RhoGDI (3 isoforms) [23]. Independently of its type, GDI interacts with GDP-bound GTPases and binds with high affinity in the nanomolar range to their lipid anchor that is inserted into the membrane [31–33]. Thus, GDI shields the C-terminal hydrophobic moiety and enables the GTPase extraction from the membrane shuttling it to the cytosolic pool [16]. Moreover, GDIs target multiple GTPases of the same small GTPase family [3].

1.1.3 The role of Ras in the cell

The most important factor for the growth and development of organisms is the cell division controlled by the cell cycle. Such a complex process requires multiple control mechanisms, regulated by cellular proteins, among which the Rho and Ras GTPases are also present [34]. The cell cycle regulation by Ras relies on the activity state of the GTPase as well as on its membrane or cytosolic localization. In order, to be internalized into the target membrane of cellular compartments, C-terminus of Ras must undergo multiple post-translational modifications (PTMs) i.e. lipidation, proteolysis, and methylation by diverse enzymes (Figure 4A) [35]. The intracellular localization of different Ras isoforms is controlled by different means. Usually, the main mechanism controlling membrane association and dissociation of Ras is represented by the reversible lipidation with a palmitoyl group [35]. The activation of Ras occurs via the receptor tyrosine kinase-mediated recruitment of the Ras GEF termed Son of Sevenless (SOS) to the target membrane, where it can activate Ras, thereby enabling its internalization into the membrane. Activated Ras can interact with a variety of effectors stimulating numerous signaling pathways (Figure 4B). The best-studied signaling pathways include the Ras–mitogen-activated protein kinase (MAPK), Ral guanine nucleotide dissociation stimulator (RalGDS), and phosphoinositide 3-kinase (PI3K) pathways (Figure 4C) [35–37]. Active Ras triggers all three pathways culminating in multiple cellular functions like gene transcription, cell proliferation, and apoptosis [5]. Thus, Ras activates RalGDS, which, in turn, facilitates the GDP to GTP nucleotide exchange in Ral GTPase by its GEF activity. The activated Ral provokes the association of Sec5 and TANK-binding kinase (TBK1), thereby elevating the kinase catalytic activity. Thereafter, TBK1 phosphorylates and promotes nuclear translocation of the NF-κB transcription factor cRel, resulting in the NF-κB

activation [36,38]. Consequently, the transcription of important cell-cycle-controlling factors is induced, which eventually initiate cell division. This highlights the role of Ras as a proto-oncogene. The hyperactivation of Ras due to oncogenic point mutations results in an increased cell division and significantly contributes to the development of cancer in humans [39,40]. This is also supported by the COSMIC (the catalogue of somatic mutations in cancer) database, confirming 22% of all cancer cases exhibit point mutations in KRas [40]. Thus, KRas is the most frequently mutated Ras isoform. Generally, there are three hotspots for cancer-related mutations in Ras: G12, G13, and Q61. The occurrence of a mutation in each position is isoform-dependent [41]. Moreover, six different amino acid substitutions were observed for each position in Ras (G to A, C, D, R, S, V, and Q to E, H, K, L, P, R) [40]. Interestingly, these mutations occur either in the nucleotide-binding P-loop (G12 and G13) or at the position of the catalytic Gln in the G3 motif of switch II (Q61). Thus, these mutations trap Ras in a constitutively active state by different means. They either reduce the response of Ras proteins to GAPs or reduce the intrinsic GTP hydrolysis of Ras, thereby inhibiting Ras inactivation in both cases [40].

Altogether, Ras GTPases play a pivotal role in the cell and the development of cancers, thereby representing a prominent therapeutic target.
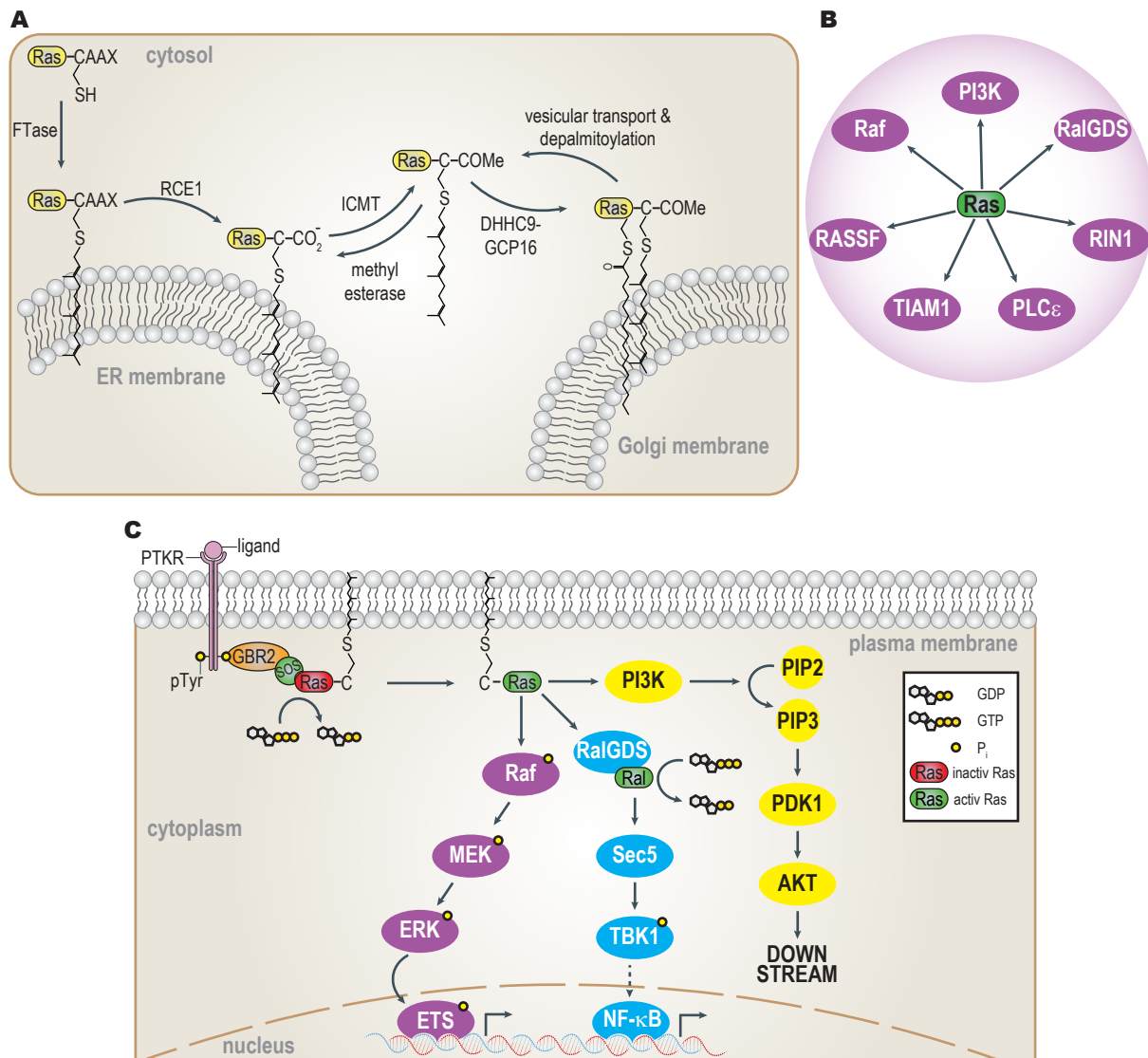
Figure 4 | Ras' fate in the cell. (A) *C-terminal processing of Ras by different enzymes ensures its proper cellular function. Once lipidated (see section 1.1.7.1 p. 25), Ras is internalized into the membrane of the endoplasmic reticulum (ER). Further, Ras is transferred to Golgi where the palmitoyl moiety can be attached. Afterwards, Ras can undergo vesicular transport to the plasma membrane before coming back to Golgi after depalmitoylation. FTase: farnesyl transferase; RCE1: RAS-converting enzyme 1; ICMT: isoprenylcysteine carboxylmethyltransferase; DHHC9–GCP16: DHHC domain-containing 9–Golgi complex-associated protein of 16 kDa. Depalmitoylation can be mediated by multiple enzymes [42]. **(B)** Active Ras can activate multiple downstream effectors. **(C)** Simplified scheme of Ras-mediated activation of different signaling pathways. Upon ligand binding, the protein tyrosine kinase receptor (PTKR) autophosphorylates and binds growth factor receptor-bound 2 (GBR2), which in turn recruits GEF Son of sevenless (SOS). Subsequently, SOS activates Ras and starts multiple downstream cascades. MEK: MAPK/ERK kinase; ERK: RAS–RAF1–extracellular signal-regulated kinase; RalGDS: Ral guanine nucleotide dissociation stimulator; TBK1: TANK-binding kinase 1; PDK1: PI3K-dependent kinase 1; PIP2: phosphatidylinositol (4,5)-bisphosphate; PIP3: phosphatidylinositol (3,4,5)-trisphosphate ETS and NF-κB: transcription factors.*

1.1.4 Rab GTPases as the masters of vesicular logistics

Intercellular communication and cellular nutrient supply occur mainly via endocytosis [43,44]. Exocytosis plays an equally important role in signal transduction and cellular clearance [45,46]. Both cellular processes involve Rab GTPases. E.g. Rab3 and Rab10 regulate lysosomal exocytosis and plasma membrane repair [47]. Rab5 and Rab11a, in turn, are involved in the regulation of the epidermal growth factor receptor (EGFR) recycling process [48]. Once EGFR is endocytosed by the

cell, it is transported to the destination point via vesicles. Thus, vesicular traffic represents a transportation system of the eukaryotic cell responsible for the specific and site-directed transport of molecules between cellular compartments. Although the course of vesicle transport depends on the cargo, it can be divided into the following general steps: vesicle formation (budding), movement between cellular compartments, tethering, and fusion [49,50]. Each of these steps requires strict spatial and temporal coordination to ensure the specificity and, ultimately, the identity of the membranes of cellular organelles. To fulfill such complex coordination, the cell utilizes the family of Rab GTPases. These G proteins control and regulate all main stages of vesicular transport (Figure 5). After Rab GTPases are synthesized in the cytosol, they are recognized by the Rab escort protein (REP) and presented to the Rab geranylgeranyl transferase (RabGGTase) for the addition of one or two geranylgeranyl lipid moieties to the Cys residues situated in their C-termini [51,52]. Lipidated Rabs can then be internalized into the donor membrane and activated by GEFs *in situ*. Active Rabs can activate sorting adaptors and engage the budding process on the donor membrane. Once the vesicle is loaded with cargo and fully formed, it can be delivered to the acceptor membrane along the cytoskeletal track composed of actin filaments or microtubules. For the vesicle motility, Rab GTPases recruit motor adaptors or bind directly to the motor, thereby ensuring the transport to the acceptor membrane. Prior to the vesicle fusion with the acceptor membrane, the vesicle has to be tethered to it by a combination of a GTP-bound Rab and tethering factors followed by the formation of a complex between vesicle (v) and target (t) soluble NSF attachment proteins receptors (SNAREs) engaging the fusion [49]. The Rab protein involved in vesicle transport is subsequently deactivated on the acceptor membrane by a GAP. The inactive Rab is then extracted from the membrane by GDI and returned to the donor membrane as a Rab:GDI complex [3]. The specific membrane targeting of Rabs has not been fully elucidated and represents a topic of future research. However, two main possible routes for the targeted Rab insertion into the donor membrane were proposed. A membrane-bound GDI displacement factor (GDF) represents the one of them and is suggested to be responsible for the recognition of the Rab:GDI complexes on the donor membrane and their dissociation, thereby ensuring targeted insertion of the Rab protein back into the donor membrane [53,54]. Consequently, the Rab protein can be reactivated by a GEF and start a new cycle of vesicular transport. Other research suggests that local GEF-mediated reactivation of Rabs enables the targeting of Rab proteins to the desired membrane [28,55]. Since GDI binds exclusively to inactive Rabs, GEF-mediated reactivation can provoke a dissociation of the Rab:GDI complex and, therefore, ensure the reinsertion of the Rab into the donor membrane.
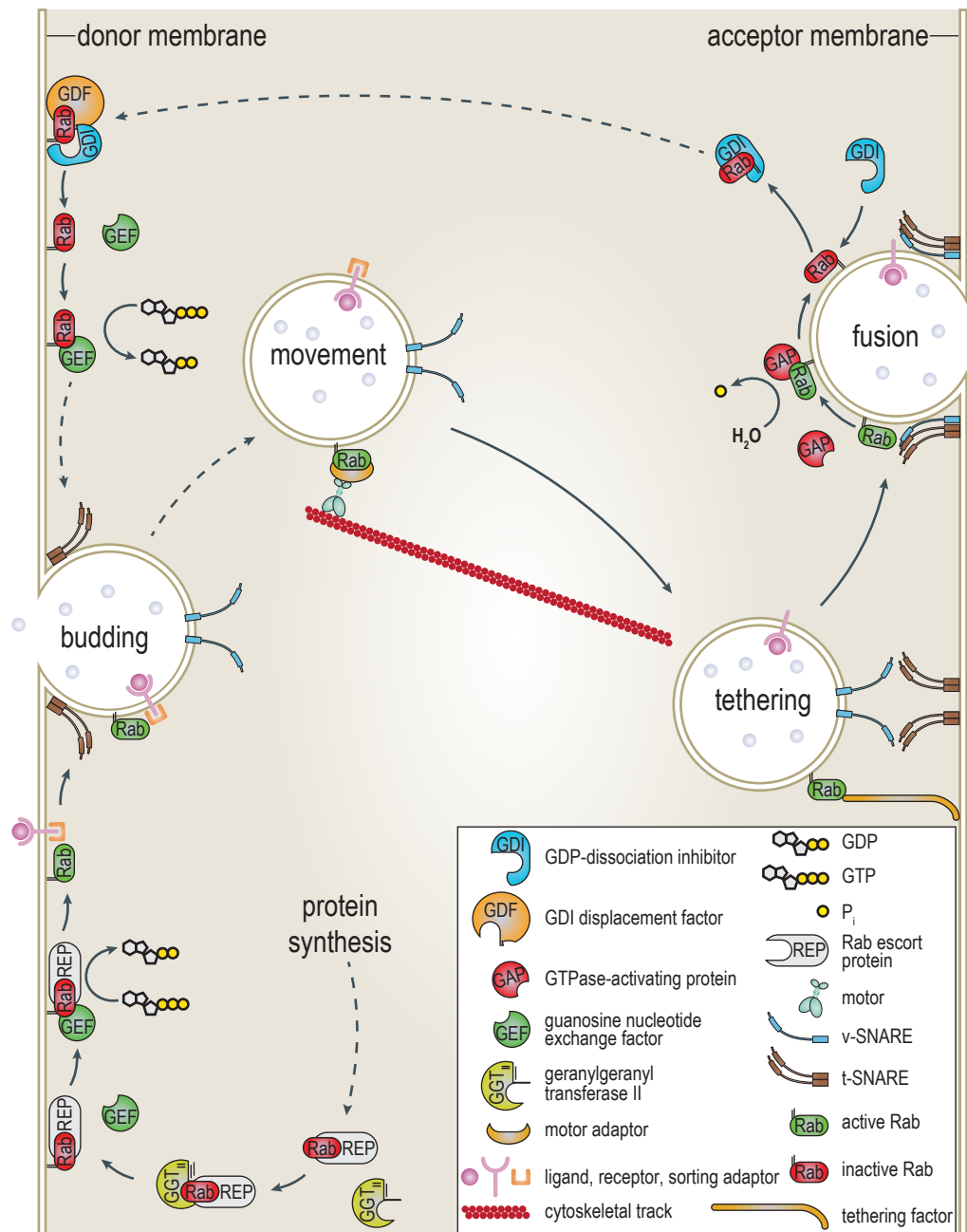
Figure 5 | Rab GTPases in vesicular transport. *Schematic overview of the Rab-mediated vesicle transport. Newly synthesized unlipidated Rab proteins interact with Rab escort protein (REP), which presents them to the geranylgeranyl transferase II (GGTase II) for the geranylgeranylation. After GEF-mediated Rab activation, the budding at the donor membrane and the vesicle transport to the acceptor membrane take place. SNARE-mediated membrane fusion is followed by GAP-mediated Rab inactivation at the acceptor membrane. Inactive Rab is provided to a donor membrane for a new transport cycle via GDI-mediated membrane recycling. Dashed lines represent multi-step or not fully understood processes. The figure was adapted and modified with permission from Stenmark, 2009 [6]. Copyright (2020) Springer Nature Limited. License number 4933921463334.*

Due to interactions with different effectors and regulators, the same Rabs can be involved in vesicle transport to different destinations depending on the cell type. Rab3, for instance, stimulates amylase release in pancreatic cells and is also involved in the regulation of synaptic transmission in neuronal cells [56,57]. The concatenation of interactions, e.g. via GEF and GAP recruitment, leads to the realization of different signal circuits. The functions of individual Rab

GTPases have been implemented in numerous studies and in many cases could be assigned to specific membrane-associated processes (Figure 6).

Malfunctions in Rab-mediated vesicle transport are associated with a variety of pathologies such as Parkinson's disease (PD), cancer, or lysosomal storage disease [58–62]. Moreover, Rabs can act as oncogenic drivers or oncogenes themselves [63,64].
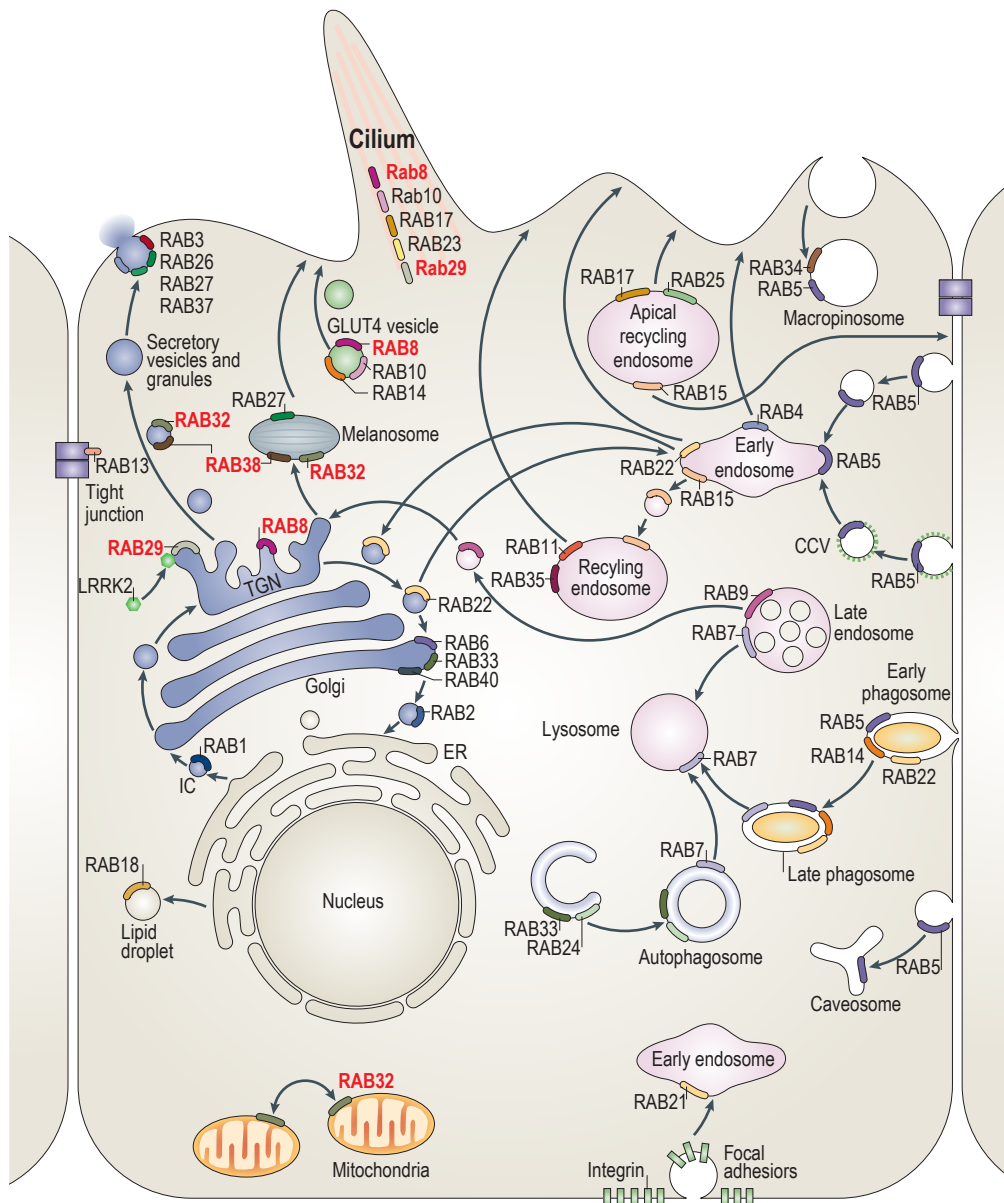
Figure 6 | Function and localization of Rab GTPases in overview. *The vesicle transport pathways and localizations of selected Rab GTPases within an epithelial cell. Rab8 and members of the Rab32 subfamily are highlighted in red. CCV: clathrin-coated vesicle; ER: endoplasmic reticulum; GLUT4: glucose transporter Type 4; IC: intermediate compartment; TGN: trans-Golgi network. The figure was adapted and modified with permission from Stenmark, 2009 [6]. Copyright (2020) Springer Nature Limited. License number 4933921463334.*

1.1.5 Cellular functions of Rab8

Rab8 is represented by two isoforms in humans: Rab8a and Rab8b, which display over 81 % of sequence identity and differ only in their C-termini [65]. The functional difference between both isoforms is poorly understood. The Rab8a localizes i.a. on GLUT4 vesicles and participates in the

regulation of GLUT4 translocation based on the direct interaction of Rab8a and Myosin Va (Figure 6) [66]. GLUT4 is an insulin-responsive glucose transporter, which is crucial for glucose transport into muscle and adipose cells [67]. In this context, it has been shown that Rab8a regulates apical protein localization and is responsible for the absorption and digestion of diverse nutrients in the small intestine [68]. Additionally, Rab8a is involved in the biogenesis of primary cilia – a hair-like structured organelle responsible for hedgehog signaling (Hhs) in mammals [69–71]. Hhs is a signaling pathway frequently used for intracellular communication which is involved in the development of multiple organs and the regulation of apoptosis [69,72]. Rab8a also functions in the endocytic recycling pathway and regulation of autophagy [73,74]. Moreover, Rab8a can be recruited to the phagosomes and stressed lysosomes by the leucine-rich repeat kinase 2 (LRRK2) in a kinase-dependent manner [75,76]. Multiple small GTPases serve as a substrate for LRRK2 [77]. Interestingly, the hyperactive G2019S-variant of LRRK2 present in PD patients impairs the function of Rab8a via phosphorylation and, thereby alters the endolysosomal trafficking [78]. Thereupon, it has been revealed that redundant phosphorylation of Rab8a by LRRK2 can alter ciliogenesis [79]. However, the LRRK2-mediated Rab8a phosphorylation plays a significant role in ciliary trafficking pathways [80]. In contrast to Rab8a, there is not much known about Rab8b. The Rab8b is downregulated in pancreatic cancer [58]. Recently, Rab8b was identified in the proteome of a pathogen-containing compartment in macrophages and suggested to be a part of the control mechanism of *Salmonella* proliferation in the host [81]. Moreover, Rab8b was linked to *Legionella pneumophila,* in which it interferes with the integrity of *Legionella*-containing vacuoles [82]. Both of the Rab8 isoforms are present on *Salmonella*-induced filaments (SIF) indicating the association of *Salmonella* with recycling compartments in macrophages [83].

1.1.6 Cellular functions of the Rab32 subfamily

The Rab32 subfamily of small GTPases is represented by three members: Rab29, Rab32, and Rab38, which are evolutional closely related to the Rab7 subfamily. Similarly to the Rab7 subfamily, the members of the Rab32 subfamily are mainly involved in endo-lysosomal signaling [84]. However, other roles of these GTPases were reported previously.

1.1.6.1 Rab29

Due to its genetic homology with Rab7, Rab29 was first designated as Rab7-like 1 [85]. This protein is present in all tissues but it is predominantly expressed in the kidneys [86]. First insights into the Rab29's cellular functionality have shown its localization at the Golgi and its role in the integrity of the trans-Golgi network [87,88]. Further research during the past decade suggested Rab29 to be linked to neuronal diseases like PD. Since LRRK2 is one of the genes mutated in the rare genetic Parkinsonism resulting in the kinase hyperactivation, it plays an important role in neurodegenerative disorders [77,89]. Rab29 is involved in the regulation of LRRK2 by recruiting and

activating it on the Golgi membrane in a GTP-dependent fashion [90–92]. Additionally, Rab29 has been shown to recruit LRRK2 onto stressed lysosomes [75]. LRRK2 and Rab29 both provoke centrosomal alterations and regulate neurite morphology [93–95]. Rab29 may also play a role in viral replicase formation [96]. Furthermore, the misregulation of Rab29 caused by mutations in the RabGEF C9orf72 results in the disruption of the trans-Golgi vesicle transport [97]. Moreover, Rab29 was shown to be involved in the regulation of ciliogenesis in immune cells [98]. Interestingly, broad-host infecting *Salmonella* secretes a protease GtgE that specifically cleaves Rab29, which is normally recruited to the *Salmonella*-containing vacuoles (SCV) in infected cells and can hinder bacterial replication in macrophages [99].

1.1.6.2 Rab32/38

Rab32 and Rab38 are paralogues displaying over 60 % of sequence identity and originating from a vertebrate whole-genome duplication [100]. Whereas Rab32 is present in different types of tissues in humans, Rab38 is expressed specifically in melanocytes and thrombocytes [101–103]. Primary research has connected Rab32 and its paralogue with the regulation of melanosome biogenesis. In this context, Rab32 has also been shown to interact with Myosin Vc maintaining the trafficking of integral membrane proteins to melanosomes [104]. Mutation in Rab38 results in the chocolate (*cht*) mouse coat color phenotype [105]. It was shown that Rab32/38 localize with end-stage melanosomes (a member of lysosome-related organelles (LRO)) and are responsible for the sorting of tyrosinase, the tyrosinase-related protein 1 (Tyrp1), and dopachrome tautomerase (Dct) in mouse melanocytes [105–107]. Moreover, Rab32 can compensate for the function of depleted Rab38 and enable nearly normal pigmentation in *cht* melanocytes [107]. In contrast, only Rab32 is critical for the trafficking of Tyrp2 [108]. For a successful melanogenesis, Rab32 and Rab38 must interact with several binding partners such as adaptor protein complex-1 (AP1), adaptor protein complex-2 (AP2) as well as biogenesis of lysosome-related organelle complex (BLOC)-2 [107]. The latter one is a heterotrimeric protein consisting of HPS3, HPS5, and HPS6 subunits [109]. HPS stands for Hermansky-Pudlak syndrome, an autosomal recessive disorder associated with e.g. oculocutaneous albinism, that displays mutations within the coding genes for HPS subunits causing the disease [110]. Another heteromeric complex of HPS subunits 1 and 4 is termed BLOC-3 and functions as a GEF for Rab32 and Rab38 [111,112]. The antagonist of BLOC-3 was also revealed previously – RUTBC1, a physiological TBC-GAP facilitating the inactivation of Rab32/38 [106,113]. Another physiologically relevant binding partner of Rab32/38 is the vacuolar protein sorting (VPS9)-ankyrin-repeat protein (Varp). Varp binds Rab32/38 via its first ankyrin repeat (ANK1) in a nucleotide-dependent manner [114–116]. This interaction was confirmed by a structural analysis of the heterocomplex between both proteins (Figure 7) [114].
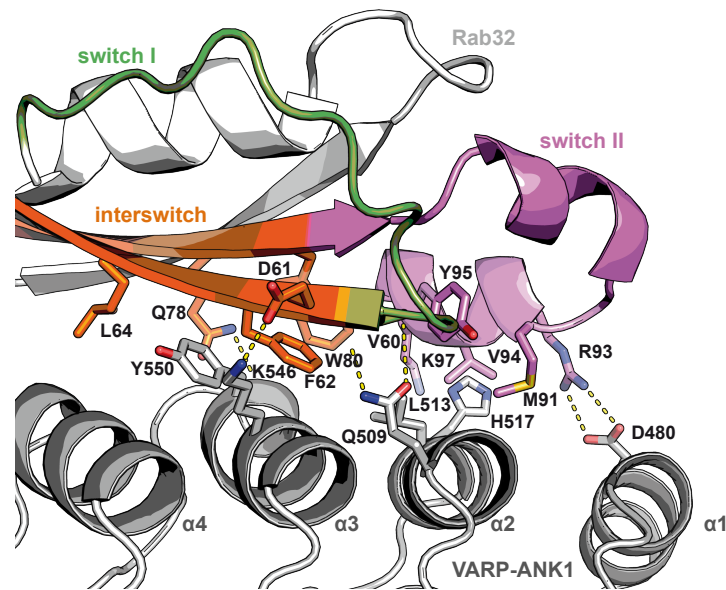
Figure 7 | Crystal structure of Rab32:VarpANK1 complex. *Varp interacts with Rab32 mainly via the residues of the interswitch region and switch II. Ion pairing is indicated with dashed yellow lines. Residues important for the establishment of interaction are depicted with sticks. PDB ID: 4CYM [114].*

Varp, in turn, is involved in the regulation of endosomal trafficking by binding not only to small GTPases (Rab32, 38, and Rab40c) but also to the retromer complex (a sorting nexin dimer, VPS29, and VPS35) and the v-SNARE (also called an R-SNARE) VAMP7 [117]. Interestingly, sorting nexin 6 was suggested to bind preferentially GTP-bound Rab32 and to affect the retromer-dependent Golgi trafficking [118]. The function of the Rab32-Varp interaction has not been fully elucidated yet. Noteworthy, similarly to Rab29, both Rab32 and Rab38 interact with the N-terminal armadillo domain of LRRK2 in a GTP-dependent manner [91]. Rab32 also controls the recruitment of the cAMP-dependent protein kinase (PKA) thereby regulating the mitochondrial fission and dynamics [119,120]. Additionally, Rab32 was suggested to regulate lysosomal mTOR trafficking and support the mTORC1 signaling, which play a pivotal role in cellular metabolism [121]. Further reports have linked Rab32 to the maturation of the autophagosomes and phagosomes during bacterial infection, in which Rab32 regulates the recruitment of cathepsin D to the phagosomes and controls the survival of intracellular pathogens [122–125]. Moreover, in a recent study it has been shown that Rab32 facilitates the delivery of itaconate, a mitochondrial metabolite with antimicrobial activity, to the SCVs restricting *Salmonella* replication [126].

1.1.7 The role of post-translational modifications in the function of small GTPases

Prokaryotic as well as eukaryotic cells do not only rely on the chemical repertoire and information content of the 20 proteinogenic amino acids. In order to expand their functionality, living cells employ covalent modifications attached to the proteins. Since such modifications usually occur after the protein synthesis, which is accomplished through a process called translation, they are designated as post-translational. Post-translational modifications (PTMs) are crucial for the regulation of a number of cellular processes like targeted protein degradation, DNA damage
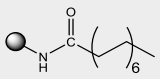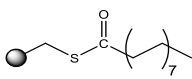
repair, cell division, signaling, etc. [127–130]. PTMs can be a result of spontaneous reactions between proteins and small molecules due to the surrounding chemical environment or they can be driven by the enzymatic activity of other proteins [131]. Despite their origin, PTMs require accurate regulation to maintain the balance between all cellular processes. However, such balance can be disturbed endogenously by pathological misregulation or exogenously by pathogens to secure their survival in the host organism [132].
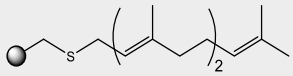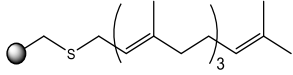
1.1.7.1 Physiological PTMs of small GTPases

Small GTPases require not only GEFs, GAPs, or GDIs for their proper functionality, but also PTMs, especially regarding the interaction with GDIs. The most important feature of small GTPases connected to PTMs is the C-terminal lipidation. It is crucial for the membrane insertion and the interaction with GDI, enabling the cycling of small GTPases between cytosolic and membrane-bound pools. Based on the C-terminal recognition sequence they can be modified with different lipid moieties and by different enzymes (Table 2). Thus, the members of the Ras family can be farnesylated by farnesyl transferase (FTase) on the Cys of the CaaX motif, followed by proteolysis of three terminal amino acids by the Ras-converting enzyme 1. The resulting free carboxyl group is subsequently methylated by isoprenylcysteine carboxylmethyltransferase (ICMT) in order to shield the hydrophilic tail which may hinder a proper membrane insertion. Additionally, Ras proteins can be palmitoylated by a palmitoyl acyltransferase (PAT) enabling their localization to the Golgi. Only the processes mediated by ICMT and PAT are reversible under physiological conditions [35]. On the contrary, Rab GTPases are only subject to irreversible lipidation by geranylgeranyl transferase II (GGTase II or also referred to as RabGGTase). GGTase II can attach one or, in most cases, two geranylgeranyl moieties to the Rab proteins when they are bound to the REP. Two geranylgeranyl groups ensure the high membrane affinity of Rab GTPases [8]. Interestingly, exactly these lipids are required for proper interaction with GDI during the Rab extraction from the membrane [33].

Table 2 | Lipidation as a PTM of small GTPases. Overview of lipid moieties with their structures and target proteins, with relevant catalyzing enzymes and recognition motifs. FTase recognition CaaX motif consists of a conserved Cys, two variable aliphatic amino acids "a" and one variable amino acid "X". Aliphatic amino acids are also present in the GGTase I recognition sequence. GGTase II requires mainly C-terminal Cys residues for the successful modification.

Lipid group	Structure	GTPase	Enzyme	Motif
Myristoyl		Arf [133], Ras [35]	NMTs	MGxxxS/T
Palmitoyl		Ras [35], Rho [134]	PATs	not consistent

| Farnesyl		Ras [35], Rho [134]	FTase	CaaX
Geranylgeranyl		Rho [134] Rab [8]	GGTase I GGTase II	CaaL CC, CxC, CC(x)$_{n=1-3}$

Other PTMs have also been discovered in addition to lipidation. Among them are serotonylation [135,136], S-nitrosylation [137], N-terminal acetylation [138], SUMOylation, and ubiquitination [35,139] as well as phosphorylation mediated by multiple kinases [35,77,140,141] (Table 3).

Table 3 | Further PTMs of small GTPases involved in their cellular regulation.

Functional group	GTPase (position)	Enzyme	Effect
Acetyl	Arf (N-terminus) [138]	N-terminal acetyltransferase	facilitated recognition by the membrane receptor Sys1p/hSys1
Phosphate	Ras [35], Rab [77,140,141], Rho [142]	multiple kinases e.g. LRRK2, Src tyrosine kinase	diverse effects e.g. impaired interaction of Rab with GDI
Serotonyl	Rab3a, Rab27a [136], RhoA [135]	transglutaminase	constitutive activation
S-nitrosyl	Ras (C118) [35]	non-enzymatic	enhanced nucleotide exchange
SUMO	Rac1 (K183, K184, K186, K188) [139]	E3 ligase PIAS3	cell migration
Ubiquitin	Ras [35], Rho [142], Rab6a, Rab8a, Rab11a [143]	E3 ligase	enhanced activation and regulation of Ras compartmentalization, protein degradation, Rab activation
	Arf6 [144]	Fbx8	downregulation of Arf6

1.1.7.2 Pathological PTMs of small GTPases by bacteria

The function of small GTPases is frequently steered and altered by bacterial effectors and regulatory enzymes mimicking the activity of host proteins [145,146]. To this end, pathogens secret a plethora of proteins during the infection directed onto the modification of host GTPases (Figure 8). Reported PTMs arising during the bacterial infection include phosphorylation [147], phospho-ribo-ubiquitination [148,149], deamination [150–152], lipidation [153], phosphocholination [154], ADP-ribosylation [155,156], glycosylation [35,142,157], adenylylation [158–160], and proteolysis [99,161,162].
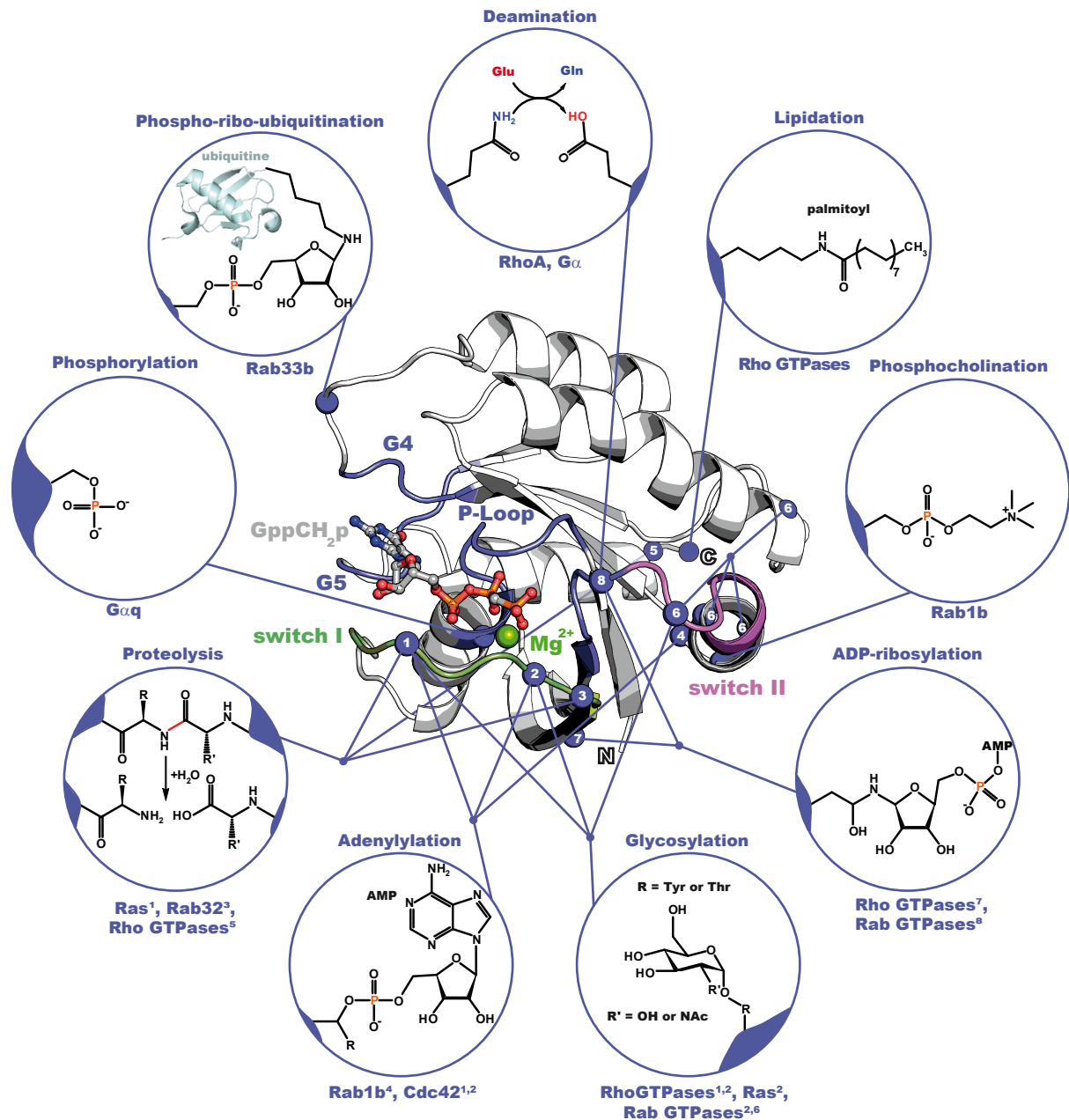
Figure 8 | Structural overview of posttranslational modifications of small GTPases introduced by bacterial enzymes. *The protein crystal structure (PDB ID: 121P) represents a typical structural organization of small G proteins [14]. PTMs, their structures, and target proteins are displayed in circles. Positions of PTMs within the protein structure are indicated with blue spheres and labeled with numbers corresponding to the superscripts next to the protein names (if necessary). Green sphere: Mg^{2+} ion; balls and sticks: $GppCH_2p$ (non-hydrolyzable GTP analog); switch regions and G motifs are indicated. Adapted and modified from Dr. Rudolf Wachtel [163].*

Thus, the structural diversity ranges from the cleavage of a single peptide bond (proteolysis) or the exchange of small functional groups (deamination), the introduction of small (charged) molecules (phosphate, phosphocholine, or glucose) to the attachment of sterically-demanding functional groups (ADP-ribose or AMP) or even small proteins (ubiquitin). Interestingly, some modifications like proteolysis are irreversible, while other PTMs e.g. adenylylation are reversed by complementary bacterial enzymes. Many of these modifications are targeting exclusively Rab GTPases, thereby enabling the supply of bacteria with nutrients and building blocks via vesicles

or disturbing the host defense systems (Table 4) [11,126]. Thus, for instance, *Legionella pneumophila* secretes multiple enzymes during the infection, in order to survive and replicate in the host by diversely manipulating the functionality of Rab1. Enzyme pairs DrrA/SidD and AnkX/Lem3 secreted by *Legionella* have been shown to reversibly modify residues located in the switch II region of Rab1b with AMP or phosphocholine moieties, respectively, resulting in a reshaped interaction profile of Rab1 with its GAPs, GEFs, and GDI [3]. Similarly, *Salmonella* typhimurium employs the protease GtgE to enhance its survival chances in the host by cleaving exclusively the members of the Rab32 subfamily [99,164]. Recently, glycosylation (arginine GlcNAcylation) has been reported to occur during Salmonella infection in the host disturbing the functionality of Rab1 and contributing to the survival and replication of the pathogen [157].

In conclusion, PTMs of small GTPases mediated by pathogen enzymes are vital for the infection progression as well as for the survival and replication of bacteria in the hosting organism. Therefore, it is of utmost importance to understand the source and effects of such modifications as well as to find possible ways to prevent them.

Table 4 | Overview of post-translational modifications of small GTPases mediated by bacterial enzymes in the host cell.

PTM	GTPase (position)	Enzyme/Bacteria	Effect
Adenylylation	Rab1b (Y77) [160]	DrrA/*Legionella pneumophila*	recruitment of Rab1b to LCVs by its constitutive activation [165]
	Cdc42 (Y32) [159]	IbpA/*Histophilus somni*	disruption of the host actin cytoskeleton [166]
	Cdc42 (T35) [158]	VopS/*Vibrio parahaemolyticus*	disruption of effector binding and downstream signaling [167]
ADP-ribosylation	RhoA, B, C (N41) [168]	C3 toxin/*Clostridium botulinum*	increased binding to GDI
	Rab5 (Q79), Rab31 (Q64) [169]	YART/*Yersinia mollaretii*	constitutive activation, increased binding to R5BD, and interaction with early endosomes
Deamination	RhoA (Q63) [150]	dermonecrotizing toxin/*Bordetella bronchiseptica*	constitutive activation, actin stress fiber formation
	multiple G_i and $G\alpha$ (GTP catalyzing Q in switch II) [151,152]	*Pasteurella multocida* toxin *Photorhabdus asymbiotica* protein toxin	constitutive activation following by Rho activation through $G\alpha_{q/11}$
Glycosylation	Rab5 (T52), Rab31 (T36) [169]	YGT/*Yersinia mollaretii*	inactivation, reduced binding to R5BD, and association with early endosomes
	Ras (T35) [170]	TcsL toxin/*Clostridium sordellii*	disruption of effector binding and MAPK/ERK pathway
	Rho (T37) [170]	TcdA/B toxin/*Clostridium difficile*	breakdown of the actin cytoskeleton

	Rho (Y34) [151]	*Photorhabdus asymbiotica* protein toxin	same effect like in the case of *C. difficile*
Lipidation	Rac1 (K183, K184) [153]	RID/*Vibrio vulnificus*	inhibition of Rho-mediated signaling, deformation of the cytoskeleton
Phosphocholination	Rab1b (S76) [154]	AnkX/*Legionella pneumophila*	displacement of GDI [171]
Phospho-ribo-ubiquitination	Rab33b (S154) [148,149]	SdeA/*Legionella pneumophila*	reduced GTP hydrolysis
Phosphorylation	$G\alpha_q$ (S47) [147]	YpkA/*Yersinia pseudotuberculosis*	decreased GTP binding, inhibition of multiple $G\alpha_q$ signaling pathways
Proteolysis	Rab29 (G41-V42) Rab32 (G59-V60) Rab38 (G43-V44) [99,172]	GtgE/*Salmonella enterica*	disruption of effector binding and downstream signaling
	HRas, KRas, NRas, Rap1a,b (Y32-D33) [161]	RRSP/*Vibrio vulnificus*	disruption of effector binding and MAPK/ERK pathway
	RhoA, Rac, Cdc42 (C-terminally) [162]	YopT/*Yersinia pestis*	loss of the prenyl group, membrane detachment

1.2 *Salmonella enterica* – a prominent human pathogen

Salmonella enterica is a Gram-negative, facultative anaerobe, and bacilli-formed bacteria belonging to the family of *Enterobacteriaceae* that can infect a broad range of hosts [173]. Salmonella is represented by more than 2600 serovars worldwide and is one of the most pathogenic species [174,175]. *Salmonella enterica* ssp. Typhimurium (further referred as to *S.* Typhimurium) is of clinical interest in both developed and developing countries, where it is one of the main reasons for food-borne illnesses [174]. *S.* Typhimurium can infect a broad range of hosts including human usually causing local salmonellosis by invading epithelial cells and macrophages of the gastrointestinal tract, leading to vomiting, inflammation, and diarrhea [176,177]. Untreated, *S.* Typhimurium can invade various organs down to the brain accompanied by a cytokine-mediated inflammation, eventually causing life-threatening sepsis [178–181]. *S.* Typhi is another *Salmonella* serovar that adjusted its infectious machinery exclusively to humans. Due to various deletions in genes encoding for pathogenic proteins (e.g. protease GtgE of *S.* Typhimurium), *S.* Typhi possesses a reduced genome, which, together with loss-of-function mutations of multiple enzymes (e.g. RabGAP SopD2) and secretion of exclusive typhoid toxin, explains the host restriction of *S.* Typhi to humans. Independently of the serovar, all *Salmonellae* are in possession of multiple pathogenicity islands (SPIs), encoding a variety of infection-associated machineries, especially the type 3 secretion system (T3SS), which is crucial for the host invasion process by Salmonella [182,183]. Generally, in 2017, Salmonella infected a multi-million human population worldwide that resulted in 33,300 – 98,100 and 76,900 – 218,900 deaths caused by invasive non-typhoidal and by

(para)typhoidal serovars, respectively [184]. Therefore, Salmonella represents a relevant bacteriological research field.

1.2.1 Host invading strategy of *Salmonella* Typhimurium

S. Typhimurium is a sophisticated representative of intracellular pathogens. After the bacteria reach the intestine, they can invade host epithelial cells or macrophages. The cell invasion, the establishment of SCVs, and further pathogen-host interactions are carried out mainly via bacterial proteins (also called bacterial effectors) encoded within the SPIs. The most important SPIs among many are the SPI-1 and SPI-2, which are employed by *S.* Typhimurium at different stages of infection. Whereas SPI-1 encodes machineries required for the first interaction with the host cell, SPI-2 is necessary for the development of a systemic infection. Therefore, SPI-1 encodes i.a. the T3SS-1 and the effector proteins required for the successful invasion of the host and the beginning of the infection [185]. The T3SS-1 is a huge needle-shaped multidomain protein complex responsible for the delivery of the Salmonella effector proteins into the host cell [186]. The T3SS's base is situated in the bacterial membrane and the protruding needle tip penetrates the membrane of the host cell, thereby establishing a connection between both organisms and enabling the translocation of bacterial effectors. Thus, *S.* Typhimurium adapts the membrane surface and intracellular environment of the host to its need. To this end, the bacterium secretes SopE and SopE2, mimicking GEF activity towards Cdc42 and Rac, which are crucial for the organization of the actin cytoskeleton [187]. Due to the activation of Rho GTPases, *S.* Typhimurium can rearrange the actin cytoskeleton resulting in membrane ruffling, which, in turn, leads to the pathogen macropinocytosis and bacterial invasion (Figure 9). Another important effector at this stage is SptP, that is translocated during the entry of the bacteria into the host. SptP possesses a GAP activity towards the same Rho GTPases, thereby downregulating the membrane ruffling [158,186]. After successful invasion, bacteria usually remain in the SCVs, which, after manipulations by *S.* Typhimurium, provide them with an appropriate intracellular replication niche. One of the secreted effectors manipulating the composition of the SCVs is SopB. SopB (encoded by SPI-1) is an inositol phosphatase that recruits Rab5 and its effector phosphoinositide 3-kinase Vps34 in order to generate phosphatidylinositol-3-phosphate (PI3P) on the SCV membrane, enabling further SCV maturation [188]. Additionally, SopB reduces levels of acidic lipids on the SCV, which may alter the trafficking of Rab GTPases and hinder SCV fusion with lysosomes [189]. After the SCVs are established, *S.* Typhimurium engages the next step of the infection. For this purpose, the bacteria assemble the T3SS-2 (encoded by SPI-2) on the SCV membrane. Both secretion systems are structurally similar, but the effectors translocated with their help fundamentally differ from each other [190]. The SPI-2 effectors secreted into the cytosol via T3SS-2 are responsible for SCV maintenance, maturation, and formation of replicative SCV with characteristic Salmonella-induced filaments (SIFs), which are crucial for the supply of replicating bacteria with

nutrients [191,192]. Thus, Salmonella has developed multiple mechanisms to manipulate the host cell and complete its intracellular infection cycle. However, many functions and mechanisms of action of numerous secreted proteins are not completely understood in detail on the molecular level. Furthermore, the difference in host specificity of *S.* Typhi and *S.* Typhimurium and a possible link to the different arsenal of effectors in this context is the subject of current discussions.

Figure 9 | Comparison between host invasion by wild type (WT) and noninvasive bacteria (ΔinvA/Inv). *After a successful injection of pathogenic effectors via T3SS, WT Salmonella enters the host cell via micropinocytosis. Hereafter, the bacteria run through the multiple steps of SCV maturation resulting in the formation of mature SCVs connected to the Sifs. The bacteria lacking SPI-1 (ΔinvA/Inv) cannot replicate in the host and are degraded in the phagolysosomes. vATPase (vacuolar proton pump) is responsible for the acidification of SCVs and (phago)lysosomes. Rab GTPases typically residing on the SCVs and intracellular compartments are indicated. Rab proteins and Salmonella effectors relevant for this work are highlighted in red. CCV: clathrin-coated vesicle; EEA1: early endosome antigen 1; LAMP1: lysosome-associated membrane protein 1; TGN: trans-Golgi network; PI3P: phosphatidylinositol-3-phosphate.*

1.2.2 The cysteine protease GtgE from *Salmonella* Typhimurium

The GtgE-encoding gene was identified as a part of the Gifsy-2 bacteriophage contributing to the pathogenicity of *S.* Typhimurium in mice [193]. In contrast to *S.* Typhimurium, GtgE is absent in the human-adapted *Salmonella* serovar Typhi. GtgE is a product of SPI-2 and secreted via T3SS-2 during the maturation of SCVs [191]. Further studies revealed that GtgE is a cysteine protease cleaving exclusively the inactive members of the Rab32-subfamily (Rab29, Rab32, and Rab38) of small GTPases [99,164,183]. Interestingly, GtgE is not present in the genome of the human-adapted *Salmonella* serovar Typhi, which explains the host restriction of the typhoid Salmonella [172]. The result of the GtgE activity is the proteolytic PTM occurring within the regulatory switch I of Rab32 between residues G59 and V60 (equivalent positions in relatives proteins are indicated in Table 4), presumably leading to its inactivation. The catalytic center of GtgE is represented by a triad of C45, H151, and D169 where C45 functions as a nucleophile supported by basic properties of H151, and D169 stabilizes H151 by the carboxyl group (Figure 10A). The catalytic residues are located between three Rab binding platforms termed spikes 1-3 (Figure 10B). These spikes form the interaction interface between the protease and its substrate via multiple polar and hydrophobic interactions, which ensure a high affinity between both proteins. Interestingly, spikes 1 and 2 form a deep cavity, in which GtgE catches and proteolytically cleaves the flexible switch I of the inactive Rab. Additionally, it has been shown, that the side-chain of F88 in Rab32 is an important determinant for GtgE specificity towards the inactive form of Rab32, disturbing the interaction of K194 of GtgE and the switch II of Rab32 in the active state [164].
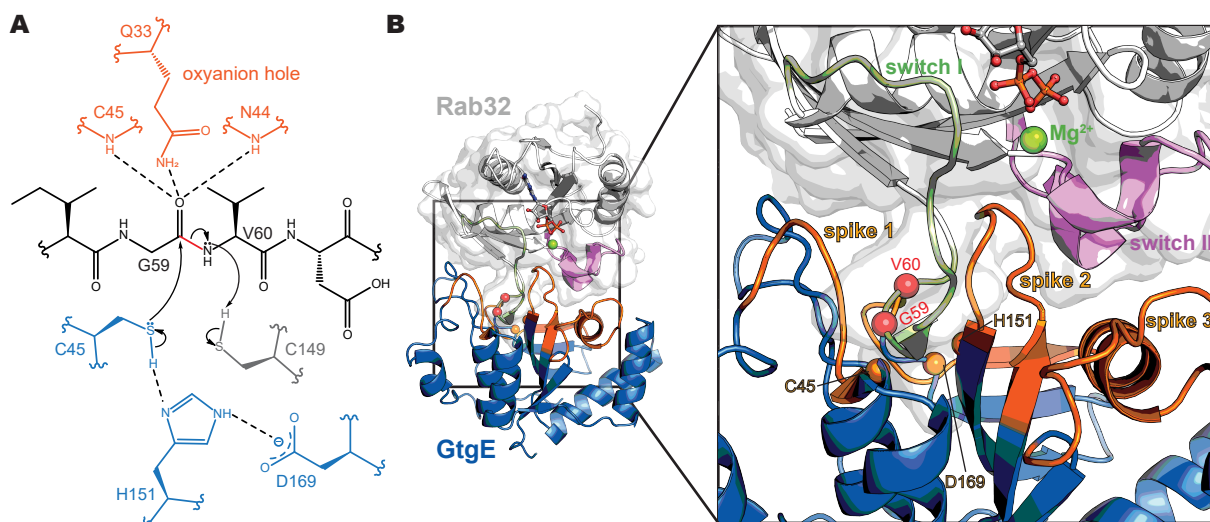
Figure 10 | Mechanism and crystal structure of GtgE in complex with Rab32. (A) *Overview of the catalytic mechanism of GtgE. The cleavage site resides between G59 and V60. Catalytic residues are depicted in blue. The oxyanion hole (orange) is composed of GtgE's backbones of C45 and N44 with the support of the side-chain of Q33. C149 serves as a proton donor in the reaction.* **(B)** *Crystal structure of Rab:GtgE complex (PDB ID: 5OEC) [164]. The interaction interface between proteins is formed by spikes 1-3 of GtgE, which form a deep cavity and trap switch I in there.*

1.2.3 RabGAP *Salmonella* outer protein D2 and its homolog D

Salmonella outer proteins (Sops) SopD and SopD2 are homologous effector proteins displaying 43% of sequence identity and 63% of similarity [194]. Both proteins are secreted by *S.* Typhimurium into the host during the infection, but at different stages [195,196]. SopD is encoded on the SPI-1 and is, thus, secreted during the beginning of the infection, whereas SopD2 belongs to the effectors encoded on the SPI-2 and is secreted after the bacteria have entered the host cell. Despite such high structural similarity, both proteins have different localizations during the infection in the host. SopD was reported to be distributed within the cytosol, whereas SopD2 localized at the SCVs [195]. SopD plays a significant role in the development of diarrhea and gastroenteritis in calves [196,197]. Additionally, both effectors play an important role in the survival and replication of bacteria in the host [146,194]. However, the detailed mechanisms of the SopD function are unknown. In contrast, SopD2 has been connected with the development of SCVs and their membrane dynamics in previous reports [195,198,199]. Moreover, studies of the past five years shed light on the role of SopD2 in the pathogen-host interaction and its substrates. The N-terminus of SopD2 interacts directly with Rab7 and inhibits its nucleotide exchange, thereby impairing its activation and the interaction with its effectors as well as the fusion of SCVs with lysosomes [200]. Additionally, SopD2 modulates the function of Rab34 and contributes to infection development [201]. Interestingly, since the C-terminus of SopD2 was reported to possess GAP activity towards Rab32 and other GTPases, it represents, thereby, a bifunctional protein targeting different small GTPases in a diverse manner [146]. Whereas the mechanism underlying Rab7 inhibition by SopD2 has not been completely clarified yet, the SopD2 GAP activity was investigated in more detail. The C-terminal R315 residue of SopD2 facilitates the GTP hydrolysis in Rab32, thereby mimicking the fundamental aspects of host GAPs [146]. Despite its mimicry, SopD2 shares neither sequence nor structural similarities with mammalian GAPs. The SopD2 GAP activity fully abolishes the recruitment of Rab32 to the SCVs. Moreover, *S.* Typhi, possessing SopD2 just as a pseudogene, engineered to express SopD2, could also suppress the recruitment of Rab32 to SCVs. Additionally, it has been shown, that the virulence-deficient ΔSopD2/ΔGtgE double-mutant *S.* Typhimurium strain could successfully replicate in BLOC-3^{-/-} deficient mice, indicating that both effectors impair the Rab32-BLOC-3-defense pathway [146]. Thus, *S.* Typhimurium employs SopD2 in order to deactivate Rab32 and provide GtgE with a substrate for proteolytical modification, thereby enabling the bacterial survival and replication in the host organism (Figure 11).
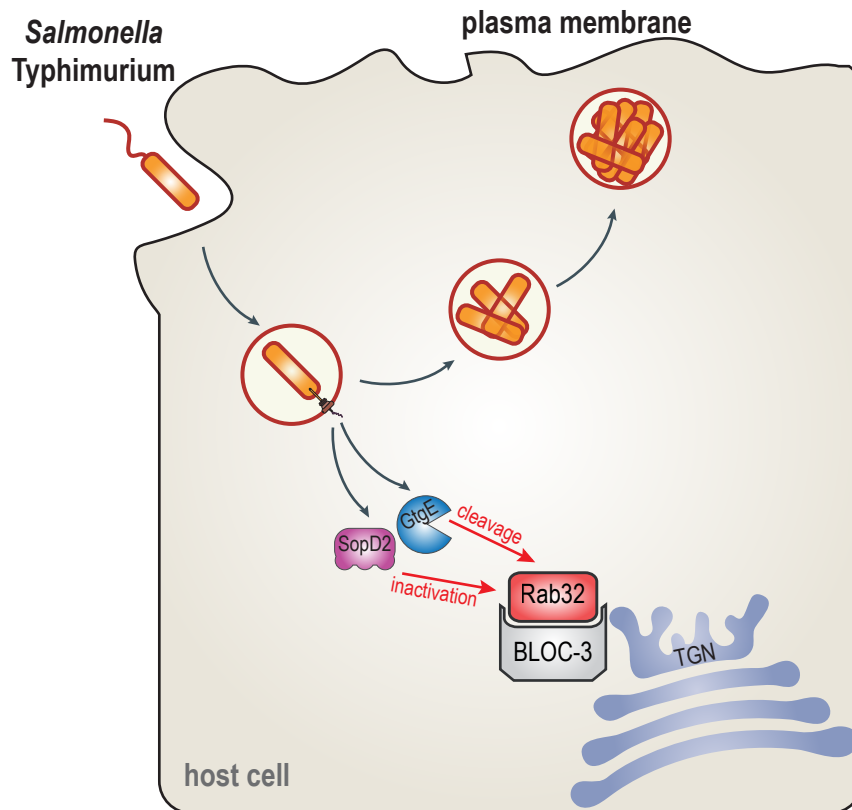
Figure 11 | Graphical representation of SopD2- and GtgE-mediated inactivation of Rab32. *Secretion of both SPI-2 effectors SopD2 and GtgE blunts the Rab32-BLOC-3-defense pathway and enables S. Typhimurium's successful propagation in the host. TGN: trans-Golgi network.*

1.3 Cytotoxicity of *Vibrio vulnificus*

Vibrio vulnificus is a human opportunistic pathogen belonging to Gram-negative facultative anaerobe halophilic motile bacteria, that are present predominantly in the sea and brackish waters of tropical and subtropical ecosystems. Similarly to Salmonella, *V. vulnificus* is a foodborne pathogen, however, it has a much higher fatality rate of ca. 50% [202]. *V. vulnificus* usually enters the human host through the ingestion of contaminated seafood and can provoke gastroenteritis or fatal sepsis in untreated cases. Additionally, *V. vulnificus* can infect open wounds while the person comes in contact with contaminated waters [203,204]. In contrast to Salmonella, *V. vulnificus* resides extracellularly in the mucosa of the intestine and has developed strategies to counter the cellular immune system and induce cell death of various cell types via secreted toxins, resulting in the invasion of the bloodstream and development of systemic disease [204–206]. The most studied toxin of *V. vulnificus* is the multifunctional auto-processing repeats-in-toxins (MARTX)$_{Vv}$ (also called RtxA$_1$) toxin. It is a crucial virulence factor for an intestinal infection, which belongs to the class of the RTX family of protein toxins like pore-forming α-hemolysin from *Staphylococcus aureus* and *Escherichia coli* [207,208]. The MARTX$_{Vv}$ toxin is a multidomain protein secreted by *V. vulnificus* extracellularly via the type 1 secretion system (T1SS) (Figure 12A). The N- and C-termini of the MARTX toxin are highly conserved and are required for its embedding into the cell membrane by

a pore formation. Interestingly, pores formed by the MARTX$_{Vv}$ toxin are not membrane-penetrating but serve as a delivery platform for further effector proteins [209]. Once the pore is formed, the bacterial effector proteins are released auto-catalytically into the host cytosol through the activity of the cysteine protease domain (CPD) (Figure 12B) [210]. However, the genuine composition of the (MA)RTX toxin varies among the species and *vibrio* bacteria. For instance, the MARTX$_{Vv}$ toxin from *V. vulnificus* delivers five effector proteins into the host: a domain of unknown function 1 (DUF1), Rho GTPase-inactivation domain (RID), an α/β hydrolase domain (ABH), a Makes Caterpillars Floppy-like domain (MCF) and a Ras/Rap1 site-specific endopeptidase (RRSP) (Figure 12A) [211].
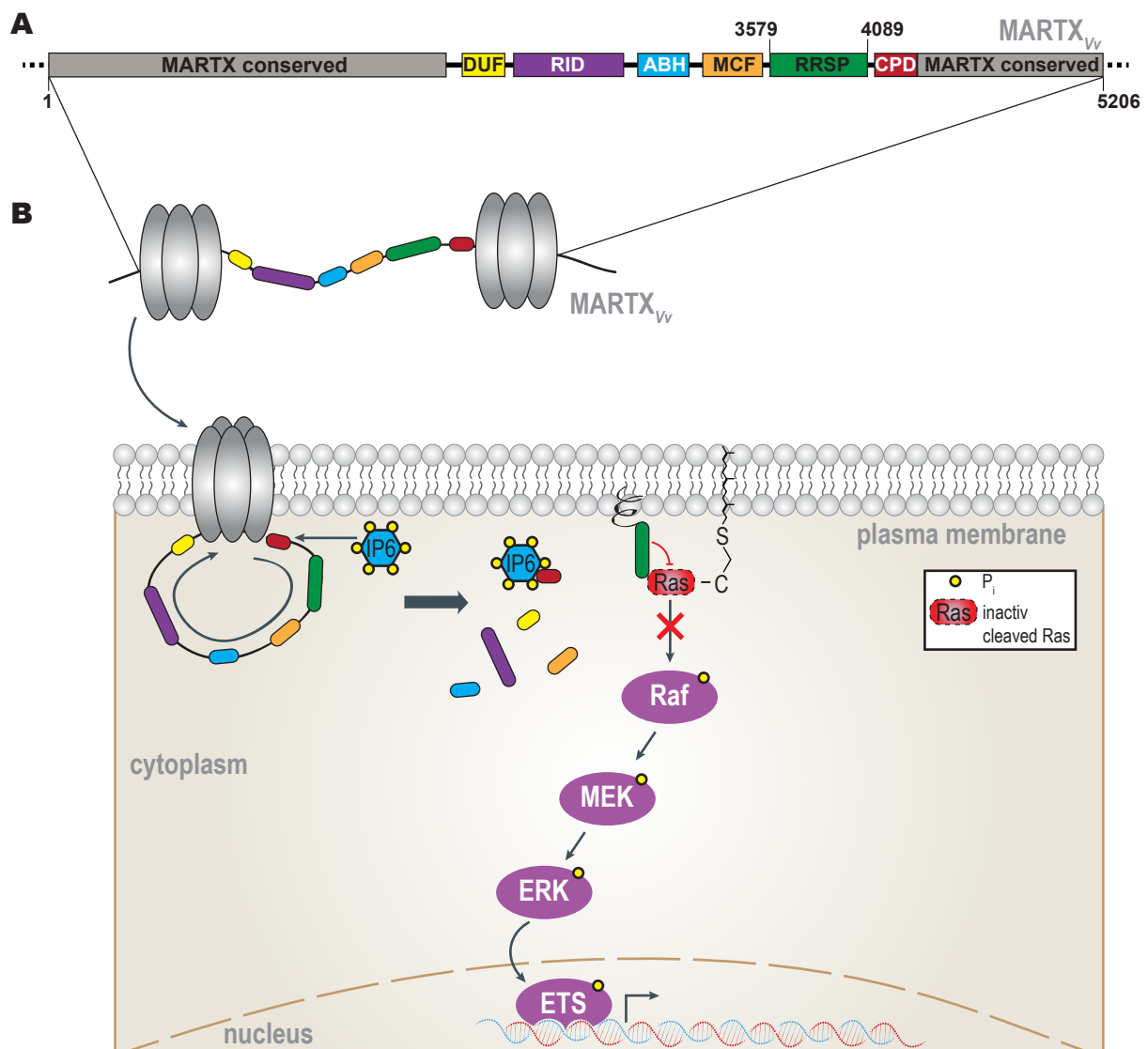
Figure 12 | Model for delivery of MARTX toxin into the host cell. *(A) Composition of the MARXT$_{Vv}$ toxin. Domain of unknown function 1 (DUF1), Rho GTPase-inactivation domain (RID), α/β hydrolase domain (ABH), Makes Caterpillars Floppy-like domain (MCF) and Ras/Rap1 site-specific endopeptidase (RRSP) are indicated. (B) After MARTX$_{Vv}$ is secreted by the V. vulnificus into the extracellular space via T1SS, it incorporates into the plasma membrane of the host cell and forms a pore-like structure. Thereafter, multiple effectors are delivered into the host and auto-processed by CPD (red) upon activation by inositol hexaphosphate (IP6). Auto-processing begins with RRSP. Thus, liberated RRSP (green) associates with the plasma membrane and cleaves the regulatory switch I of Ras resulting in the inhibition of e.g. Raf signaling pathway.*

1.3.1 Ras/Rap1 site-specific endopeptidase from *Vibrio vulnificus*

RRSP is a cytotoxic factor of *V. vulnificus* located within the 3579-4089 amino acids of MARTX$_{Vv}$. RRSP is composed of three domains: C1, C2A, and C2B [212]. Whereas the first N-terminal part (N1) of the C1 domain forms a hydrophobic core enabling the membrane association, the C2 domains bear the catalytic center of the endopeptidase (Figure 13A, B) [161,213]. After RRSP is released into the host cell cytosol by CPD activity, it targets exclusively Ras and Rap1 GTPases. Similarly to GtgE from Salmonella, RRSP cleaves the switch I region of small GTPases, or rather the peptide bond between Y32 and D33 (KRas), which is located near the N-terminal part of the switch I (Figure 13C). The RRSP-mediated proteolysis of Ras results in the disruption of the MAPK/ERK pathway and cytotoxicity [214]. The MAPK/ERK pathway inhibition by RRSP can be explained by the inability of the cleaved Ras to bind its physiological effector Raf, normally starting the MAPK/ERK signaling pathway [161]. Recent studies have revealed, that RRSP utilizes a 2His/2Glu motif similar to the endopeptidases of the TIKI superfamily in order to facilitate Ras/Rap1 proteolysis (Figure 13A). However, in contrast to the typical members of the TIKI superfamily like Bcr135, RRSP is not a metalloprotease [161,213]. The C1 and C2A domains are connected with an inter-lobe linker (3723-3739aa), which includes residues crucial for the proteolytic functionality of the C2 domain. The inter-lobe linker is suggested to function as a hinge ensuring flexibility between the connected domains [213]. Noteworthy, D3721 and R3841, located in the proximity of the inter-lobe linker are also vital for the cytotoxicity of the RRSP [212]. Moreover, the R3988E and R4001F mutations have been shown to abolish the Ras proteolysis due to a possible contribution to the substrate recognition [213]. In contrast, the R4001A mutation does not affect the cleavage of Ras [161]. Despite the contribution of previous studies, the genuine proteolytic mechanism on the molecular level remains elusive.
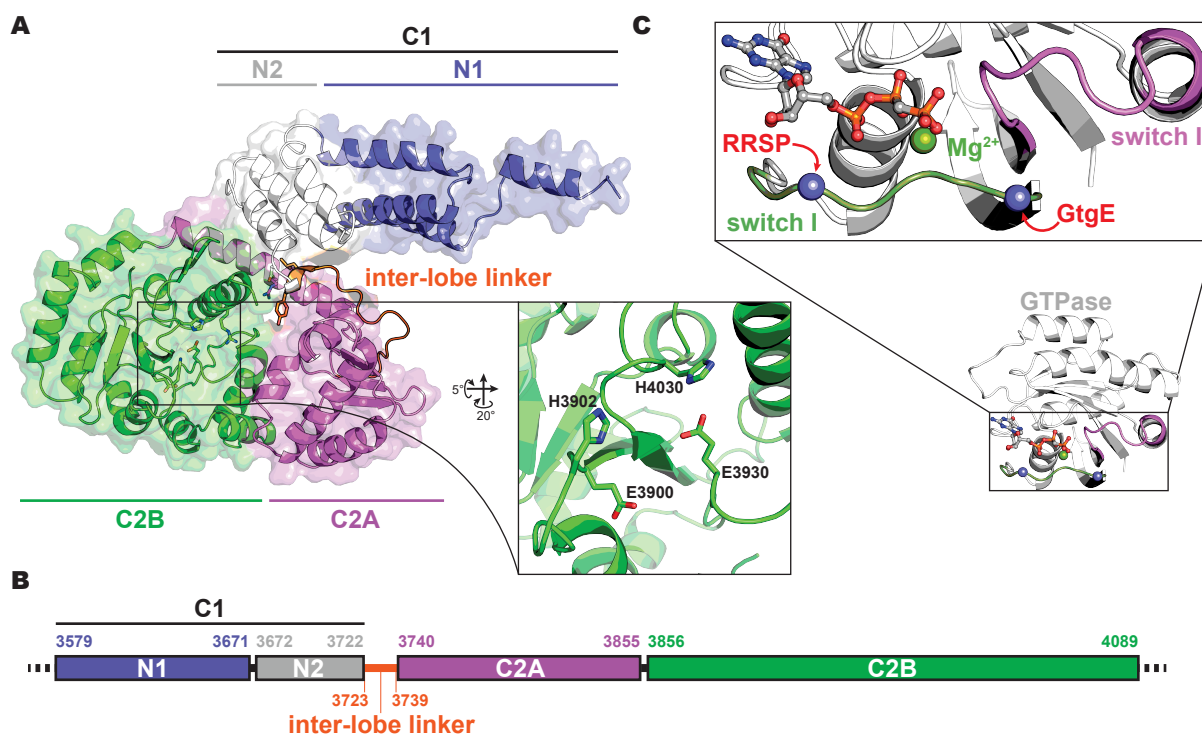
Figure 13 | Structural composition of RRSP and the cleavage site within Ras. (A) *Structural organization of the domains in RRSP (PDB ID: 6A8J)* [213]. *N1 (blue) part of C1 is crucial for the membrane insertion of the protease. N2 further contributes to the stabilization of the membrane localization domain (C1). The inter-lobe linker connects C1 and C2A domains and contributes to the flexibility between them, which is apparently vital for the substrate recognition. The function of C2A remains unknown. C2B (green) provides the catalytic quartet for Ras processing (catalytic residues are shown in the magnified section).* ***(B)*** *Scheme of RRSP domain composition.* ***(C)*** *Schematic representation of the cleavage positions (blue spheres) for RRSP and GtgE within the switch I of Ras and Rab32 (PDB ID: 121P)* [14]. *Green sphere: Mg^{2+} ion; balls with sticks: $GppCH_2p$.*

1.4 Sortase A – a transpeptidase with a broad biochemical application range [a]

Previous reports from various fields of biological sciences have proven the importance of protein immobilization techniques on a solid support, which have found indispensable applications in such scientific fields as biosensors, continuous flow biocatalysis and targeted drug delivery [216–218]. Therefore, various solid supports such as magnetic nanoparticles (MNPs) have been developed, providing a large surface area, good biocompatibility, and versatility [219,220]. During the past decade, significant progress in the development of various approaches has been made that allows the oriented immobilization of macromolecules [221]. In particular, enzyme-mediated protein immobilization allows for site-specific and efficient coupling under physiological buffer conditions, thereby preserving the functionality of immobilized proteins [222]. Immobilized proteins often demonstrate a higher resistance to organic solvents, pH, and temperature fluctuations [223,224]. The most renowned enzymes used in protein immobilization are microbial transglutaminase as well as sortase A (SrtA), which ligates a C-terminal LPXTG motif to substrates carrying an N-terminal poly-Gly (Figure 14) [225–228]. SrtA was discovered in *Staphylococcus aureus,* a Gram-

---

[a] The text in this section was modified and reprinted with permission from Fauser *et al*, 2020 [215]. Copyright (2020) American Chemical Society.

positive bacteria, where it catalyzes the immobilization of target proteins to the bacterial cell wall [229,230]. Recently, more efficient SrtA variants (e.g., SrtA 5M and SrtA 7M) have been developed [231–233]. SrtA has found an application in diverse scientific fields such as protein immobilization on crystalline cellulose nano-scaffolds, functionalization of proteins with small molecules, ligation of proteins to macromolecular nanocages, site-specific immobilization on microgels, and partial isotope labeling of multi-domain proteins for NMR [234–238]. Most recently, SrtA-mediated ligation was also applied for site-specific ubiquitylation of proteins both *in vitro* and *in cellulo* [239]. Although SrtA-mediated ligation has been well characterized, the determination of enzymatic activity of immobilized proteins remains challenging due to the lack of methods for their quantification on a solid support. This thesis represents a useful application for the fluorescent-based quantification method of immobilized GtgE protease on MNPs, that was designed by Dr. Burak Gülen and Joel Fauser, thereby expanding the SrtA application field and providing it with an alternative quantification system of immobilized proteins [215]. The immobilized GtgE was successfully used herein to produce pure cleaved Rab32 for subsequent highly sensitive FRET analyses, where even GtgE traces may influence the resulting data.

Hence, SrtA represents a versatile biochemical tool for the immobilization, bioconjugation, and labeling of proteins, despite challenges related to the quantification of immobilized proteins.
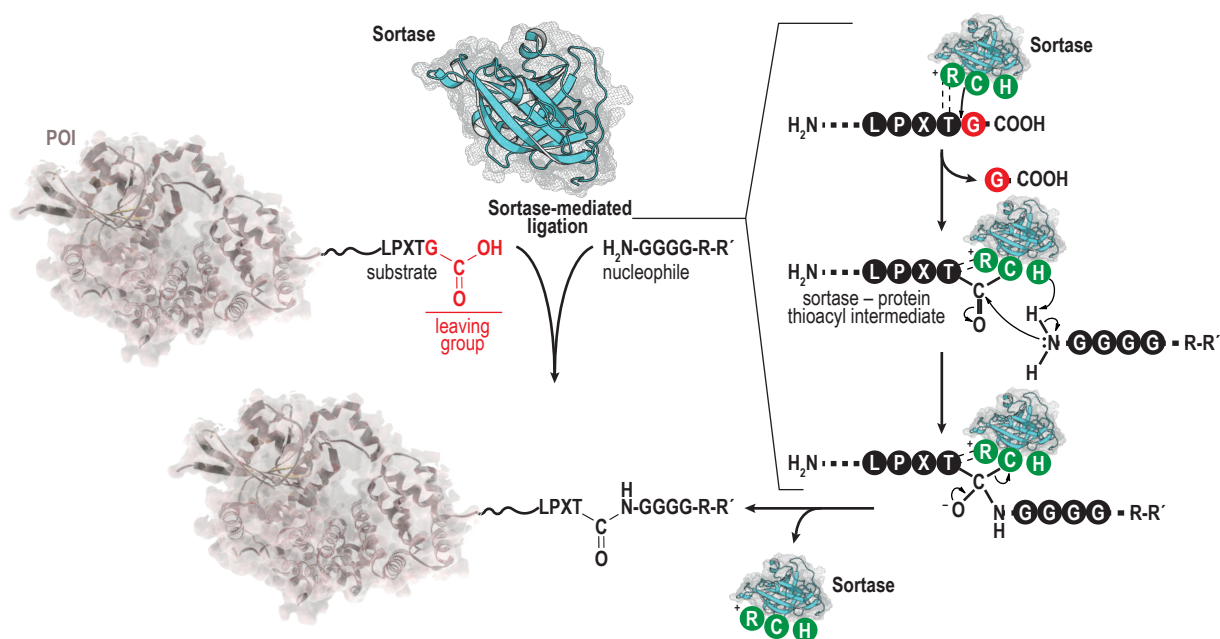
Figure 14 | Schematic representation of SrtA-mediated ligation. SrtA identifies the LPTXG motif on the C-terminus of the protein of interest (POI) and initiates the ligation between the POI and the substance bearing N-terminal poly-Gly tail. The catalytic site of SrtA is represented by a triad (green) of Cys, His, and Arg. Arg together with Thr from the recognition motif form an oxyanion hole, thereby stabilizing the catalytic complex. Cys, in turn, performs a nucleophilic attack on the carbonyl carbon of the Thr and forms the first tetrahedral intermediate complex. Afterward, His deprotonates the amine group of another ligation partner, thereby supporting the nucleophilic attack on the carbonyl carbon. Thereafter, the second tetrahedral intermediate collapses releasing SrtA and the ligation product [240]. R: flexible linker; R': variable substance (e.g. small molecules, nanoparticles, proteins, etc.).

2. AIMS

The main aim of this work was to investigate the consequences of proteolytic post-translational modifications of small GTPases by bacterial enzymes (virulence factors). To this end, two proteases from different bacteria were employed as an experimental system: GtgE from *Salmonella* Typhimurium targeting an inactive Rab32 and its homologs, and RRSP from *Vibrio vulnificus*, targeting Ras. Both proteases cleave their substrates within the switch I region. In contrast to GtgE, RRSP-mediated cleavage is independent of the nucleotide-bound state of the substrate. The consequences in terms of conformational changes and effector binding by GTPases upon cleavage should be investigated. In order to fulfill this goal, a multidisciplinary approach combining biochemical characterization of processed substrates and their binding behavior to the physiological effectors, single-pair FRET measurements, molecular dynamics simulations, and NMR spectroscopy. Since the effects caused by RRSP on Ras proteins were comprehensively covered by two independent laboratories in 2018, it was decided not to proceed with any further investigation on this topic.

Additionally, this work aimed at identifying the function and the putative targets of the virulence factor SopD secreted by the bacterial pathogen Salmonella at the beginning of the infection process. For this purpose, a yeast two-hybrid approach should have been applied using SopD as prey for screening through the Rab bank. Subsequently, the putative targets must have been validated *in vitro*.

Lastly, a project devoted to development of a sortase-mediated protein immobilization on magnetic nanoparticles was successfully closed, in order to obtain highly pure proteolytically processed Rab32 free of any residual GtgE for single-pair FRET measurements.

3. RESULTS

3.1 Sortase-mediated GtgE immobilization on magnetic nanoparticles [b]

This section is a product of the collaborative work with Dr. Burak Gülen, Joel Fauser, Maximilian Fottner, Vanessa Trauschke, and the author of this thesis. The results presented here are part of a recent publication in bioconjugate chemistry [215]. Whereas Dr. Burak Gülen and Joel Fauser designed the method, the data related to Rab32 and GtgE in this dissertation are contributed by the author and represent an application for the developed immobilization method. Maximilian Fottner provided the plasmid for sortase A and supported the project with his ideas. Vanessa Trauschke generated and analyzed all presented FRET data in here.

3.1.1 Design of a modular platform for GtgE immobilization

In order to couple GtgE to solid supports, Sortase A (SrtA) was chosen to enable oriented immobilization under physiological coupling conditions, thus preserving the functionality of coupled enzymes. In recent years, magnetic nanoparticles (MNPs) emerged as a new standard for protein immobilization mainly because of their versatility and easy handling [241,242]. Therefore, it was decided to combine the advantages of SrtA-mediated protein immobilization and MNPs. In order to equip MNPs with a polypeptide that serves as a SrtA substrate, a peptide (peptide 1) was chosen based on repeating sequences of commonly used poly-Gly/Ser motifs providing flexibility and solubility [243]. Besides, peptide 1 displays an N-terminal poly-Gly moiety which serves as an acceptor nucleophile in the SrtA-mediated transpeptidation, thus permitting specific SrtA-mediated coupling of target proteins to MNPs [244]. By using standard solid-phase peptide chemistry, peptide 1 was successfully activated and coupled via its C-terminus to the amino moiety of the MNPs. The Fmoc-protection group at the N-terminus of peptide 1 prevents polymerization upon chemical activation of the C-terminus and is removed with piperidine after coupling (Figure 15A). The chemically-coupled peptides can be directly used for the C-terminal immobilization of recombinant proteins and enzymes equipped with a C-terminal tag bearing the SrtA 5M recognition sequence (GSSG**LPETG**G) [231]. SrtA 5M contains five mutations that lead to 140-fold increased catalytic activity and therefore minimizes the "charging time" of the enzymes to the MNPs [231]. GtgE for immobilization was designed with an N-terminal GFP tag that is cleavable by the tobacco-etch virus (TEV) protease. After the SrtA-mediated coupling of the purified fusion construct to the MNPs, the N-terminal GFP tag is cleaved by TEV protease leaving the functional enzyme covalently linked to MNPs (Figure 15B). The release of GFP allows sensitive quantification of the immobilized enzyme via fluorescence spectroscopy. In this regard, the monitoring of TEV cleavage efficiency is crucial for accurate quantification. Fluorescence of immobilized GFP

---

[b] The text and figures in this section were modified and reprinted with permission from Fauser *et al*, 2020 [215]. Copyright (2020) American Chemical Society.

constructs, however, is quenched due to its proximity to the iron core of the MNPs [245]. Consequently, quantification of immobilized enzymes would help to control reaction conditions in biochemical assays using immobilized GtgE.
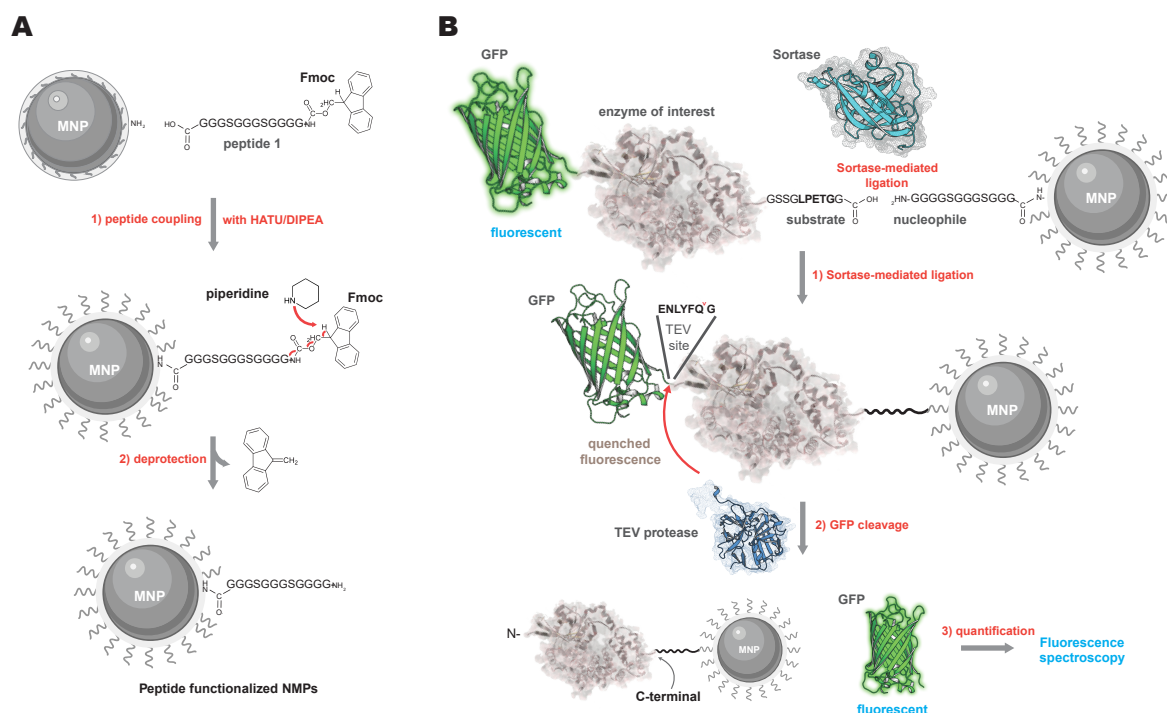
Figure 15 | Concept of SrtA-mediated MNP-based protein immobilization and GFP-based quantification. *MNP: magnetic nanoparticles. (A) Schematic representation of the coupling of peptide 1 to MNPs via standard solid-phase peptide chemistry. (B) Schematic representation of SrtA-mediated ligation of GFP-tagged substrates and subsequent cleavage by TEV protease. The released GFP is quantified via fluorescence spectroscopy. The figure was reprinted with permission from Fauser et al, 2020 [215]. Copyright (2020) American Chemical Society.*

3.1.2 Quantification of immobilized GtgE

GtgE GFP-fusion construct was successfully coupled to peptide-functionalized MNPs via SrtA 5M under physiological buffer conditions. Ligation was performed in 6-fold molar excess of GtgE to SrtA 5M within 1 h at 37 °C. After washing of GtgE-coupled MNPs, the amount of immobilized enzyme was quantified via fluorescence spectroscopy. Therefore, both immobilized and soluble GFP-fusion GtgE variants were simultaneously proteolyzed by the TEV protease, providing a reference for quantification as well as a control for cleavage efficiency. SDS-PAGE analysis shows that soluble GFP-fusion GtgE is quantitatively cleaved by TEV protease (Figure 16A). Since the cleavage efficiency of immobilized substrates may be affected by steric hindrance, TEV in 2.5-fold molar excess (compared to a molar ratio of 1:1 for the soluble reference) was used. Noteworthy, the accuracy of quantification relies on TEV cleavage efficiency which depends on the GFP-fusion constructs used. Any uncleaved GFP would cause an inaccuracy regarding the quantification of immobilized proteins. Serial dilutions of the cleaved soluble GFP-fusion construct were used to produce a standard curve for fluorescent measurements and quantification (Table 5 and Figure S1). GFP fluorescence revealed that 5.23 ± 0.15 nmol of GtgE were coupled to 1 mg MNPs (Table 5). Noteworthy, the same experimental setup can be used for the C-terminal protein

41

immobilization directly from the complex lysates. Additionally, a reverse approach in which MNPs are functionalized with a peptide bearing the SrtA recognition sequence, can be used for the N-terminal immobilization of proteins bearing a poly-Gly moiety on their very N-termini [215].

Table 5 | Overview quantification of immobilized GtgE. *The table was modified and reprinted with permission from Fauser et al, 2020* [215]. *Copyright (2020) American Chemical Society.*

	molecular weight [Da]	linear function[c]	measured fluorescence y [a.u.]	calculated concentration x [µM]	volume [µL]	total amount [nmol enzyme/1 mg MNP]
GtgE (C-terminal)	27,233	y = 2.0427x	33.39 ± 0.93	16.35 ± 0.46	100	5.23 ± 0.15

3.1.3 Assessment of the activity of immobilized GtgE

Quantification of the immobilized GtgE enabled the analysis of its functional integrity. Thus, the reaction kinetics of the immobilized and soluble GtgE were compared. Reaction kinetics of GtgE-mediated proteolysis are monitored by SDS-PAGE (Figure 16B) [164]. The results suggest that a coupled GtgE exhibited equivalent reaction kinetics compared to its soluble counterpart. The determined k_{cat}/K_M parameters for immobilized and soluble GtgE are $(6.2 \pm 1.1) \times 10^5$ M^{-1} s^{-1} and $(4.3 \pm 1.0) \times 10^5$ M^{-1} s^{-1}, respectively. Overall, the reaction kinetics are consistent with previously published data [164]. It could be inferred from those results that the quantification of immobilized enzymes proved reasonably accurate due to comparable kinetics. Since SrtA also hydrolyzes the created covalent linkage at extended incubation times, residual SrtA may lead to the removal of enzymes from MNPs [246]. To ensure complete removal of the uncoupled enzyme and SrtA, an extensive washing procedure was applied. The washing steps included high salt conditions and EGTA chelation of Ca^{2+}. Since Ca^{2+} is a cofactor of SrtA, the depletion of Ca^{2+} decreases the affinity of SrtA to coupled peptides bearing the SrtA 5M recognition sequence [247]. Additionally, a washing step containing excess (>40-fold) of a peptide bearing the LPETG motif (peptide 2), thus competing for the binding pocket of SrtA, was applied. Finally, a specific SrtA inhibitor, 4-hydroxymercury benzoic acid, was used to inactivate any residual SrtA. After washing, enzymatic activity was exclusively mediated by the immobilized GtgE as shown by testing the MNP supernatant for possible enzymatic activity (Figure 16C). The data showed that GtgE immobilized to MNPs led to complete substrate conversion within 2-3h. Minor enzymatic activity of the GtgE supernatant was observed, which cleaved about 8% of Rab32 only after prolonged incubation (Figure 16C).

---

[c] See Figure S1 for linear regression.
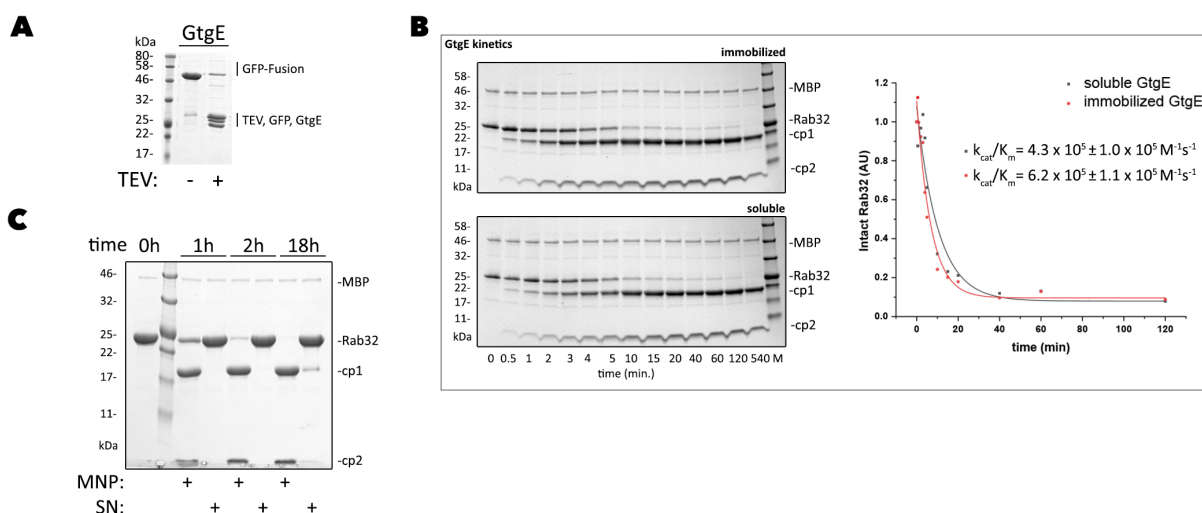
Figure 16 | Determination of the activity of immobilized enzymes. (A) *SDS-PAGE demonstrating the cleavage efficiency of the substrates GFP-IbpA and GFP-GtgE fusion constructs by the TEV protease in solution. The TEV protease was used at equimolar amounts to cleave the substrates.* **(B)** *Kinetic measurements of GtgE: SDS-PAGE displaying proteolysis of Rab32 mediated by either immobilized GtgE or soluble GtgE. MBP represents the maltose-binding protein as a loading control, cp1 and cp2 represent the resulting cleavage products of GtgE-mediated Rab32 cleavage. Calculated kinetic parameters are indicated. Quantified band intensities are plotted against the time and fitted with a single exponential function.* **(C)** *SDS-PAGE displaying enzymatic activity mediated by either immobilized GtgE (MNP) or supernatant (SN) as a negative control, The figure was modified and reprinted with permission from Fauser et al, 2020 [215]. Copyright (2020) American Chemical Society.*

3.1.4 Single-pair FRET-based enzymatic assessment

Generally, in biochemical experiments, small amounts (catalytic amounts) of enzymes are used to catalyze the desired reaction. Usually, these catalytic amounts do not interfere with the subsequent analysis of the product. However, in some applications such as single-pair FRET, even minimal impurities (such as catalytic amounts of an enzyme) may interfere with signal detection of the product. In order to assess the advantages of enzyme removal after GtgE-mediated cleavage of Rab32, the protease was immobilized on MNPs and the cleavage product was analyzed via single-pair FRET. The goal of these experiments was the monitoring of conformational changes of the Rab32 structure upon GtgE-mediated cleavage (see section 3.2.3 p. 48). To this end, Rab32 was proteolyzed by catalytic amounts of either soluble GtgE or MNP-immobilized GtgE. Quantitative proteolysis was verified via SDS-PAGE (Figure S2). After enzymatic proteolysis, the MNP-immobilized GtgE was removed from the reaction mixture, whereas in the parallel reaction, catalytic amounts of soluble GtgE remained in the sample submitted for FRET analysis (molar ratio of 1:180 of GtgE:Rab32). A Rab32 variant displaying two cysteine moieties for subsequent modification with maleimide fluorophores via Michael addition (Alexa488-maleimide, Alexa647-maleimide) was used for this experiment. Of note, GtgE bears five endogenous cysteines, which are prone to multiple cysteine labeling with the fluorophores and therefore may lead to substantial FRET signals even at catalytic quantities (Figure S2). Therefore, it was tested whether complete removal of immobilized GtgE from the reaction mixture would reduce unspecific FRET signals and improve the overall data quality. Indeed, a comparison of FRET data shows that FRET

statistics improved significantly upon GtgE removal (Figure 17A, B). Even the trace amounts of soluble GtgE negatively affected FRET efficiency, frequency, and signal distribution, whereas the removal of GtgE by MNPs exhibited a homogeneous FRET signal population with a higher signal-to-noise ratio (Figure 17C). Often, such impurities are removed by affinity-based purification techniques, which generally correlate with sample loss especially while handling analytical quantities. By simple magnetic removal of immobilized GtgE, an additional purification step was therefore avoided. Hence, the SrtA-mediated coupling of enzymes is advantageous for the production of biological samples with a high demand for purity, particularly at an analytical scale.
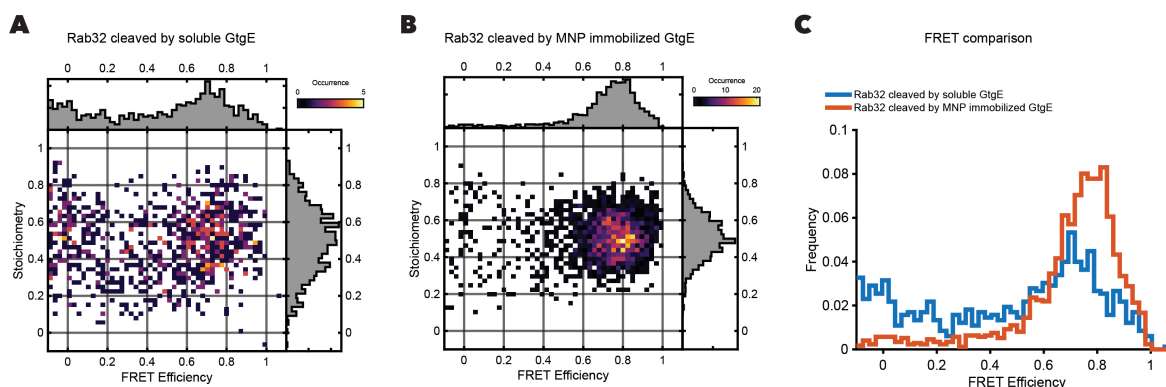
Figure 17 | FRET measurement of GtgE cleaved Rab32. *Two-dimensional stoichiometry vs FRET efficiency plot for **(A)** Rab32 cleaved by soluble GtgE and **(B)** Rab32 cleaved by immobilized GtgE (subsequently removed). **(C)** FRET efficiency histogram comparing Rab32 cleaved by soluble and immobilized GtgE, respectively. FRET data generated and processed by Vanessa Trauschke (the group of Prof. Don C. Lamb, LMU). The figure was reprinted with permission from Fauser et al, 2020 [215]. Copyright (2020) American Chemical Society.*

3.2 Effects of GtgE-mediated proteolysis of Rab32 [d]

This section represents the results of detailed biochemical, functional, and structural analyses involving combination of molecular dynamics (MD) simulations, nuclear magnetic resonance (NMR) experiments, and single-pair Förster resonance energy transfer (spFRET) analyses directed to investigate the effects of GtgE-mediated cleavage of Rab32 *in vitro*. The results presented in this section are the achievement of collaboration between the laboratories of Prof. Aymelt Itzen, Prof. Don C. Lamb, Prof. Michael Sattler, Prof. Martin Zacharias, and their co-workers. The author produced all proteins and conducted biochemical and biophysical experiments and analyzed the data (exception is stated on p. 48). Vanessa Trauschke performed protein labeling and FRET measurements with subsequent data analysis. Danial P. J. Dehkordi performed all MD simulations and helped with data interpretation. Dr. Hyun-Seo Kang collected and analyzed HSQC NMR spectra. The final version of the composed manuscript is under review in iScience (2020) [248].

---

[d] The text and figures in this section were modified and reprinted with permission from Savitskiy et al, 2020 [248]. Copyright (2020) Elsevier.

3.2.1 Proteolytic modification of Rab32 affects its nucleotide binding

After GtgE-mediated cleavage of Rab32, the GTPase domain remains a stable and monomeric protein in solution [164]. In order to dissect the functional consequences of Rab32 cleavage, cleaved and uncleaved Rab32 variants in both nucleotide-bound states were biochemically characterized in detail.

The protein melting temperature (T_M) was monitored via changes in circular dichroism (CD) as a proxy for the stability of intact and cleaved Rab32 in both GTP-bound and GDP-bound states, to elucidate whether the GtgE-mediated cleavage destabilizes the GTPase. CD measurements of secondary structure elements at 220 nm revealed that GtgE-mediated cleavage of Rab32:GDP results in a non-significant T_M decrease of 0.9°C (from 47.6°C to 46.7°C) (Figure 18A). Moreover, the nucleotide exchange from GDP to GppNHp (a non-hydrolyzable GTP analog) causes an increase of T_M value (50.0°C), which can be explained by the structural rigidification of the switch regions [19]. However, this stabilizing effect is not reflected in the $Rab32_{cleaved}$:GppNHp melting temperature (Figure 18B). Cleavage of Rab32:GDP followed by a nucleotide exchange does not affect the T_M (46.7°C) of none of the nucleotide states. Taken together, the CD studies demonstrate that GppNHp stabilizes neither the cleaved Rab32 nor its switch regions in contrast to the uncleaved Rab32. Additionally, CD spectroscopy reveals that there are no notable structural changes after GTPase cleavage (Figure 18C).

Both switch regions contribute to the stabilization of the nucleotide in the nucleotide-binding pocket of small GTPases [19,249,250]. Thus, the nucleotide dissociation properties may be used to investigate the impact of GtgE-mediated cleavage on the stability of the switch regions. In order to investigate the nucleotide dissociation rates, Rab32 was loaded *in vitro* with modified GDP or GppNHp bearing the fluorescent 2'/3'-O-(N-Methyl-anthraniloyl) (mant) moiety attached to the ribose (mGDP or mGppNHp). The nucleotide dissociation was monitored by the decrease in mant fluorescence intensity as a function of time after the addition of an excess amount of non-fluorescent counterparts (GDP or GppNHp). The nucleotide dissociation rate (k_{off}) of the proteolytically cleaved Rab32 increased regardless of the nucleotide state. Rab32:mGDP shows a k_{off} value of $1.4 \pm 0.002 \times 10^{-3}$ s^{-1} for the non-modified and $3.3 \pm 0.003 \times 10^{-3}$ s^{-1} for the cleaved state. On the other hand, Rab32:mGppNHp has a k_{off} value of $0.9 \pm 0.009 \times 10^{-3}$ s^{-1} for the non-modified and $2.6 \pm 0.014 \times 10^{-3}$ s^{-1} for the modified state (Figure 18D, E). Thus, the nucleotide dissociation rate is doubled for mGDP or tripled for mGppNHp in cleaved Rab32 (Figure 18F). Since GtgE proteolytically cleaves the switch I region, which is involved in nucleotide binding and Mg^{2+} ion coordination, it is not surprising that the cleavage leads to an increased nucleotide dissociation rate caused by destabilization of the switch I.
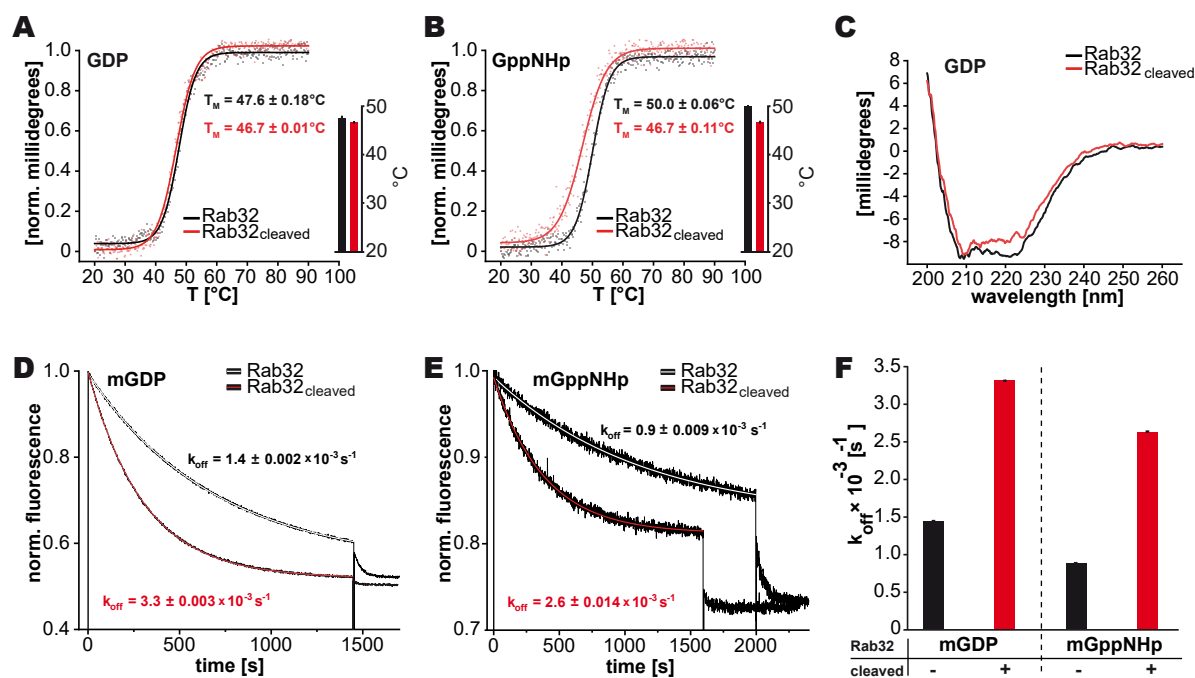
Figure 18 | The biochemical and biophysical characterization of non-modified and cleaved Rab32 in both the activated and inactive states. (A) *GtgE-mediated proteolysis does not significantly impact the thermal stability of Rab32:GDP. Left: Normalized thermal unfolding curves of cleaved and non-modified Rab32:GDP monitored via CD spectroscopy at 220 nm is plotted. The data are fitted with a Boltzmann function yielding the corresponding melting temperature (T_M). Right: Comparison of T_M in both modification states using a bar graph representation. The data are presented as a mean ± SEM (n = 2).* **(B)** *The thermal stability of Rab32:GppNHp is decreased upon GtgE-mediated proteolysis. Left: Normalized thermal unfolding curves of cleaved and non-modified Rab32:GppNHp monitored via CD spectroscopy at 220 nm are plotted. The data are fitted with a Boltzmann function yielding the corresponding melting temperature (T_M). Right: Comparison of T_M in both modification states using a bar graph representation. The data are presented as mean ± SEM (n = 2).* **(C)** *CD spectra of non-modified and cleaved Rab32:GDP. The comparison does not reveal any structural differences.* **(D)** *GDP dissociation from Rab32 is elevated in the cleaved state. Mant-fluorescence-based nucleotide release of mGDP (0.5 µM Rab32:mGDP) induced after the addition of a high concentration of non-fluorescent GDP (200 µM final). The fluorescence intensity and the time axis were normalized to the start of the reaction.* **(E)** *The nucleotide dissociation rate increases in Rab32:GppNHp after cleavage. Mant-fluorescence-based nucleotide release of mGppNHp (0.5 µM Rab32:mGppNHp) induced after the addition of a high concentration of non-fluorescent GppNHp (200 µM final). The fluorescence intensity and the time axis were normalized to the start of the reaction.* **(F)** *Quantification of nucleotide dissociation from non-modified and cleaved Rab32 in both the activated and inactive states are plotted in a bar graph. The figure was modified and reprinted with permission from Savitskiy et al, 2020 [248]. Copyright (2020) Elsevier.*

3.2.2 Proteolysis reduces binding of Rab32 to the VARP-ANK1 domain

Since GtgE-mediated cleavage of Rab32 may lead to an altered interaction profile with its binding partners, it was decided to investigate whether the cleaved Rab32 is still able to bind to its physiological interaction partners, the ANK1-domain of VARP and GDI. VARP is an effector of Rab32 that specifically binds to the active GTPase through its ANK1-domain [115]. Assuming the nucleotide exchange from Rab$_{cleaved}$:GDP to Rab$_{cleaved}$:GTP is not impaired by the GtgE-mediated proteolysis, Rab$_{cleaved}$:GTP may still bind to VARP. In case the nucleotide exchange is impaired due to the cleavage, it would render Rab32$_{cleaved}$:GDP a dead-end for the downstream signaling with VARP; however, it may still be able to bind to GDI. In order to test both scenarios, the uncleaved and the cleaved Rab32 variants in each nucleotide-bound states were prepared *in vitro*, and their potentials to bind to VARP and GDI were tested via analytical size exclusion chromatography (aSEC) (Figure 19).

As expected, neither Rab32:GDP nor its proteolytically modified counterpart formed a complex with the VARP-ANK1, whereas Rab32:GppNHp formed a stable complex with the ANK1-domain (Figure 19A, B) [114]. However, no binding was observed between Rab32$_{cleaved}$:GppNHp and VARP-ANK1 (Figure 19B, left). Thus, GtgE-mediated cleavage of Rab32 impairs its binding to VARP-ANK1 *in vitro*.

GDI specifically interacts with the inactive prenylated Rab GTPases [33,251]. The C-terminal lipid anchor of Rab GTPases is a prerequisite for the interaction with GDI [33]. For this purpose, Rab32 bearing the CVIM-sequence on its C-terminus for farnesylation was produced [252]. Subsequently, it was proteolyzed by catalytic amounts of GtgE, loaded with the desired nucleotide, and farnesylated, as described in the material and methods section (see section 6.4 Biochemical methods). Farnesylation was confirmed by mass spectrometry of the intact proteins before and after lipidation (Figure S3). Surprisingly, farnesylated Rab32$_{cleaved}$:GDP appears to form a complex with GDI, as indicated by the reduced elution time of the complex as well as the decreased Rab32 peak (Figure 19C, Figure S4). In contrast to the well-known binding preference of GDI for GDP-bound Rab proteins, the chromatographic data suggest that GDI is also able to form a complex with Rab32$_{cleaved}$:GppNHp (Figure 19D). Peak decomposition indicates distinct complex formation between GDI and Rab32 in the cases of Rab32:GDP, Rab32$_{cleaved}$:GDP, and Rab32$_{cleaved}$:GppNHp (Figure S5).

Moreover, any complex formation between Rab32:GppNHp and the Armadillo domain of LRRK2 could not have been detected on aSEC although the reported K$_d$ value for these two proteins lies in the low µM range (Figure S6) [91].

In conclusion, the proteolytic modification of Rab32 disrupts its interaction with VARP-ANK1. In contrast, the proteolytic cleavage does not affect the interactions with GDI in the case of Rab32$_{cleaved}$:GDP; furthermore, Rab32$_{cleaved}$:GppNHp displays an increased binding to GDI compared to its non-modified state.
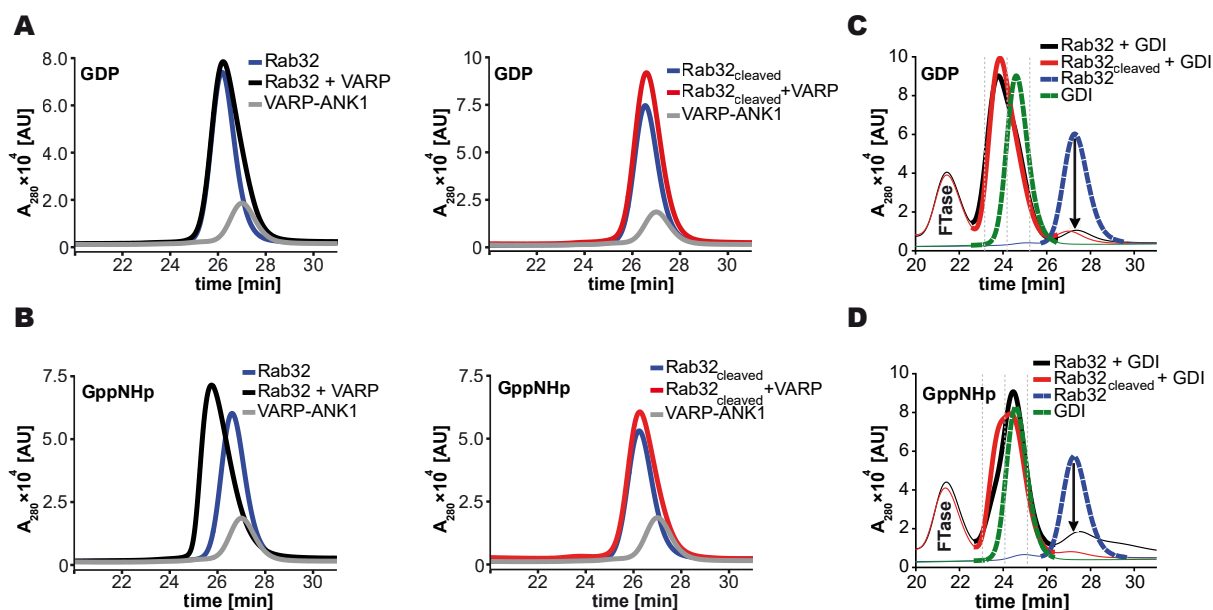
Figure 19 | Binding of Rab32 with its physiological interaction partners is selectively impaired by the proteolytic modification[e]. *To investigate the interaction of Rab32 with other proteins, aSEC measurements were performed during which the intensity at 280 nm was monitored, and the resulting peaks were deconvolved into the individual species. **(A)** Left: aSEC measurements of Rab32:GDP in the presence of VARP. VARP-ANK1 does not bind Rab32:GDP in vitro. Rab32 (50 μM) was preparatively loaded with GDP (98%) and equilibrated for complex formation with 50 μM VARP-ANK1 for 1 h at 15°C. Subsequently, 50 μl were chromatographically separated via aSEC. The individual runs of single proteins serve as a reference. Right: aSEC measurements of cleaved Rab32:GDP in the presence of VARP. Cleaved Rab32:GDP also does not form a complex with VARP-ANK1. **(B)** Left: Complex formation between active Rab32 and VARP-ANK1 investigated using aSEC. The analysis corresponds to that used in panel A starting with Rab32:GppNHp (90% loaded). Here, a clear complex formation is observed. Right: aSEC measurement of the interaction between cleaved Rab32:GppNHp and VARP-ANK1. Cleavage of Rab32 impairs the complex formation between Rab32 and VARP-ANK1. **(C)** aSEC measurements of the interaction of Rab32:GDP with GDI in the non-modified and cleaved state. Inactive Rab32 (100% loaded with GDP) binds GDI regardless of its modification state. **(D)** aSEC measurements of the interaction of Rab32:GppNHp with GDI in the non-modified and cleaved state. Rab32cleaved:GppNHp can more efficiently form a complex with GDI in comparison to the non-modified Rab32. This can be clearly seen in the reduction of the Rab32 only peak for Rab32cleaved:GppNHp in comparison to Rab32:GppNHp (arrow). 30 μM of B12 was used as an intern standard for each aSEC run. The figure was reprinted with permission from Savitskiy et al, 2020 [248]. Copyright (2020) Elsevier.*

3.2.3 GtgE-mediated cleavage destabilizes switch I and indirectly impacts switch II of Rab32

Next, it was decided to examine the impact of the GtgE-mediated proteolysis of the switch I of Rab32 on the conformations of both switch regions of the protein. For this purpose, a single-pair FRET (spFRET) was employed, which detects distance variations between the two fluorophores. This method suits ideally for the determination of conformational changes within disordered protein regions [253]. In order to enable labeling with fluorescent dyes, several pairs of Cys substitutions were strategically positioned within Rab32, thereby providing labeling sites for fluorophores. Given that Rab32 is a small protein, an attempt was made to maximize the distances between the labeling positions on the static portion of the protein (Q160C or S156C) and a potentially dynamic counterpart in either switch I (R55C) or switch II (N90C) region of the protein (Figure S7). Subsequently, spFRET suitable fluorophores (Alexa488-maleimide, Alexa647-maleimide) bearing a maleimide moiety were covalently coupled to Cys-containing

---

[e] Data showed in **(A)** and **(B)** were generated by Dr. Rudolf Wachtel [163].

Rab32$_{R55C/Q160C}$ or Rab32$_{N90C/S156C}$ constructs ([Figure 20A, left](#)). In order to avoid off-target labeling, intrinsic Cys residues (C145, C162) were mutated to Ser. The identity of the purified double mutants was confirmed via intact mass spectrometry ([Figure S8](#)). The coupled fluorophores contained flexible linkers, allowing free rotation while increasing the volume in which the dye molecule can be located ([Table S1](#)). The presence of fluorescent dyes on the analyzed Rab32 mutants were confirmed via in-gel fluorescence ([Figure S9](#)). Additionally, the accessible volume calculations were performed, estimating the possible locations of the fluorophore based on its size and the dimensions of the linker, in order to visualize the spatial distribution of the possible locations of the fluorescent dye [254]. Figure 20A presents the accessible volume calculations for both Rab32 double mutants. The main goal of spFRET experiments was the detection of conformational changes after GtgE-mediated proteolysis of switch I in Rab32 between G59 and V60. Thus, pure cleaved Rab32 variants were produced and subsequently submitted for fluorophore labeling and spFRET measurements ([Figure 20B](#)). The proteolytic modification of Rab32$_{R55C/Q160C}$ labeled in the switch I generated two species with equal contributions of 50% after peak decomposition ([Figure 20C](#)). Whereas the distance of the first species corresponded to non-modified Rab32, the distance of the second species between the fluorophores after cleavage is increased by 8.6 Å ([Figure 20C](#)). In the case of the Rab32$_{N90C/S156C}$ labeled in switch II, only minor changes were observed. Thus, the cleavage reduced the distance between the fluorophores by ~2 Å ([Figure 20D](#)).

In summary, spFRET data indicate a strong destabilization of the switch I region as well as an indirect minor influence on switch II of Rab32 caused by the GtgE-mediated proteolysis.
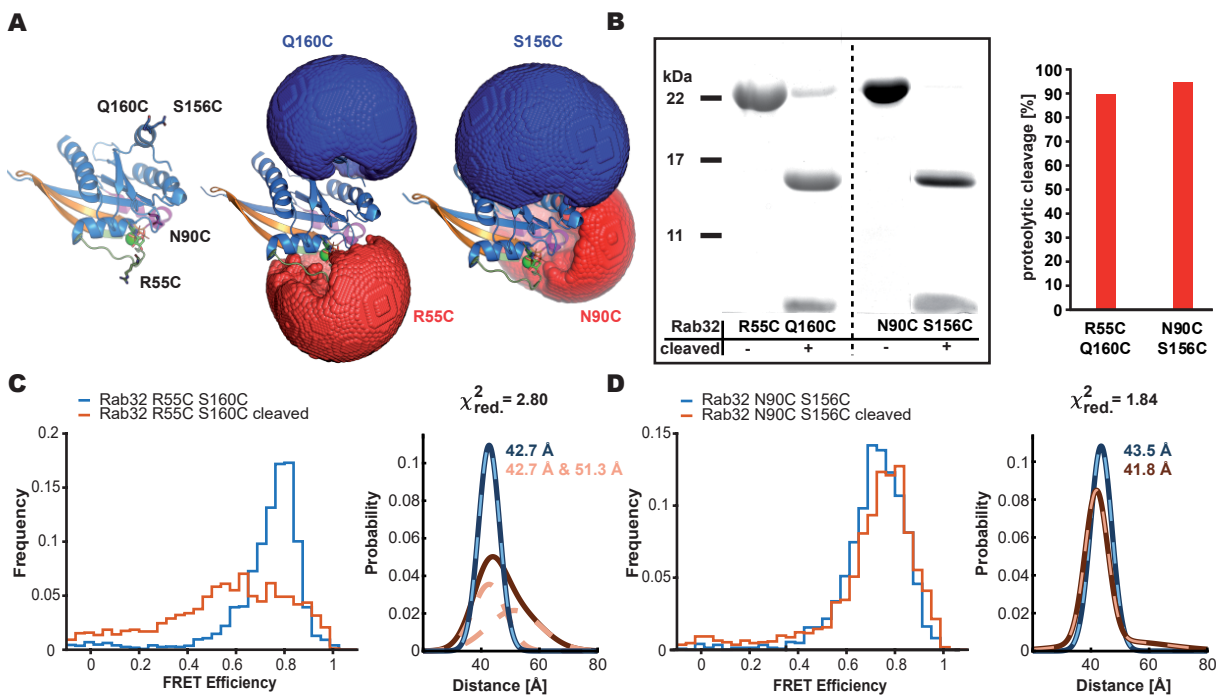
Figure 20 | Single-pair FRET reveals changes in the conformation of Rab32 upon proteolytic modification. (A) *Position of Cys mutations within the Rab32 for covalent fluorophore linkage. Left: Ribbon structure representation of*

*Rab32 where the selected amino acid positions for protein labeling with FRET pairs are shown as sticks. Middle and right: Visualization of the accessible volume calculations for Rab32_{R55C Q160C} and Rab32_{N90C S156C} double mutants, respectively. The Rab32 structure used for the current representation is deposited in PDB under ID 6FF8 [91]. **(B)** Quantification of cleavage efficiency for spFRET. Rab32 mutants. Left: Rab32:GDP mutants were proteolytically cleaved and run on an SDS-PAGE gel. Right: Densitometric quantification of the gel bands for modification completion in both double mutants plotted in a bar graph. **(C)** SpFRET histograms for the non-modified and cleaved Rab32_{R55C Q160C} mutant revealing a change in distance between fluorophores upon cleavage. The distances calculated using the probability distribution analysis approach are indicated. Orange dashed lines show the decomposed peak after proteolysis with two equally populated species. **(D)** SpFRET histograms for the non-modified and cleaved Rab32_{N90C S156C} mutant. Cleavage of switch I lead to minor distance differences in the switch II region of the protein. All calculated distances represent the separation of the fluorophores, which are attached to the protein via flexible linkers. FRET data were generated and processed by Vanessa Trauschke (the group of Prof. Don C. Lamb, LMU). The figure was reprinted with permission from Savitskiy et al, 2020 [248]. Copyright (2020) Elsevier.*

### 3.2.4 Rab32_{cleaved}:GppNHp exhibits structural similarities with its GDP state

In order to understand the structural consequences of GtgE-mediated proteolysis of Rab32 better, nuclear magnetic resonance (NMR) studies were conducted (Figure 21, Figure S11). To this end, the effects of Rab32 proteolysis in the presence of different nucleotides (GDP, GppNHp) were identified by collecting and comparing ^{1}H, ^{15}N heteronuclear single quantum correlation (HSQC) NMR spectra of the four states (schematics in Figure 21B). Preliminary HSQC NMR spectra of Rab32_{wt} revealed a big area of signals belonging probably to unstructured parts (N- and C-termini) of the Rab protein around ^{1}H/^{15}N: 8/120 ppm (Figure S10). Therefore, it was decided to truncate Rab32 N- and C-terminally, to remove flexible parts of it, and to possibly reduce overlapping signals in the indicated ppm area. Indeed, the truncated Rab32₂₀₋₂₀₁ displayed a much clearer spectrum in contrast to the Rab32_{wt} (Figure S10). Thus, further experiments were conducted with the truncated version of Rab32.

First, the exchange of GDP to GppNHp (non-hydrolyzable GTP analog) in Rab32 displayed significant spectral differences, whereas most signals were shifted or broadened in the GppNHp state, which represents the GTP-bound form (Figure 21A, black vs green). Thus, it can be assumed that the transition to the active state upon GTP binding is not limited to local changes in the switch regions of Rab32, but rather results in more global conformational changes in the protein. Next, the GtgE-mediated cleavage of Rab32 in the presence of GDP or GppNHp was examined. After the Rab32:GDP is cleaved, a handful of NMR signals were clearly shifted or broadened (Figure 21A, black vs red), probably corresponding to the residues vicinal to the cleavage site in the switch I region. On the contrary, nearly no spectral changes were observed for Rab32:GppNHp after the addition of a catalytic amount of GtgE (Figure S11). This demonstrates that the nucleotide exchange to GppNHp was complete and confirms GtgE preference to interact with inactive Rab32 [164]. In the last step, the effect of GppNHp-binding to the cleaved Rab32:GDP (Rab32_{cleaved}:GppNHp) was investigated. Spectral changes indicated a nucleotide exchange from GDP to GppNHp for cleaved Rab32, but, most of the signals did not reach the fully active GppNHp-bound state – rather, they appeared between the two states and closer to the GDP-bound state (Figure 21B). In short, the comparisons of NMR spectra indicated that (i) GppNHp-binding triggers conformational changes beyond the switch regions and protects the switch I region from

proteolysis, and that (ii) GtgE-mediated proteolysis results in local changes in the protein structure, which subsequently lock Rab32 in an inactive-like conformational state despite its nucleotide state.
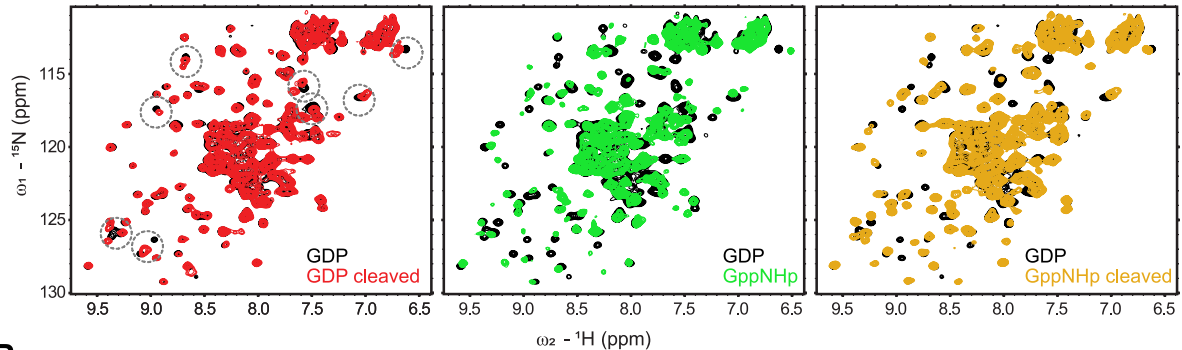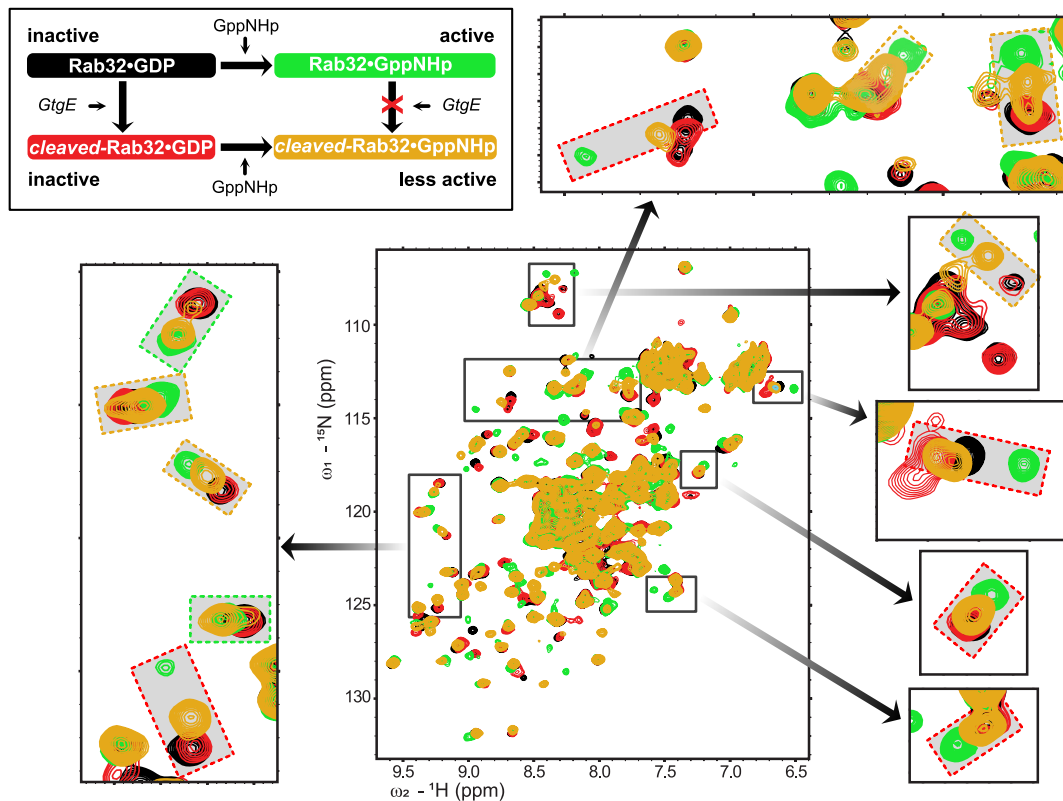
Figure 21 | NMR analysis of structural effects of proteolysis and nucleotide binding on Rab32. *(A) Superposition of ^1H, ^{15}N NMR correlation spectra of ^{15}N-labeled Rab32 with GDP (black) or GppNHp (green) and their cleaved states (red and orange, respectively) by GtgE. Note that the cleaved Rab32:GppNHp (orange) has been produced by proteolysis of Rab32:GDP followed by the addition of GppNHp. Specific spectral changes of GDP state upon cleavage are shown with dashed circles. **(B)** Summary of the states of Rab32 used for NMR analysis. Spectral overlays of the four states indicate that the NMR signals of the cleaved GppNHp-bound state (orange) generally are intermediate between the GppNHp-bound active (green) and GDP-bound (black) state, closer to the inactive state (grey boxes). Proteins and sample sets for NMR were produced by the author. Data were recorded and processed by Dr. Hyun-Seo Kang (the group of Prof. Michael Sattler, TUM). The figure was reprinted with permission from Savitskiy et al, 2020 [248]. Copyright (2020) Elsevier.*

3.2.5 GtgE-mediated cleavage destabilizes the switch regions and disrupts the interswitch region of Rab32

Additionally, molecular dynamics (MD) simulations on cleaved and uncleaved Rab32 in both activity states were performed. MD simulations are used as a complementary approach for gaining

further insights into the stability and time scale of dynamic changes in both switch regions upon the proteolytic modification. Furthermore, MD simulations can provide additional structural clarity around the impaired binding between the VARP-ANK1 domain and Rab32$_{cleaved}$:GppNHp. Rab32 either as an intact protein chain or cleaved between G59 and V60 in the active GTPase conformation with either a bound GDP or GTP served as a starting point for the simulations (for more details see section 6.6 Analytical methods). In the presence of GDP, proteolytic modification leads to a drastically increased root-mean-square deviation (RMSD) of both of the switch regions in the inactive state of Rab32 relative to the uncleaved state of it, indicating destabilization (Figure 22A). The sampling of conformations for the switch I and switch II regions deviating from the initial structures by ~16 Å and ~5 Å, respectively, are shown by distributions of the RMSD values (Figure 22A, B right). Subsequent simulations in the presence of bound GTP revealed that GTP binding was not sufficient to maintain the stability and structure of switch I in the cleaved form (Figure 22B, left). Similarly, the RMSD plot in the cleaved state indicated that switch I had higher flexibility compared to its uncleaved state reaching an RMSD value of around 4 Å (Figure 22B, right). That said, on the time scale of the simulations no differences in the flexibility of switch II in the case of the cleaved vs. uncleaved Rab32 with bound GTP were observed (Figure 22B, right). In fact, the simulations indicated that proteolysis of Rab32 disrupted the interswitch region of Rab32 independently of its nucleotide bound state (Figure 22C and D, left and middle). This disruption appeared after 500 ns of simulation and lead to the structural degradation of the β2 strand. Moreover, the antiparallel β-sheet strands β2 and β3 drifted apart during the simulation (Figure 22C, D middle). In order to characterize this process better, two pairs of C$_\alpha$-atoms were selected, one from V60&F62 and one from W80&I82, and the changes in the distances between the centers of mass (COM) of these two pairs were monitored over time. These residues belong to the β2 and β3 strands, which were expected to be stable in the uncleaved state, but dynamic after proteolytic modification. While the uncleaved Rab32 variants displayed no significant differences during the simulation, the distances between COM of the chosen pairs (V60&F62 and W80&I82) increased drastically in the cleaved structures, accompanied by the dissociation of the β2 strand. This was observed for both GDP- and GTP-bound Rab32 (Figure 22C and D, right). Noteworthy, the dissociation of β2 does not take place at the very beginning of the simulation. Thus, two species can be distinguished: intact β2 and dissociated β2 (Figure 22 C, two broad orange peaks on the density chart). Both species occur with a probability of approximately 50 %. Therefore, it can be suggested that NMR data reflect either the intact or slightly disordered β2 since the spectrum of cleaved Rab32 does not show any dramatic changes in comparison to its uncleaved version.

Thus, consistent with spFRET data, MD simulations demonstrate that proteolysis significantly destabilizes switch I as well as slightly impacts switch II. Furthermore, upon proteolysis, the interswitch region of Rab32 is drastically disordered regardless of its activity state. Since both of

the switches and the interswitch region reside at the interface in the complex with the VARP-ANK1 domain, disturbances of these structural regions caused by proteolysis explain the reduced interaction of cleaved Rab32 with VARP-ANK1.
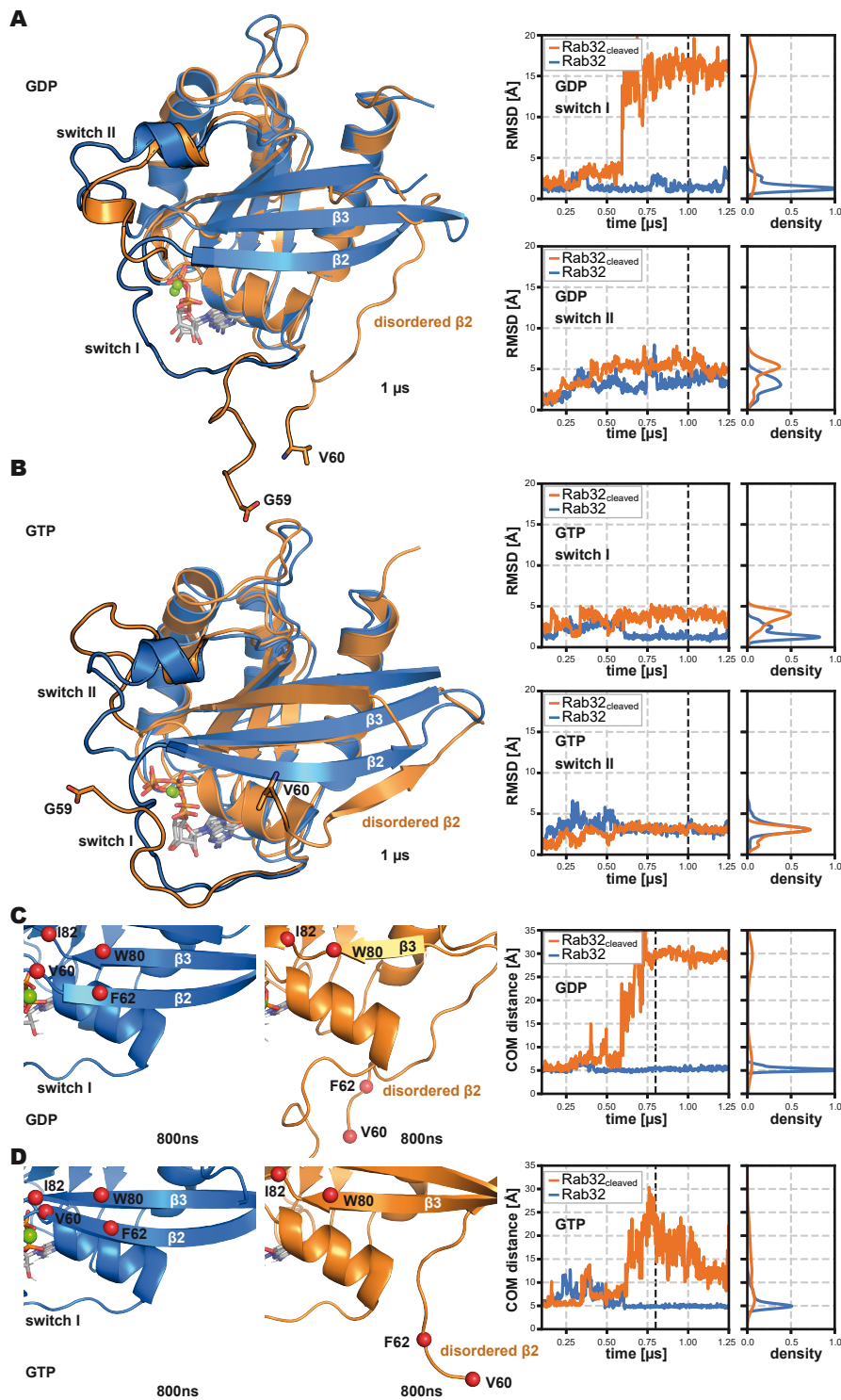
***Figure 22 | Cleavage-induced flexibility in the switch I promotes the unfolding of the β2-strand in the interswitch region of Rab32 (revealed by molecular dynamics simulations). (A)** Left: Superimposed MD simulated structures of Rab32:GDP (blue) and Rab32cleaved:GDP (orange, the disordered β2-strand is indicated) after 1 μs of MD simulations. The switch regions are highlighted with a black stroke. Right panels: RMSD vs. simulation time for switch I and II regions of Rab32:GDP and Rab32cleaved:GDP. The black dashed lines indicate the sampling time of the corresponding snapshots shown on the right.* **(B)** *Superimposed MD simulated structures of Rab32:GTP (blue) and Rab32cleaved:GTP (orange) after 1 μs. Right panels: same as in (A) for the Rab32:GTP and Rab32cleaved:GTP.* **(C)** *Left and middle: The interswitch region of*

*Rab32:GDP (blue) and Rab32$_{cleaved}$:GDP (orange) presents the β2 strand at 800 ns of the MD simulation with a large change of the COM (center-of-mass) distances of V60 & F62 and W80 & I82 in the cleaved vs. uncleaved states. Red spheres indicate the C$_α$-atoms of the amino acids V60, F62, W80, and I82. Right: V60 & F62 - W80 & I82 COM distances vs. simulation time. The point of 800 ns, indicated by the black dashed line, highlights the time point of the snapshots shown in the left and middle panels. **(D)** Same as in (C) but for the Rab32$_{cleaved}$:GTP vs. Rab32:GTP case. Data generated and processed by Danial P. J. Dehkordi (the group of Prof. Martin Zacharias, TUM). The figure was reprinted with permission from Savitskiy et al, 2020 [248]. Copyright (2020) Elsevier.*

3.3 Effects of RRSP-mediated proteolysis of Ras

In order to investigate the effects caused by RRSP-mediated proteolysis on Ras isoforms, the complex formation between Ras and its genuine binding effectors cRaf and RalGDS was investigated. First, the native PAGE of single proteins as well as their complexes in the absence and presence of RRSP was performed. Subsequently, the migration patterns of proteins were analyzed. Preincubation of HRas with the RRSP resulted in the disappearance of the band present in not proteolyzed HRas (GppNHp loaded) and cRaf, indicating that the proteolysis of the switch I region prevents the interaction between HRas and cRaf (Figure 23A). This observation is in line with recent publications [161,213]. Co-incubation of HRas and RalGDS did not result in a clearly defined complex band like in HRas:cRaf case. Only smears (blurry bands) between both proteins were observed, which were reduced upon HRas proteolysis (Figure 23A). Next, the same experimental setup for HRas, RalGDS, and its mutant was analyzed via aSEC. Since wt RalGDS showed just a minor reduction of elution time, it was decided to introduce a point mutation N54R in order to increase the affinity between the proteins, like it was achieved in the Ras:RalGDS complex by E31K mutation in Ras [255]. In contrast to the approach applied by Huang and colleagues, the mutation in RalGDS does not alter proteolysis of HRas by RRSP: The E31K mutation in Ras may impair the RRSP-mediated proteolysis due to proximity of the mutated residue to the cleavage site between Y32 and D33 in Ras. The selection of the position for the site-directed mutagenesis was based on the analysis of available complex crystal structures of Ras/Rap1 and its effectors (Figure 23B). Indeed, RalGDS$_{N54R}$ formed a complex with HRas indicated by decreased elution time. However, the presence of RRSP impaired complex formation between HRas$_{cleaved}$ and RalGDS as indicated by elution time identical to the individual proteins. RalGDS$_{wt}$ and RalGDS$_{N54R}$ did not produce a complex, suggesting that the complex between HRas and RalGDS variants is sensitive to RRSP-mediated proteolysis. (Figure 23C, D).

Next, the structural consequences of RRSP-mediated proteolytic modification of Ras were addressed. For this purpose, a ^{15}N labeled KRas was produced and the ^{1}H^{15}N HSQC spectra of KRas in non-modified and proteolytically modified states were collected. The recorded spectra of cleaved species display dramatic global conformational changes upon proteolysis in comparison to the uncleaved ones. The resulted patterns of the collected spectra and the observed spectral changes caused by RRSP-mediated proteolysis recapitulate the data reported by the Satchell laboratory (Figure 23E) [161]. It has been shown, that RRSP-mediated cleavage affects drastically not only the switch regions but also α2 and β2 substructures of KRas [161]. Additionally, KRas$_{cleaved}$

shows slight structural alterations in the β1 [161]. Since this research topic was investigated and reported by two independent laboratories, it was decided to stop further investigations on it. Taken together, these analyses suggest that RRSP-mediated cleavage of Ras provokes global structural changes in Ras and impairs int binding to the cRaf and RalGDS.
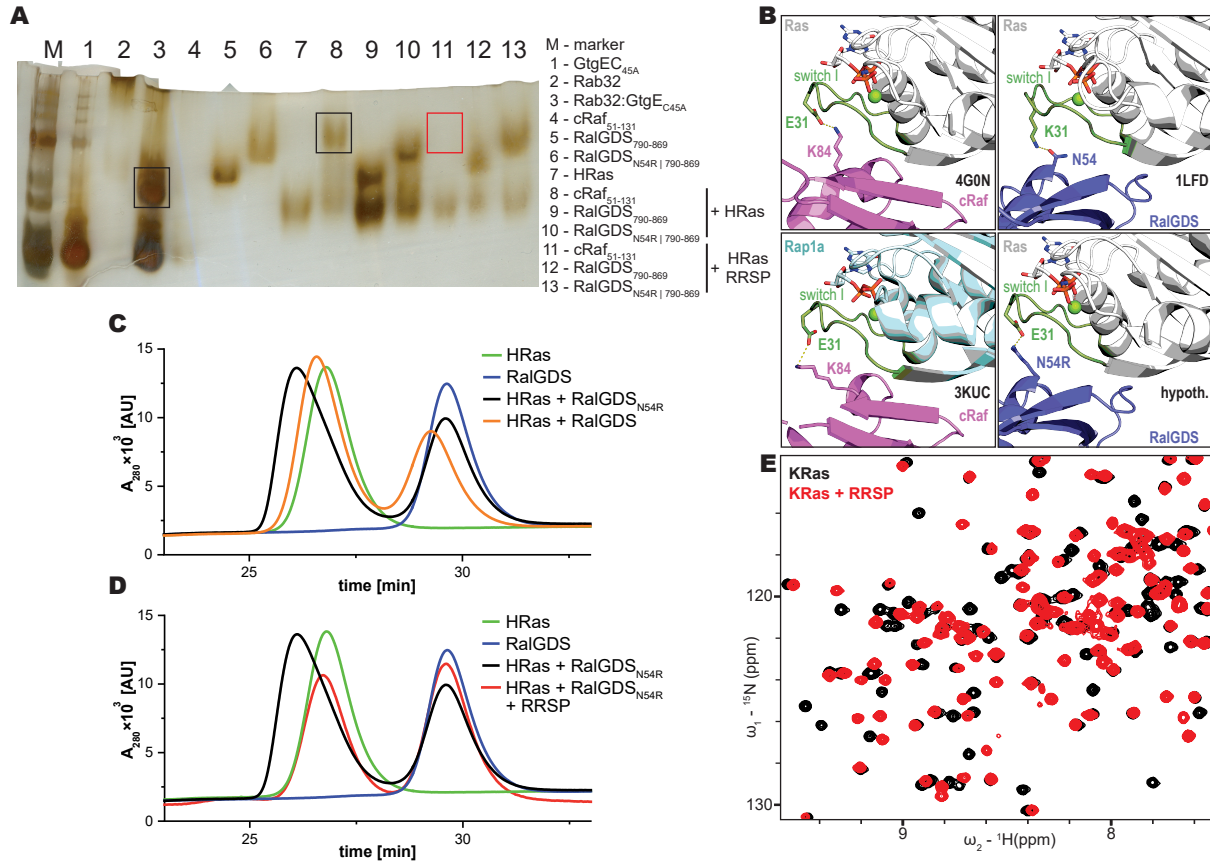
Figure 23 | Effects of RRSP-mediated proteolysis of Ras. (A) *Native PAGE gel (pH 8.5) demonstrates a complex formation between HRas and cRaf (lane 8, black box), which disappears upon RRSP-mediated cleavage of HRas (lane 11, red box). Lanes 9 and 10 show smearing signals, which are reduced in the presence of RRSP in the solution (lanes 12 and 13). Rab32:GtgE$_{C45A}$ was used as a positive control. PI values of proteins: 7,40 (Rab32 $_{20-201}$), 5,04 (HRas), 9,72 (cRaf$_{51-131}$), 5,06 (RalGDS$_{790-869}$), 5,63 (RalGDS$_{N54R | 790-869}$), 5,46 (RRSP), 4,34 (GtgE$_{C45A}$).* **(B)** *Overview of available complex crystal structures (PDB IDs are indicated black) [255–257] used for the generation of RalGDS$_{N54K}$ mutant (hypoth.).* **(C)** *Complex formation between active HRas and RalGDS as well as RalGDS$_{N54R}$ investigated using aSEC. A stable complex between HRas and both RalGDS variants could be formed. Noteworthy, the mutated RalGDS displays reduced elution time indicating the increased binding abilities between both proteins.* **(D)** *The analysis corresponds to panel A. RRSP-mediated cleavage abolishes the binding of HRas to its mutated effector RalGDS$_{N54R}$.* **(E)** *$^1H^{15}N$ HSQC of KRas in cleaved and not cleaved states. NMR data were recorded and processed by Dr. Hyun-Seo Kang (the group of Prof. Michael Sattler, TUM).*

3.4 Identification and validation of SopD targets
3.4.1 A yeast two-hybrid screen suggests Rab proteins as SopD targets

In order to identify the putative targets of SopD, it was decided to screen a library of 46 small GTPases using a yeast two-hybrid (Y2H) assay for interaction with SopD (Figure 24A) [2]. The used library was kindly provided by the laboratory of Bruno Goud (Institut Curie, Paris). Since SopD2's catalytic arginine is located at its C-terminus (Figure 25) [146], SopD gene was cloned into the pGAD-HA vector as prey with the GAL4 activation domain (AD) at its N-terminus leaving the C-terminus free for possible interactions with GTPases. If the proteins bearing AD and DNA binding domain (BD) interact, it results in the activation of the reporter gene HIS3 enabling the histidine biosynthesis and survival of the yeast on the selective agar lacking histidine. Thus, yeast colonies on the selection agar indicate the interaction between the proteins present on the transformed plasmids in the yeast [258,259]. The Y2H screen revealed 11 putative interaction partners of SopD: Homologs of Rab3 (Rab3a-d) and Rab8 (Rab8a+b) as well as Rab10, Rab14, Rab29, Rab30, and Rab32 (Figure 24A). Five of those targets – Rab3d, Rab8a, Rab8b, Rab10, and Rab14 – were confirmed with a Y2H replicate focusing on the putative SopD targets (Figure 24B).
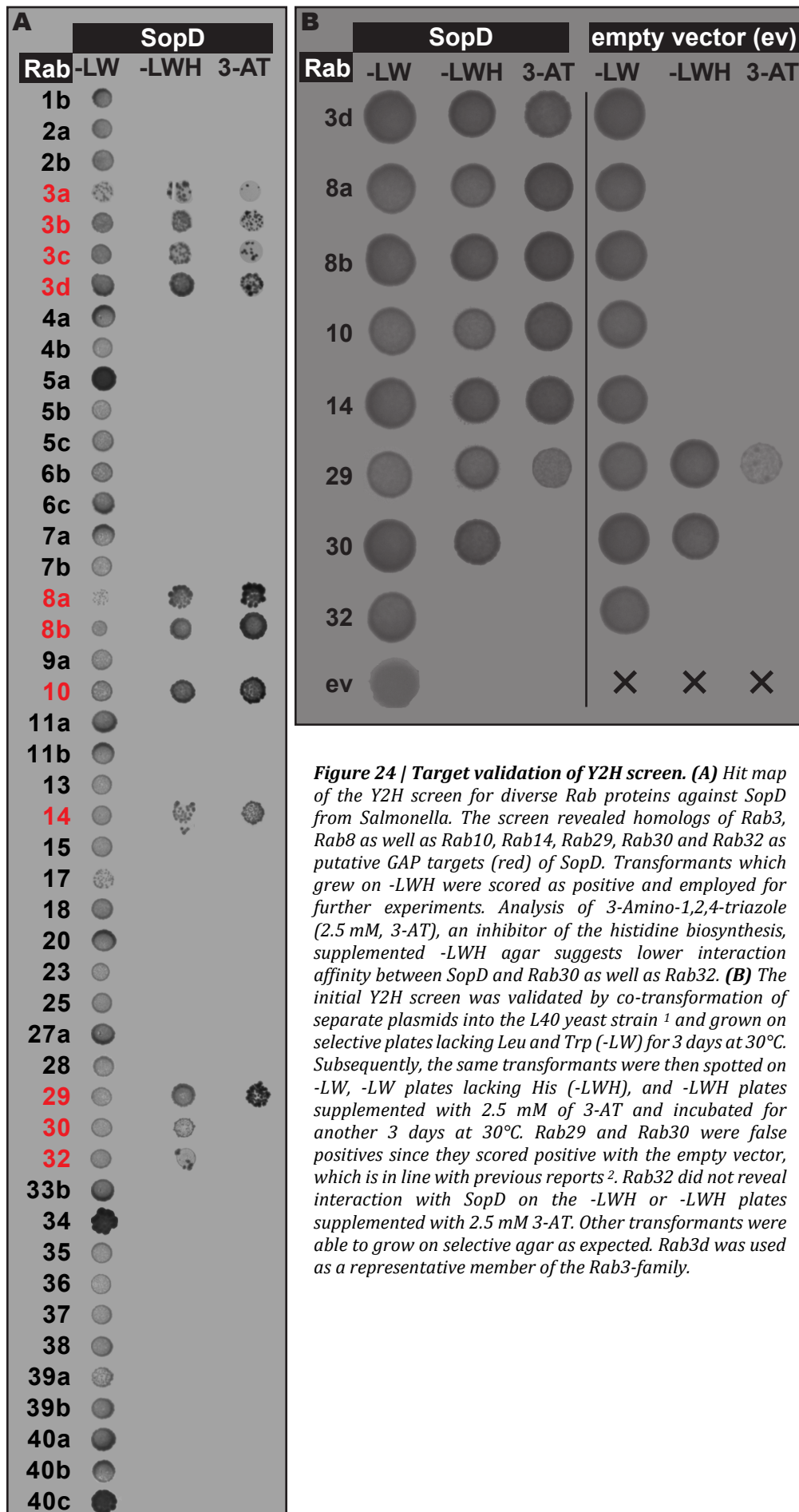
Figure 24 | Target validation of Y2H screen. (A) *Hit map of the Y2H screen for diverse Rab proteins against SopD from Salmonella. The screen revealed homologs of Rab3, Rab8 as well as Rab10, Rab14, Rab29, Rab30 and Rab32 as putative GAP targets (red) of SopD. Transformants which grew on -LWH were scored as positive and employed for further experiments. Analysis of 3-Amino-1,2,4-triazole (2.5 mM, 3-AT), an inhibitor of the histidine biosynthesis, supplemented -LWH agar suggests lower interaction affinity between SopD and Rab30 as well as Rab32.* **(B)** *The initial Y2H screen was validated by co-transformation of separate plasmids into the L40 yeast strain [1] and grown on selective plates lacking Leu and Trp (-LW) for 3 days at 30°C. Subsequently, the same transformants were then spotted on -LW, -LW plates lacking His (-LWH), and -LWH plates supplemented with 2.5 mM of 3-AT and incubated for another 3 days at 30°C. Rab29 and Rab30 were false positives since they scored positive with the empty vector, which is in line with previous reports [2]. Rab32 did not reveal interaction with SopD on the -LWH or -LWH plates supplemented with 2.5 mM 3-AT. Other transformants were able to grow on selective agar as expected. Rab3d was used as a representative member of the Rab3-family.*

3.4.2 SopD specifically targets Rab8

In order to exclude possible Y2H false positives, the putative SopD targets were validated independently *in vitro.* For this purpose, recombinantly expressed and purified proteins were used. Incubation of catalytic amounts of SopD (1 µM) with GTP-loaded Rabs (50 µM) and subsequent GTP quantification via reversed-phase high-performance liquid chromatography (RP-HPLC) revealed Rab8a as its preferable target *in vitro* since GTP-hydrolysis is stimulated 16-fold under the given conditions (Figure 26A) [164]. To a lower extent, SopD has an impact on the GTP-hydrolysis of Rab10, but none of the other putative Rabs were susceptible to SopD (Figure 26A). Since SopD is specifically stimulating GTP-hydrolysis in only two Rab proteins, it was verified whether SopD2 is also targeting the Rab32-homologs Rab29 and Rab38. Therefore, the same HPLC-supported experimental setup as for SopD was chosen. Consistent with previous studies, the incubation of diverse Rab GTPases with SopD2 showed that SopD2 has minor GAP activity towards Rab8a and Rab10 (Figure 26B) [146]. Additionally, SopD2 also targets Rab32-homologs Rab29 and Rab38. Rab1b and Cdc42 were chosen as negative controls. Surprisingly, SopD2 has a negligible effect on the GTP-hydrolysis in Rab1b (Figure 26B).
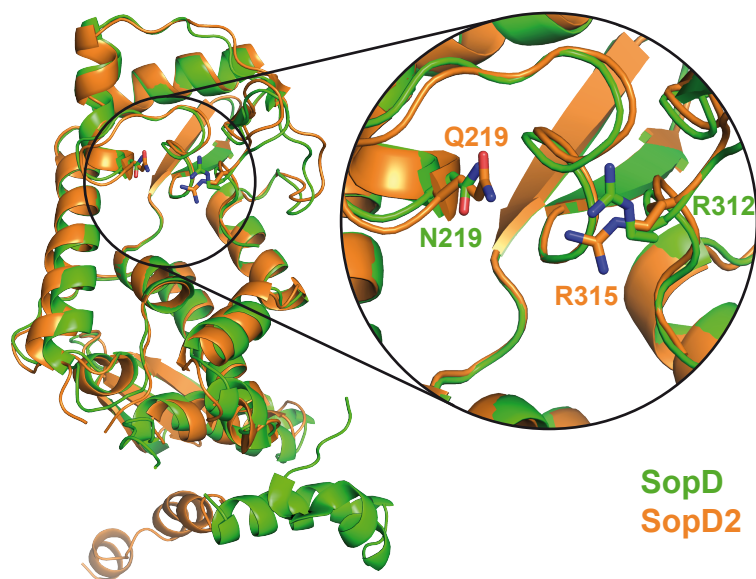
Figure 25 | *Superimposed crystal structures of SopD (PDB ID: 5CPC) in green and SopD2 (PDB ID:5CQ9) in orange with suggested catalytic residues showed with sticks* [200]

Next, it was presumed that SopD might share the catalytic mechanism with its homolog SopD2. Previously, R315 of SopD2 was reported to be important for the GTP-hydrolysis [146]. R312 in SopD is homologous in position and sequence to R315 of SopD2 (Figure 25). Therefore, the impact of an R312A$_{SopD}$ substitution for Rab8a:GTP hydrolysis was evaluated. Moreover, it was investigated whether further amino acid residues in SopD are relevant for its activity. Since the catalytic site for GAP-mediated activity is typically represented by a pair of Gln/Arg or possibly by Asn/Arg, Gln and Asn residues were screened in the SopD structure using alanine substitutions. To reduce the effort of the mutagenesis study, the following selection criteria were used: the close structural proximity of the second catalytic residue to R312 and its location in the same possible interaction

surface with Rab. Thus, N219 was selected first as a possible complementary partner of R312 (Figure 25). Indeed, SopD$_{R312A}$ or SopD$_{N219A}$ did not confer GAP-activity towards Rab8 (Figure 26C).

Since GAPs with two catalytic residues are able to catalyze GTP-hydrolysis even in the constitutively active, hydrolytically deficient Rabs [260], an experiment with a constitutively active Rab32$_{Q85A}$ mutant was set up and GAP activity of SopD2 towards it was tested. The Gln residue in the G3 motif of Rab proteins is typically responsible for their GTPase activity [3]. Surprisingly, SopD2 was not able to stimulate GTP hydrolysis in Rab32$_{Q85A}$ (Figure 26D, E). Moreover, inactivating point mutations (N219A or R312A) in SopD do not impact the interaction with its target Rab8a (Figure S12). Interestingly, the deletion of 76 N-terminal aa in SopD$_{77-317}$ and SopD2$_{77-319}$ reduced the GTP hydrolysis compared to the wild type (Figure S13). Thus, SopD and SopD2 require both residues (N219/R312 and Q219/R315 respectively) together with the catalytic Gln of Rab protein to achieve successful and efficient Rab inactivation.
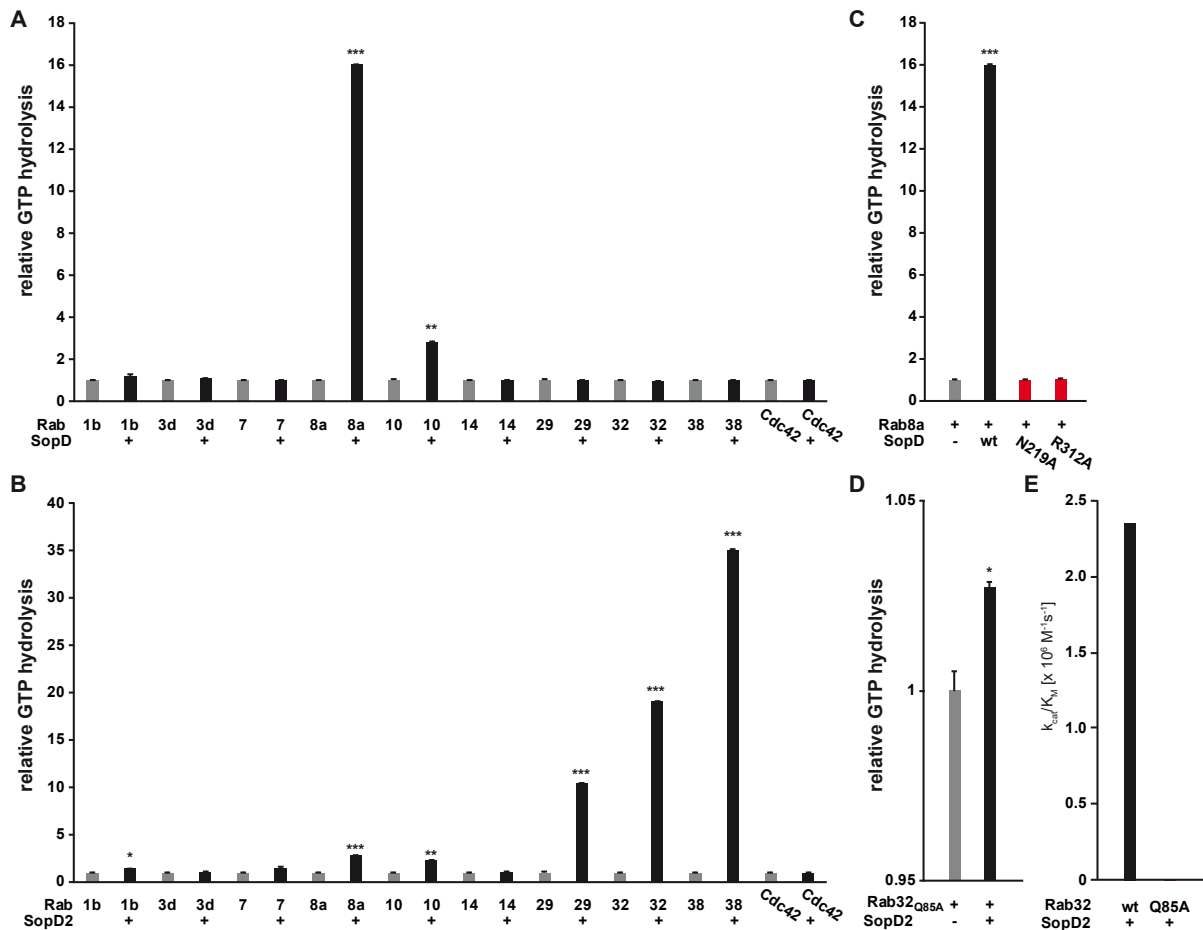
Figure 26 | In vitro validation of putative SopD targets. (A) *Recombinantly expressed and purified Rab GTPases were loaded with GTP and incubated for 30 minutes with SopD at room temperature (50:1 molar ratio). The reactions were stopped by heat denaturation (95℃) for five minutes; reaction mixtures were cleared by centrifugation at 4℃ for five minutes at 21000 g. Resulting supernatants were used for analysis on a reversed-phase HPLC (RP-HPLC). The integration of corresponding GTP and GDP peaks provided values for further verification of GTP hydrolysis. Data were normalized for each Rab protein to its intrinsic GTP hydrolysis (n=3 ± SEM; paired Student's t-test: p<0.01 ≙ **, p<0.0001 ≙ ***). (B) Same like in A but for SopD2 (n=3 ± SEM; paired Student's t-test: p<0.05 ≙ *, p<0.01 ≙ **, p<0.0001 ≙ ***). (C) Incubation of Rab8a with N219A or R312A point mutants (red) of SopD shows no increase in GTP hydrolysis (n=3 ± SEM; paired Student's t-test: p<0.01 ≙ **, p<0.0001 ≙ ***). (D) GAP activity of SopD2 towards constitutively active Rab32 mutant is negligible.*

(E) The Gln of Rab32 is important for SopD2-mediated GTP hydrolysis. Catalytic efficiencies (k_{cat}/K_M) of SopD2 towards Rab32 and its constitutive active mutant Rab32$_{Q85A}$ are represented as a bar chart.

3.4.3 SopD and SopD2 are catalytically efficient RabGAPs

Next, the catalytic efficiencies of SopD and SopD2 towards their targets were determined and compared. For this purpose, GTP loaded Rab proteins were incubated at room temperature over time in presence of an appropriate GAP, and the progress of the GTP hydrolysis was stopped at distinct time points by the heat denaturation. Resulted mixtures were cleared from precipitated proteins by centrifugation and the nucleotides containing supernatants were analyzed via RP-HPLC (for detailed method and validation see chapter 6.6 Analytical methods). Validation of GDP/GTP loading of Rab8a in the presence of SopD resulted in an exponential reduction of GTP in time and provided the catalytic efficiency value (k_{cat}/K_M) of $(2.3 \pm 0.5) \times 10^6$ M^{-1}s^{-1} (Figure 27A). SopD2 showed similar catalytic efficiency of $(2.3 \pm 0.2) \times 10^6$ M^{-1}s^{-1} towards Rab32 (Figure 27B). However, the stronger observed effect of SopD2 on Rab38 during *in vitro* validation raised the interest to it. Thus, it was investigated whether SopD2 facilitates GTP hydrolysis in Rab38 more efficiently. Indeed, SopD2 demonstrated a 2-fold higher k_{cat}/K_M value of $(5.0 \pm 0.5) \times 10^6$ M^{-1}s^{-1} for Rab38 than for Rab32 (Figure 27C).

In conclusion, SopD represents a specific GAP against Rab8, which is not typical for other known RabGAPs with multiple targets [3,260].
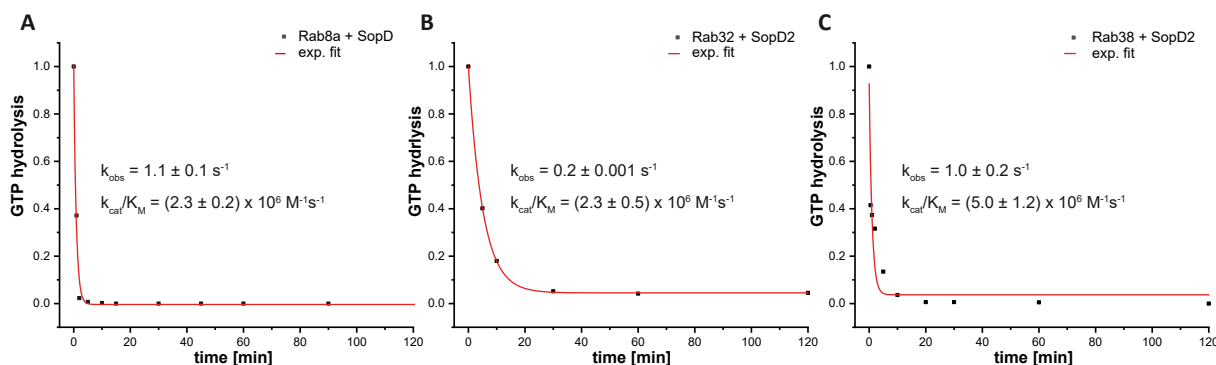
Figure 27 | Validation of catalytic efficiencies of SopD and SopD2. (A) GTP loaded Rab8a was incubated with catalytic amounts (500nM) of SopD with subsequent reaction stops at different time points by heat (95°C). Resulted mixtures were treated like in in vitro validation and analyzed via RP-HPLC. The starting point was normalized to the GTP amount in Rab protein at the time point 0 of the reaction. Data points were fitted to a single exponential function. (B) and (C) Same as in (A) but with Rab32 and SopD2 (85nM) or Rab38 and SopD2 (200nM), respectively. All data represent the mean of 2-3 independent experiments with ± SEM.

3.4.4. Rab:GAP complex crystallization attempts

In order to understand the GAP mechanisms of SopD and SopD2 on a molecular level, multiple crystallization setups of Rab proteins with their GAPs were tried out. Crystallization of a stable complex between a GAP and its substrate provides insights into the mechanistic details of GTP hydrolysis by resolving e.g. the orientation of both proteins to each other, positioning of catalytic residues, the role of other aa residues contributing to the complex formation[23]. Therefore, a crystallographic approach is an appropriate tool for the determination of mechanisms of

enzymatically supported hydrolysis reactions. First, attempts were made to obtain a complex between Rab8 and SopD via aSEC. However, neither the preincubation of Rab8:GDP with SopD in the presence of AlF$_4^-$ (AlCl$_3$+NaF) nor the GppNHp-loaded Rab8 and SopD provided a stable complex that should elute before SopD alone (Figure 28A, B). Additionally, co-crystallizations of Rab8 with SopD and Rab32 with SopD2 at protein concentrations over 10 mg/ml were conducted. Only the co-crystallization of Rab32 with N-terminally truncated SopD2 (the N-terminal flexible region of the protein was removed) resulted in rectangular crystals (Figure 28C). Unfortunately, the grown crystals did not diffract and could not deliver any usable data.
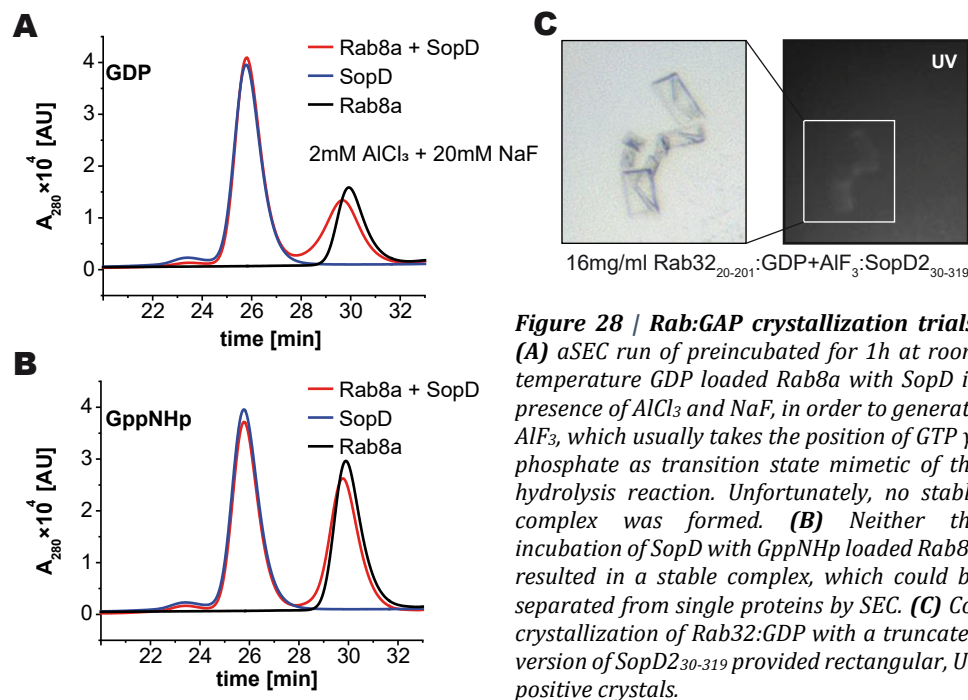
Figure 28 | Rab:GAP crystallization trials. **(A)** *aSEC run of preincubated for 1h at room temperature GDP loaded Rab8a with SopD in presence of AlCl$_3$ and NaF, in order to generate AlF$_3$, which usually takes the position of GTP γ-phosphate as transition state mimetic of the hydrolysis reaction. Unfortunately, no stable complex was formed.* **(B)** *Neither the incubation of SopD with GppNHp loaded Rab8a resulted in a stable complex, which could be separated from single proteins by SEC.* **(C)** *Co-crystallization of Rab32:GDP with a truncated version of SopD2$_{30-319}$ provided rectangular, UV positive crystals.*

4. DISCUSSION
4.1 SrtA – a tool for protein immobilization

During the past decades, scientists constantly expanded the biochemical toolbox for multiple applications ranging from protein labeling with small molecules to protein immobilization on nano-scaffolds and enzyme supported assembly of multi-domain proteins for NMR [235,238,261]. The method of protein immobilization on magnetic nanoparticles presented in this work extends the set of such biochemical tools and provides researchers with new application opportunities for sortase A. This method enabled the immobilization of GtgE and generation of highly pure cleaved Rab32 samples free of any GtgE traces. Subsequent spFRET measurements of the samples prepared via this method showed distinct improvement of the resulting data. Moreover, the method developed in here permits not only instant purification of reaction mixtures from immobilized catalysts via magnet, but also pull-down experiments. MNPs proved advantageous for the enrichment of specific proteins since they produce lower background noise compared to agarose beads. A combination of MNP enrichment and methods such as co-substrate-mediated covalent capture, a recently developed technique in our group, could enable a fully covalent immobilization of the AMPylating enzymes with their targets. Subsequently, the target proteins can be cleaved from the immobilized enzymes through oxidation of the ribose vicinal diols by sodium periodate, allowing the direct identification of targets [262]. Alternatively, the covalently immobilized targets could be trypsinized directly on the MNPs and submitted to MS/MS analysis. Additionally, the SrtA-mediated immobilization described in this work proposes a quantification method for immobilized proteins via GFP-fluorescence, which significantly increases the accuracy of protein quantification compared to the previously applied methods [263,264] [f]. Noteworthy, other methods such as thermogravimetric analysis or enzyme-linked immunosorbent assay (ELISA) could be used for quantification purposes. However, such methods require a large number of analytes or specific antibodies. In contrast, the presented herein fluorescence-based quantification method is fast, sensitive, nondestructive, and compatible with analytical applications. Moreover, the simultaneous immobilization of multiple enzymes fused to different fluorescent proteins and their individual quantification is conceivable by applying the proposed method. However, fluorescence-based quantification might not be suitable for some enzymes due to the production of fusion constructs, which is where other methods could still prove valuable.

---

[f] This and following sentences in this section (4.1) are reprinted with permission from Fauser *et al*, 2020 [215]. Copyright (2020) American Chemical Society.

4.2 GtgE induces an inactive GTPase conformation of Rab32 [g]

The consequences of GtgE-mediated cleavage of inactive Rab32 were investigated using structural and biochemical analyses. The results demonstrate that the GtgE-mediated cleavage of switch I does not affect the global structural stability of the protein but results in local changes in the structure and destabilization of the switch regions. Moreover, the regioselective cleavage of switch I indirectly alters the interswitch region of Rab32 leading to the unfolding of the β-sheet structure of the β2 strand. Furthermore, Rab32$_{cleaved}$:GppNHp cannot bind to its effector VARP-ANK1. In contrast, GtgE-mediated cleavage does not impair the interaction between Rab32:GDP and GDI. Surprisingly, proteolytic modification of Rab32 permits the interaction between Rab32$_{cleaved}$:GppNHp and GDI that is not the case for the uncleaved Rab32:GppNHp.

The interaction surface between Rab32 and VARP-ANK1 is composed of amino acid residues from switch I (V60, D61, and F62), switch II (M91, V94, R93, Y95, and K97) and the interswitch region (D61, L64, and W80) (Figure 29A, B) [114]. Interestingly, the M91 and R93 residues from switch II in Rab32 are conserved only in the Rab32-subfamily and are crucial for the interaction with the ankyrin repeats [92,114]. The importance of the interswitch region of small GTPases for the interaction with their effectors has been reported previously [22,265–268]. This is supported by herein presented spFRET data and MD simulations showing that the gain in structural flexibility of the switch regions of cleaved Rab32 accompanied by the unfolding of the interswitch impairs the interaction between Rab32$_{cleaved}$:GppNHp and VARP-ANK1. Additionally, the proteolytic modification of Rab32 forces β2 and β3 strands to drift apart, as indicated by the increased COM distances between these two β strands in the MD simulations. This, in turn, displaces all residues of the β2 strand involved in the interaction with VARP-ANK1 and contributes in this fashion to the breakdown of the Rab32:VARP-ANK1 interaction. However, it should be noted that MD simulations generate not only one Rab32 species with dissociated β2 strand, but two species. The second species with an intact β2 strand is also present. Both species occur in a ratio of approximately 50 %. Thus, it can be suggested that NMR experiments detected none of the radical examples (intact or fully disordered) generated by MD simulations, but probably the species with slightly disordered β2 strand. This could explain the fact that NMR HSQC spectra of cleaved Rab32 do not differ dramatically from the uncleaved Rab32. However, these minor structural alterations are sufficient to impair the binding between cleaved Rab32:GppNHp and VARP-ANK1. VARP participates in the trafficking of melanogenic enzymes and has been suggested to control the transport in the endosome-to-cell surface route by regulating the retromer activity [106,114,115,269]. However, the role of Rab32 as a binding partner of VARP is not entirely understood [114]. The destruction of the interaction between Rab32 and VARP may lead to an aberrant sorting and

---

[g] The text in this section was modified and reprinted with permission from Savitskiy *et al*, 2020 [248]. Copyright (2020) Elsevier.

degradation of melanogenic enzymes or disruption of trafficking out of the endosome in the cell periphery [106,108,114,115,269].

Moreover, a recent study has shown that proteolytic modification of the switch I in KRas by the Ras and Rap1 specific protease (RRSP) from *Vibrio vulnificus*, similarly to the activity of GtgE in Rab32, impairs the interaction with its effector RAF [161]. In contrast to GtgE, RRSP cleaves switch I of KRas in the center and not near its C-terminal end. Similarly to GtgE-mediated proteolysis, cleavage by RRSP impacts the β2 strand of KRas [161]. However, Rab32 and KRas differ in the nucleotide-binding properties after proteolytic modification: cleaved Rab32 – but not KRas – shows elevated GDP/GTP dissociation rates. Stabile nucleotide binding in KRas is assumed to be ensured by F28 binding to the guanine moiety [161], but the identically positioned F50 in Rab32 is not sufficient for nucleotide stabilization after proteolytic modification. Furthermore, the results of spFRET experiments and MD simulations demonstrate that switch I gains structural flexibility after cleavage and, thus, likely does not contribute to the stabilization of the nucleotide in its binding pocket. The existence of two species with two different distances between fluorophores determined by spFRET of cleaved $Rab32_{R55C/Q160C}$ could be explained by the dynamic behavior of the cleaved switch I region. Thus, switch I of $Rab32_{cleaved}$ is not displaced from the protein core continuously but attaches and detaches dynamically. Therefore, the position of the cleavage site within switch I plays an important role in its conformational stability and the nucleotide-binding ability.

Structural changes in Rab32 caused by GtgE-mediated cleavage are not sufficient to impair its binding to GDI. Comparing Rab32 with Ypt1 in complex with GDI, G59, and D61 from the switch I, N90, R93, V94, and K97 from switch II and only D81 from the interswitch region form the binding interface of Rab32:GDI complex (Figure 29C, D) [270]. Due to a dramatic influence of the proteolytic modification on the organization of the interswitch region and the stability of switch I, they are apparently not vital for the interaction with GDI. Therefore, the Rab32 binding to GDI is presumably determined by the structural organization of switch II. Noteworthy, bulky PTMs on switch II (such as AMPylation – enzymatic transfer of AMP moiety to a target molecule) of Rab1b impair the interaction with GDI [141,171,271]. Nonetheless, the indirect minor impact of GtgE-mediated cleavage on the switch II has a big consequence for the interaction of Rab32 with GDI resulting in the ability to bind to $Rab32_{cleaved}$:GDP and $Rab32_{cleaved}$:GppNHp. Recently, it has been shown that bacteria can lock Rab1b in the active state using AMPylation [165]. Consequently, *Salmonella* may use proteolysis in order to force Rab32 into an inactive-like conformation as demonstrated here by NMR. That may explain the ability of $Rab32_{cleaved}$ to interact with GDI in the GDP and GTP states.

Once proteolyzed, cellular Rab32-signaling could hypothetically develop in two ways: 1) immediate interaction with GDI and withdrawal from the membrane or 2) GEF-mediated nucleotide exchange to GTP followed again by GDI interaction and withdrawal from the

membrane (Figure 29E). Whereas the first route seems to be possible, the second one is questionable, since Rab32 must be first activated by its GEF BLOC-3. Whether cleaved Rab32 can interact with BLOC-3 has yet to be elucidated. BLOC-3 belongs to heterodimeric RabGEF complexes and exhibits similarities with the Mon1-Ccz1 complex. Therefore, BLOC-3 probably utilizes the same mechanism for the nucleotide exchange as the Mon1-Ccz1 complex does [272,273]. Furthermore, Rab32 possesses an R55 matching with the K38 of Ypt7, which is crucial for its interaction with Mon1-Ccz1 [272]. Since the results show that cleaved switch I has higher flexibility and is dislocated, it would not be surprising if proteolytically modified Rab32 cannot be activated by BLOC-3. Therefore, the reduced amount of Rab32-positive SCVs caused by secretion of GtgE and SopD2 [146], may be explained by GtgE-mediated proteolysis resulting in a constitutive conformational locking of the small GTPase in the inactive state, providing GDI with an appropriate binding partner and ensuring the full removal of Rab from the SCVs [123,172]. An additional effect of $Rab32_{cleaved}$:GDP and $Rab32_{cleaved}$:GppNHp may be a GDI depletion from the host cell securing the enhanced membrane localization of other Rab GTPases. Furthermore, the proteolytic constitutive deactivation of Rab32 may explain the impairment of itaconate delivery into the SCVs in a Rab32-BLOC3-dependent manner [126].
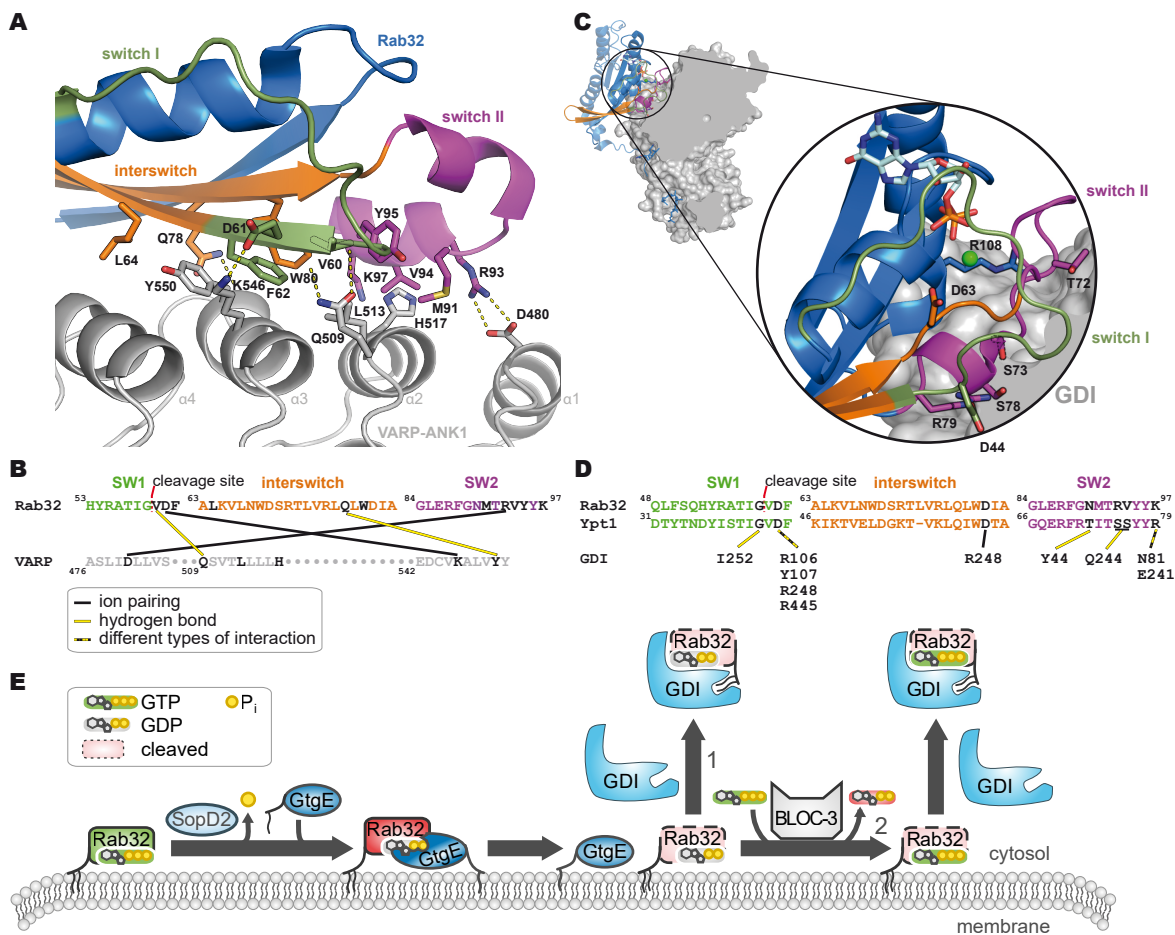
Figure 29 | Models of the molecular basis for binding effects of cleaved Rab32 with its interaction partners. (A) *Structural representation of Rab32 (colored) and VARP-ANK1 (grey) with important interaction residues presented as sticks (PDB ID 4CYM [114]).* **(B)** *The sequence of the switch I, switch II, and interswitch region of Rab32 with corresponding interacting amino acids from VARP-ANK1 depicted in black. Salt bridges between amino acids are indicated by black-yellow*

*lines. **(C)** A structural representation of Ypt1 (yeast GTPase) and GDI showing the interaction surface with important interaction residues of switch I, switch II, the interswitch region, and the C-terminal region of Ypt1 with hydrophobic moiety (PDB ID 2BCG [270]). Structural representations of the proteins were prepared using PyMol. **(D)** Sequence comparison of the GDI interacting regions of Ypt1 and Rab32 with crucial amino acids for the GDI binding depicted in black. Amino acids contributing to the interaction between the two protein structures are indicated by black sticks. **(E)** Model of the hypothetical lifecycle of Rab32 during the Salmonella infection process with possible routes for proteolyzed Rab32. Once the intrinsic hydrolysis of GTP to GDP occurs in Rab32, which is accelerated by SopD2 from Salmonella, it can be processed by GtgE protease and take one of two possible pathways, indicated with arrows 1 or 2, respectively. The figure was reprinted with permission from Savitskiy et al, 2020 [248]. Copyright (2020) Elsevier.*

GtgE also targets the Rab32 homolog Rab29 and cleaves its switch I between G41 and V42, which is homolog to the cleavage site in Rab32 [99]. Moreover, Rab29 interacts with the Armadillo domain of LRRK2 [91]. The result of this interaction is LRRK2 recruitment and activation on the Golgi [92]. Noteworthy is also the activation of the NLRC4 inflammasome by active LRRK2 during *Salmonella* infection [274]. Therefore, it would be of great interest to investigate whether Rab29 proteolysis by GtgE may impair the Rab29-mediated LRRK2 recruitment and activation on the Golgi, and reduce the activation of NLRC4 inflammasome [92,274]. It would also be beneficial to understand whether the kinase activity of LRRK2 during the infection is associated with Rab32 and plays a pivotal role in the defense mechanism of the host against *Salmonella* [274,275].

This study demonstrates that the high flexibility and dislocation of switch I, the alteration of the interswitch region, and locking of Rab32 in a GDP-like state by GtgE-mediated cleavage are responsible for the impairing the interaction between VARP-ANK1 and Rab32 as well as for binding of GDI to Rab32$_{cleaved}$:GDP or Rab32$_{cleaved}$:GppNHp. These findings expand the understanding of the consequences of GtgE-mediated proteolysis on Rab32, which facilitates the *Salmonella* infection. Taken together, these data provide insight on possible further downstream effects of proteolytic modification of Rab32 and deepen the knowledge about mechanisms of *Salmonella* infection.

4.3 RRSP-mediated proteolysis inhibits Ras downstream signaling

Ras isoforms are the subject of multiple investigations varying from inhibitors screenings and structural analysis to the complex *in vivo* experimental setups, to better understand Ras' role in cancer and finding possible ways to influence these multifunctional proteins [39,276]. Investigating Ras' interactions and the effects of Ras manipulation by bacterial toxins may provide additional means for controlling the hyperactivated Ras pathways in oncogenic cells and tissues. Previous studies have shown toxin TpeL from *Clostridium perfringens* modifying post-translationally Thr35 (switch II) in Ras by attaching a glycosyl moiety to it, thereby disrupting the MAP-kinase cascade downstream of Ras [277]. Similarly, RRSP from *V. vulnificus* impairs the binding of Ras to its effector cRaf but via specific proteolytic modification of switch I of Ras, which also results in the inhibition of the MAP-kinase cascade [161]. Results generated in this work and by Dr. Wachtel [163] are in line with recently published reports [161,213]. Additionally, this work provides evidence for the RRSP-mediated switch I cleavage disrupting the interaction between Ras and its another effector RalGDS, which is responsible for a plethora of signaling pathways downstream of Ras [36]. This

suggests that RRSP-mediated cleavage of Ras may inhibit the RalGEF-Ral effector signaling network.

4.4 SopD specifically inactivates Rab8

Additional investigations of SopD represented in this work identified Rab8 as an exclusive target of the RabGAP SopD from *Salmonella*. In contrast to SopD, SopD2 can stimulate GTP hydrolysis in Rab29, Rab32, and Rab38 *in vitro*. Moreover, both RabGAPs displayed a high catalytic efficiency toward their targets. Mutagenesis studies revealed that SopD is dependent on an Asp/Arg dual finger for the GTP hydrolysis in Rab8, pointing out the similarity to the mechanism of TBC-domain-containing GAPs in eukaryotes [26]. However, like the LepB from *Legionella*, SopD also requires the Gln located in the G3 motif of the Rab proteins for its efficient functioning [260]. Therefore, it can be suggested that SopD and SopD2 could combine mechanistic details of these diverse GAP classes. Notably, SopD and its homolog do not display structural similarities either with the TBC domain or with LepB. Moreover, the mutagenesis analysis presented in this work suggests SopD is using Asn residue for water activation instead of canonical Gln in the case of RabGAPs. This resembles the mechanism of RapGAPs, which also utilize Asp/Arg dual finger for the GTP hydrolysis [278]. However, Rap proteins are missing a catalytic Gln (replaced by Thr) in their switch II. Thus, the GTP hydrolysis is mediated solely by their GAPs with the support of conserved Thr residues situated in switch regions, which stabilize the interaction between both proteins. If SopD and SopD2 utilize the same mechanism similar to RapGAP's, they would also be able to facilitate GTP hydrolysis in the hydrolysis deficient Rab variants like TBC-GAPs. However, this was not the case. Therefore, GAPs from *Salmonella* may represent a new type of RabGAPs.

Furthermore, in contrast to SopD, its homolog SopD2 is able to inactivate multiple Rab proteins involved in different cellular processes [79,84]. Moreover, the validation of catalytic efficiencies of SopD2 towards the Rab32 subfamily suggests that Rab38 may be another SopD2 substrate. Thus, SopD2 may broadly inactivate Rab proteins involved in the biogenesis of lysosomal-related organelles and in the defense against bacteria, increasing the survival chances of the bacteria [84,92,146,274].

Unfortunately, the attempts to crystalize the Rab8:SopD and Rab32:SopD2 complexes were not successful. However, alterations to the setup might prove useful to achieve this goal in a future study. Herein, the trials of co-crystallization of these proteins at even higher concentrations (≥20 mg/ml) or in presence of fluoride salts of beryllium or magnesium could provide crystals suitable for crystallographic data collection.

5. OUTLOOK

Over the course of evolution, bacteria have developed multiple strategies that promote entry into the host and their replication in the host cells. To fulfill these strategies, bacteria secrete pathogenic proteins (effectors) into the host. Some of these effectors specifically target small GTPases and manipulate them to the benefits of bacteria. This work expands our understanding of the effects of such manipulations on small GTPases and provides new insights into effector-target interactions. The findings discovered in this work may inspire future experiments. Thus, it would be of interest to unravel the genuine role of Rab32 in the defense mechanisms of the eukaryotic cell during a bacterial invasion. It should be investigated whether Rab32 can provoke mitochondrial fission, resulting in the release of reactive oxygen species and cytochrome c into the cytosol, which engage the inflammation and apoptosis in the host cell during infection. Additionally, in order to construct a full picture of cleaved Rab32's fate, the interaction of proteolyzed Rab32 with its GEF BLOC-3 should be considered.

Another protease, RRSP, targeting small GTPases was extensively examined during the past years. However, the proteolytic mechanism underlying the Ras cleavage remains obscured. Therefore, the crystallization of Ras:RRSP complex would provide the utmost insights into the detail of RRSP functionality. Nevertheless, the affinity of RRSP for Ras in the high micromolar range represents a hindrance for the crystallographic approach, which may be overcome by the introduction of reactive unnatural amino acids into the proteins via amber codon suppression for complex stabilization. The deep knowledge and understanding of proteolytic mechanisms of GtgE and RRSP as well as the reasons for their substrate specificity may enable the generation of specific inactivating proteases for each small GTPase, thereby providing scientists with a powerful tool for fundamental and clinical research.

Bacterial GAPs secreted during the infection represent an efficient way to manipulate multiple cellular processes orchestrated by small GTPases. *Salmonella's* SopD2 inactivates Rab32 and provides, thus, a substrate for the protease GtgE, which induces an inactive GTPase conformation and impairs its functionality. Results of this work could indicate that SopD, a homolog of SopD2, catalyzes GTP hydrolysis in Rab8. Next, the effect of Rab8 inactivation by SopD during the *Salmonella* infection, needs to be investigated more thoroughly. To this end, infection studies should be conducted with *Salmonella* strains depleted from SopD or bearing its inactive mutants accompanied by the examination of e.g. the composition of SCV's membranes or cellular localization of Rab8. Additionally, co-crystallization attempts for Rab8:SopD and Rab32:SopD2 with fluoride salts other than aluminum should be undertaken to reveal the GAP mechanism of these proteins. Since SopD's homolog, SopD2, can inhibit Rab7 functionality via its N-terminus, it is possible that SopD is able to inhibit pathways controlled by Rab GTPases other than Rab8. To

identify other SopD substrates, the N-terminus of SopD should be probed for possible interactions with other Rab GTPases in a Y2H assay.

6. MATERIALS AND METHODS

6.1 Materials

Chemicals and compounds

Table M1 | *The list of chemicals and compounds used in this work.*

Chemical/compound	Provider	Chemical/compound	Provider
Acetonitrile	Fisher Scientific	HATU	Sigma Aldrich
Acetic acid	VWR Prolabo	HEPES	Carbosynth
Acetone	VWR	Hydrochloric acid	VWR Prolabo
Acrylamide/Bis-acrylamide (30%)	Serva	4-(Hydroxymercuri)benzoic acid sodium salt	Sigma Aldrich
Agarose for microbiology	Serva	Iron (III) chloride	VWR
Aluminum chloride hexahydrate	AppliChem	Isopropyl β-D-1-thiogalactopyranoside (IPTG)	Carbosynth
Amine magnetic beads (#801–113–2)	Raybiotech Inc.	Isopropanol, biology grade	VWR Prolabo
Amino acids for Y2H	Carl Roth	Kanamycin	Carl Roth
3-Amino-1,2,4-triazole	Sigma Aldrich	LB-medium (Lennox)	Carl Roth
Ampicillin	AppliChem	Lithium acetate	Carl Roth
Boric acid	VWR	Magnesium chloride	VWR Prolabo
Formaldehyde	Sigma Aldrich	Magnesium sulfate	Sigma Aldrich
Formic acid	Fluka	Manganese (II) chloride	Bernd Kraft
^{15}N Ammonium chloride	Cambridge Isotope Laboratories Inc.	mant-GDP	Jena Bioscience
Ammonium persulfate (APS)	VWR Amresco	mant-GTP	Jena Bioscience
β-Mercaptoethanol (β-ME)	VWR Prolabo	Methanol	Fluka
B1 (Thiamine)	Merck	MES	Carl Roth
B3 (Niacin)	VWR	Nickel (II) sulfate hexahydrate	Carl Roth
B7 (Biotin)	Carbosynth	Peptide 1 (Fmoc-N′-GGG-GSGGGSGGG-C′)	GenScript
B12 (Cobalamin)	Carl Roth	Peptide 2 (N′-SGGSSG-GGSSGLPETGG-C′)	GenScript
Bromophenol blue	Alfa Aesar	Piperidine	Sigma Aldrich
Calcium chloride	Carl Roth	Potassium dihydrogen phosphate	Carl Roth
Chloramphenicol	VWR	Phenylmethylsulfonyl fluoride (PMSF)	VWR Amresco
Cobalt chloride	Fisher Chemical	Select agar	Sigma Aldrich
Coomassie ® Brilliant Blue R-250	AppliChem	Silver nitrate	Sigma Aldrich
Copper (II) chloride	VWR	Sodium azide	Alfa Aesar
NAD$^+$	Carbosynth	Sodium dodecyl sulfate (SDS)	Carl Roth
dNTPs	Carbosynth	Sodium chloride	VWR Prolabo
N,N-diisopropyle-thylenamine (DIPEA)	Sigma Aldrich	Sodium dihydrogen phosphate	Carl Roth
N,N-dimethylformamide (DMF)	Sigma Aldrich	Sodium fluoride	AppliChem
Dimethyl sulfoxide (DMSO)	Fluka	Sodium hydrogen phosphate	Carl Roth
1,4-Dithiothreitol (DTT)	Carl Roth	Sodium hydroxide	Carl Roth
Ethanol, biology grade	VWR Prolabo	Sodium molybdate	Sigma Aldrich
EGTA	Fluka	Sodium selenite	AppliChem
EDTA sodium salt	Merck	Sodium thiosulfate pentahydrate	Alfa Aesar

Farnesyl Pyrophosphate	Sigma Aldrich	Tris (2-carboxyethyl) phosphine (TCEP)	Carl Roth
Gentamicin	Carl Roth	TEMED	VWR Amresco
D-glucose	Carl Roth	Tetra-n-butylammonium bromide (TnBr)	Alfa Aesar
^{13}C D-glucose	Cambridge Isotope Laboratories Inc.	Trichloroacetic acid	Fisher Chemical
Glutaraldehyde	Sigma Aldrich	Trifluoroacetic acid (TFA)	Carl Roth
Glycerin	Carl Roth	TRIS-HCl	Carl Roth
Glycine	Carl Roth	TRIS-Base	Carl Roth
Guanidinium chloride	VWR Prolabo	Xylene cyanol	AppliChem
Guanosine-5'-[(β,γ)-imido]-triphosphate (GppNHp)	Jena Bioscience	Zink chloride	Sigma Aldrich
Guanosine-5'-diphosphate (GTP)	Carbosynth	Zink sulfate	VWR

Enzymes

Table M2 | *The list of enzymes used in this work.*

Enzyme	Provider
DNAase I	AppliChem
FTase	Itzen lab
Lysozyme	Carl Roth
Q5®-DNA Polymerase	NEB
Taq ligase	NEB
T4-DNA Polymerase	NEB
T5 exonuclease	NEB
TEV protease	Itzen lab
Phusion polymerase	Itzen lab

Buffers, solutions and mixtures

Table M3 | *Buffers used for purification of proteins.*

Buffer A	
Compound	Concentration
HEPES	50 mM
NaCl	500 mM
MgCl$_2$	1 mM
β -ME	2 mM
Nucleotide (for GTPases)	10 µM
NaOH/HCl	pH 7.5

Buffer B	
A + Imidazol	500 mM

Dialysis buffer	
HEPES	50 mM
NaCl	100 mM
β-ME	2 mM
NaOH/HCl	pH 7.5

SEC buffer	
HEPES	20 mM
NaCl	50 mM
MgCl$_2$	1 mM
DTE/DTT/TCEP	1 mM
Nucleotide (for GTPases)	10 µM
NaOH/HCl	pH 7.5

C18 buffer (pH6.6)

Compound	Concentration
KH_2PO_4	50 mM
K_2HPO_4	50 mM
TnBr	10 mM
Acetonitrile	12% (v/v)

5 x ISO buffer

Compound	Volume/Mass	Stock concentration
TRIS-HCl	3 ml	1 M (pH 7.5)
$MgCl_2$	150 µl	2M
dATP	60 µl	100 mM
dCTP	60 µl	100 mM
dGTP	60 µl	100 mM
dTTP	60 µl	100 mM
DTT	300 µl	1 M
PEG-8000	1.5 g	
NAD^+	300 µl	100 mM
H_2O	6 ml	

Gibson-Assembly master mix

Compound	Volume	Stock concentration
5 x ISO buffer	320 µl	
Taq ligase	160 µl	40 U/µl
T5 exonuclease	0.64 µl	10 U/µl
Phusion polymerase	20 µl	2 U/µl
H_2O	700 µl	

DNA agarose gel loading buffer

Compound	Concentration
Glycerol	50 %
EDTA	10 mM
Bromophenol blue	0.2 %
Xylencyanol	0.2 %

TAE buffer (50x)

Compound	Amount
TRIS base	242 g
Acetic acid	57.1 ml
0.5 M EDTA	100 ml
H_2O	add to 1 l

Table M4 | *Buffers and solutions for SDS-PAGE.*

SDS-PAGE gel loading buffer (2x)

Compound	Concentration
TRIS-HCl (pH 6.8)	0.1 M
SDS	4 %
Glycerol	20 %
β-ME	10 %
Bromophenol blue	0.002 %
Stacking gel buffer (4x)	
TRIS-HCl (pH 6.8)	0.5 M
SDS	0.4 %

Resolving gel buffer (4x)

TRIS-HCl (pH 8.8)	1.5 M
SDS	0.4 %

SDS-PAGE running buffer (10x)

TRIS-HCl	0.25 M
SDS	1 %
Glycine	2 M

Coomassie staining solution

Acetic acid	12 %
Ethanol	44 %
Coomassie ® Brilliant Blue R-250	0.15 %

Destaining solution

Acetic acid	10 %

One step buffer

Compound	Concentration
Lithium acetate	200 mM
PEG 4000	40 %
DTT	100 mM

10 × M9 Salt

Compound	Concentration
Na_2HPO_4	60 g/l
KH_2PO_4	30 g/l
NaCl	5 g/l

1000x trace elements

Compound	Volume	Stock concentration
$CoCl_2$ x 6 H_2O	1 ml	0.2 M
$CuCl_2$ x 2 H_2O	2 ml	0.1 M
$FeCl_3$ x 6 H_2O	50 ml	0.1 M
H_3BO_3	2 ml	0.1 M
$MnCl_2$ x 4 H_2O	2 ml	1 M
Na_2MoO_4 x 2 H_2O	2 ml	0.1 M
Na_2SeO_3	2 ml	0.1 M
$NiSO_4$ x 6 H_2O	2 ml	0.2 M
$ZnSO_4$ x 7 H_2O	1 ml	1 M

2000x vitamin mix*

Compound	Concentration
Thiamine (B1)	100 mM
Niacin (B3)	100 mM
Biotin (B7)	100 mM
Cobalamin (B12)	10 mM

* do not autoclave, do not filter, use sterile water.

KITS

Table M5 | The list of KITS used in this work

KIT	Provider
Q5® Site-Directed Mutagenesis Kit	NEB
Monarch® DNA Gel Extraction Kit	NEB
Pierce™ Coomassie (Bradford) Protein-Assay	Thermo Scientific

PureYield™ Plasmid Midiprep System	Promega
PureYield™ Plasmid Miniprep System	Promega

Media

Table M6 | Media used for E.coli.

LB medium	
Compound	Concentration
LB (Lennox)	20 g/l
SOC medium	
Yeast extract	5 g/l
Trypton	20 g/l
NaCl	10 mM
KCl	2.5 mM
$MgCl_2$	10 mM
$MgSO_4$	10 mM
Glucose	3.96 g/l
M9 minimal medium	
M9 Salt	1 x
$MgSO_4$	2 mM
Glucose*	0.4 %
$CaCl_2$	0.1 mM <u>add first!</u>
Trace elements	1 x
Vitamin Mix	1 x
$^{15}NH_4Cl$	0.1 %
Antibiotic	1 x

* 0.2 % ^{13}C glucose for ^{13}C labeling.

Table M7 | Media and mixtures used for yeast

YAPD medium	
Compound	Concentration
Yeast extract	10 g/l
Peptone	20 g/l
Glucose	20 g/l
Adenine sulfate	1 g/l
Select agar	20 g/l (for plates)
Selection Dropout medium	
aa-4 mix	3 g/l
Yeast nitrogen base	2.8 g/l
Glucose	20 g/l
Selection aa	1 x
Select agar	20 g/l (for plates) +4 drops of 5 M NaOH
Selection aa (100x)	
Adenine-hemisulfate	1 g/l
Histidine	2.4 g/l
Leucine	7.2 g/l
Tryptophan	4.8 g/l
aa-4 mix*	
L-alanine	2 g
L-arginine	2 g
L-asparagine	2 g
L-aspartic acid	2 g
L-cysteine	2 g

L-glutamine	2 g
L-glutamic acid	2 g
Glycine	2 g
myo-Inositol (meso-Inosit)	2 g
L-isoleucine	2 g
L-lysine	2 g
L-methionine	2 g
L-phenylalanine	2 g
L-proline	2 g
L-serine	2 g
L-threonine	2 g
L-tyrosine	2 g
L-valine	2 g
Uracil	2 g
para-amino-benzoic acid	1.2 g

* all aa were homogenized in a porcelain mortar

Organisms

Table M8 | The list of bacteria and yeast strains used in this work.

Bacteria strain	Genotype	Provider
E. coli BL21 (DE3)	F$^-$ ompT gal dcm lon hsdS$_B$(r$_B$$^-m_B$$^-$) λ(DE3 [lacI lacUV5-T7p07 ind1 sam7 nin5]) [malB$^+$]$_{K-12}$(λ^S)	Promega
E. coli BL21 (DE3) RIL	B F– ompT hsdS (rB– mB–) dcm+ Tetr gal λ(DE3) endA Hte [argU ileY leuW (Cam^R)]	Stratagene, Agilent Technologies
E. coli Rosetta2 (DE3)	F- ompT hsdSB(rB- mB-) gal dcm (DE3) pRARE2 (Cam^R)	Novagen®, Merck
E. coli Mach1	ΔrecA1398 endA1 tonA	Invitrogen®, Thermo Fisher Scientific
E. coli DH10Bac	F-mcrA Δ(mrr-hsdRMS-mcrBC) Φ80lacZΔM15 ΔlacX74 recA1 endA1 araD139 Δ(ara, leu)7697 galU galK λ-rpsL nupG/pMON14272/pMON7124	Invitrogen®, Thermo Fisher Scientific
Yeast strain	**Genotype**	**Provider**
L40 ΔGal4	MATa ade2Δ0 his3Δ0 leu2Δ0 trp1Δ0 LYS::lexA-HIS3 URA3::lexA-LacZ	ATCC® MYA-3332™
Y187	MATα, ura3-52, his3-200, ade2-101, trp1-901, leu2-3, 112, gal4Δ, met–, gal80Δ, MEL1, URA3::GAL1$_{UAS}$ -GAL1$_{TATA}$-lacZ	Clontech Laboratories Inc.

Consumables

Table M9 | The list of consumables used in this work.

Consumable	Provider	Consumable	Provider
Black 96-well plates	Sarstedt	Glass Pasteur pipettes	Brand
Bottle-Top-Filter (sterile, 45 µm)	Berrytec	PCR-tubes (0.2 ml)	Sarstedt
Dialysis tubing (MWCO 12-14K)	Serva	Petri dishes (round and square)	Sarstedt
Cuvettes UV/Vis	Sarstedt	Pipette tips	Sarstedt
Membrane filters (20-45 µM)	Merck	Serological pipettes (5 ml, 10 ml, 25 ml, 50 ml)	Sarstedt
Microcentrifuge tube (1.5-2.0 ml)	Roth	Syringe filter (20 µm, 45 µm)	Carl Roth
Microcentrifuge tube (1.5 ml LoBind)	Eppendorf	Syringes and needles (1-20 ml)	Braun
Falcons (15 ml, 50 ml)	Sarstedt		

Software

Adobe Illustrator CC 2017

Adobe Photoshop CS6

ChemDraw 19.1

Citavi 6.4.0.35

GraphPad Prism 4.0

Image Lab 6.0.1

MagTran v. 1.02

Microsoft Office Excel 365

Microsoft Office Word 365

NMRFAM-SPARKY

OriginLab, 2019b, v9.65

PyMOL 2.3.2

6.2 Equipment

Table M10 | The list of instruments used in this work.

Instrument	Commercial name	Provider
Agarose gel electrophoresis chamber	Mini-Sub® Cell GT	Bio-Rad
Autoclave	Systec VE-65 Systec VX-150	Systec
Balance	ACJ 120-4M, EG 2200-2NM	Kern
Battery-powered pipette filler	pipetus®	Hirschmann
CD-Spectrometer	J-715	Jasco
Centrifuges	5424 5424R 5810R Avanti® J-26 XP Sigma 8K Sorvall Lynx 6000	Eppendorf Backmann Sigma Thermo
Drying oven	FD 240	Binder
FPLC	ÄKTAPrime Plus	GE Healthcare
Heat block	Thermomixer compfort AccuBlock™ Digital Dry Bath	Eppendorf Labnet
High-pressure fluidizer	Constant Cell Disruption Systems	Constant Systems
HPLC	Autosampler: SIL-20AC Degasing unit: DGU-20A$_{3R}$ Detector: SPD-20AV Fraction collector: FRC-10A Pumps: LC-20AD System controller: CBM-20A	Shimadzu
Imaging system	ECL CHEMOCAM	Intas-Science-Imaging Instruments
Incubator	FP 115 IPS260	Binder Memmert
Incubator shaker	Innova 44 INFORS HT multitron standard	New Brunswick Infors HT
Label printer	GK420t	Zebra
Laminar flow hood	LaminAir® HB 2448 K	Heraeus instruments
LC-MS	LC: UltiMate™ 3000 system MS: Heated-ESI-LCQFleet	Dionex Thermo
MPLC	NGC QuestTM 10	Bio-Rad
Shaker	RS-TR05 Unimax 1010	Phoenix instrument Heidolph
PAGE gel electrophoresis chamber	Mini Protean™ Tetra System	Bio-Rad
pH-meter	pHenomenal™ pHenomenal 111	VWR
Pipets	Eppendorf Research plus®	Eppendorf
Plate reader	Spark®	TECAN life sciences
Power supply	PowerPac™ Basic, EPS 601	Bio-Rad
Sonicator	Sonifier 250	Branson
Spectrofluorometer	FluoroMax®-4 FP-8300	Horiba Jasco
Thermocycler	T100™ Thermal Cycler	Bio-Rad
Transilluminator	FL-3 LED BlueLight Table	Rex Leuchtplatten Serva
Ultra-Low Temperature Freezer	U410 Freezer V86V-780.1	New Brunswick EWALD Innovationstechnik

UV/Vis- spectrophotometer	NanoDrop 2000	Thermo
	BioPhotometer	Eppendorf
Vacuum pump	Divac 2.4L	Leybold
Vortex	Vortex-Genie 2	Scientific Industries
Water system	TKA-GenPure	Thermo

6.3 Molecular biology

DNA cloning

All cloning procedures were accomplished using the Mach1 *E.coli* strain. Primers were designed manually for each cloning procedure considering the melting temperature (48-72°C), GC content (45-57%), and codon usage in *E. coli* K12 strain and *S. cerevisiae*. All primers were purchased from Integrated DNA Technologies, Inc. (IDT, Leuven, Belgium). Melting temperatures for primers were generated automatically on an online Tm Calculator (https://tmcalculator.neb.com/#!/main). Amplified by PCR (Figure M1A, Table M11) templates and inserts were purified via agarose gel electrophoresis and extracted from the gel using Monarch Gel Extraction Kit (NEB) according to a provided protocol by the manufacturer. Subsequently, purified products were ligated via SLIC (site and ligation independent cloning) or Gibson-Assembly (Figure M1B, C). All plasmids were confirmed by Sanger sequencing with Microsynth Seqlab (Table M12, Table M14).

Table M11 | Typical composition of PCR runs

Component	Volume [µl]	Concentration
Q5-reaction buffer	10	5 x
Q5 High GC Enhancer	10	5 x
5´-primer	2.5	10 µM
3´-primer	2.5	10 µM
Template	1	25 ng/µl
dNTPs	1	10 mM
ddH$_2$O	22.5	---
Q5 High-Fidelity DNA Polymerase	0.5	2000 U/ml
	Σ 50	
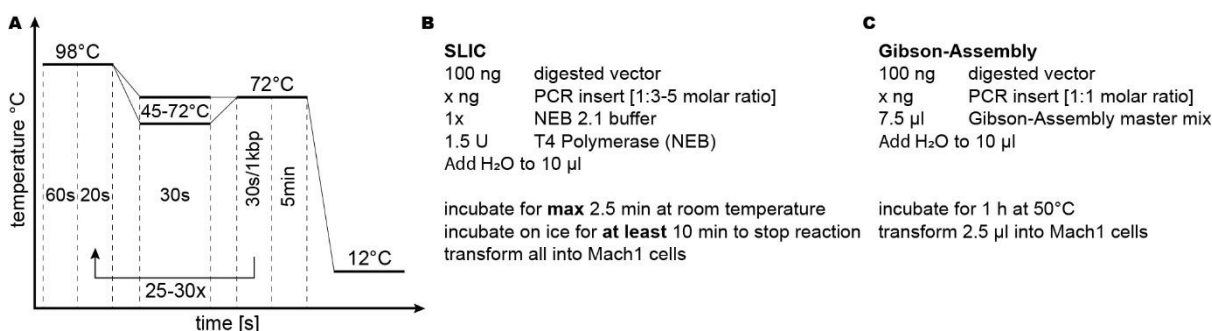
Figure M1 | Cloning procedures. (A) Schematic representation of used PCR cycling programs. (B) The standard protocol for SLIC ligation. (C) The standard protocol for Gibson-Assembly. Both ligation procedures can be used for ligation of multiple DNA fragments. For the Gibson-Assembly master mix see section 6.1 Materials.

Table M12 | List of plasmids used in this work for protein expression

Protein	Tag	Cleavage site	Vector	Resistance	NCBI #	Repository #
$Cdc42_{1-191}$	His_{10}-GFP	TEV	pSF421	Amp	NP_001034891	M2325
$cRaf_{51-131}$	His_6-MBP	TEV	pMal	Amp	NP_002871	M2157
GDI_{wt}	His_6	TEV	pFastBacHTa	Amp/Gen	NP_776489	02915
GroEL/S			pGro7	Cam		M2021
$GtgE_{wt}$	His_6-MBP	TEV	pMal	Amp	AAT12442	M0133
$GtgE_{C45A}$	His_6-MBP	TEV	pMal	Amp	- / -	M0160
$GtgE_{GSSGLPETGG}$	His_{10}-GFP	TEV	pSF421	Amp	- / -	xH0101
$LRRK2_{10-661}$	His_{10}-MBP	TEV	pSF421	Amp	NP_940980	xH0239
$Rab1_{3-174}$	His_6-MBP	TEV	pMal	Amp	NP_112243	02142
$Rab3d_{wt}$	His_6-MBP	TEV	pMal	Amp	NP_004274	xH0281
$Rab7a_{1-204}$	His_6-MBP	TEV	pMal	Amp	NP_004628	M0272
$Rab8a_{6-176}$	His_6	TEV	pET19mod	Amp	NP_005361	02443
$Rab10_{wt}$	His_6-MBP	TEV	pMal	Amp	NP_057215	xH0282
$Rab14_{wt}$	His_6-MBP	TEV	pMal	Amp	NP_057406	xH0283
$Rab29_{wt}$	His_6-MBP	TEV	pMal	Amp	NP_001129134	M0169
$Rab32_{wt}$	His_6-MBP	TEV	pMal	Amp	NP_006825	M0176
$Rab32_{Q85L}$	His_6-MBP	TEV	pMal	Amp	- / -	M0212
$Rab32_{20-CVIM}$	His_6-MBP	TEV	pMal	Amp	- / -	M2394
$Rab32_{20-201}$	His_6-MBP	TEV	pMal	Amp	- / -	M0813
$Rab32_{N90C|C145S|S156C|C162S|20-201}$	His_6-MBP	TEV	pMal	Amp	- / -	M2456
$Rab32_{R55C|C145S Q160C|C162S|20-201}$	His_6-MBP	TEV	pMal	Amp	- / -	M1928
$Rab38_{wt}$	His_6-MBP	TEV	pMal	Amp	NP_071732	M0170
$RalGDS_{790-869}$	His_6-MBP	TEV	pMal	Amp	NP_006257	M2158
$RalGDS_{N54R|790-869}$	His_6-MBP	TEV	pMal	Amp	- / -	M2351
$(K)Ras_{1-166}$	His_6-MBP	TEV	pMal	Amp	NP_001356715	M2484
$(H)Ras_{wt}$	His_6-MBP	TEV	pMal	Amp	NP_005334	M0359
$RRSP_{3596-4088}$	His_6-MBP	TEV	pMal	Amp	WP_011081430	M1248
$SopD_{wt}$	His_6-MBP	TEV	pMal	Amp	NP_461866	M2160
$SopD_{N219A}$	His_6-MBP	TEV	pMal	Amp	- / -	M2471
$SopD_{R312A}$	His_6-MBP	TEV	pMal	Amp	- / -	M2472
$SopD_{77-317}$					- / -	M2671
$SopD2_{wt}$	His_6-MBP	TEV	pMal	Amp	WP_001145561	M0941
$SopD2_{Q219A}$	His_6-MBP	TEV	pMal	Amp	- / -	M2326
$SopD2_{R315A}$	His_6-MBP	TEV	pMal	Amp	- / -	M2159
$SopD2_{30-319}$	His_6-MBP	TEV	pMal	Amp	- / -	M2672
$SopD2_{77-319}$	His_6-MBP	TEV	pMal	Amp	- / -	M2673
$Varp_{451-640}$	His_6-MBP	TEV	pMal	Amp	NP_115515	M1844

Table M13 | List of plasmids used in this work for Y2H assay

Protein	Domain	Vector	Resistance	Repository #
Rab1b	LexA BD	pLexA	Amp	M0427
Rab1b DN	LexA BD	pLexA	Amp	M0560
Rab1b DA	LexA BD	pLexA	Amp	M0505

Rab2a	LexA BD	pLexA	Amp	M0428
Rab2a DN	LexA BD	pLexA	Amp	M0561
Rab2a DA	LexA BD	pLexA	Amp	M0506
Rab2b	LexA BD	pLexA	Amp	M0429
Rab2b DN	LexA BD	pLexA	Amp	M0562
Rab2b DA	LexA BD	pLexA	Amp	M0507
Rab3a	LexA BD	pLexA	Amp	M0430
Rab3a DN	LexA BD	pLexA	Amp	M0563
Rab3a DA	LexA BD	pLexA	Amp	M0508
Rab3b	LexA BD	pLexA	Amp	M0431
Rab3b DN	LexA BD	pLexA	Amp	M0564
Rab3b DA	LexA BD	pLexA	Amp	M0509
Rab3c	LexA BD	pLexA	Amp	M0432
Rab3c DN	LexA BD	pLexA	Amp	M0565
Rab3c DA	LexA BD	pLexA	Amp	M0510
Rab3d	LexA BD	pLexA	Amp	M0433
Rab3d DN	LexA BD	pLexA	Amp	M0566
Rab3d DA	LexA BD	pLexA	Amp	M0511
Rab4a	LexA BD	pLexA	Amp	M0434
Rab4a DN	LexA BD	pLexA	Amp	M0567
Rab4a DA	LexA BD	pLexA	Amp	M0512
Rab4b	LexA BD	pLexA	Amp	M0435
Rab4b DN	LexA BD	pLexA	Amp	M0568
Rab4b DA	LexA BD	pLexA	Amp	M0513
Rab5a	LexA BD	pLexA	Amp	M0436
Rab5a DN	LexA BD	pLexA	Amp	M0569
Rab5a DA	LexA BD	pLexA	Amp	M0514
Rab5b	LexA BD	pLexA	Amp	M0437
Rab5b DN	LexA BD	pLexA	Amp	M0570
Rab5b DA	LexA BD	pLexA	Amp	M0515
Rab5c	LexA BD	pLexA	Amp	M0438
Rab5c DN	LexA BD	pLexA	Amp	M0571
Rab5c DA	LexA BD	pLexA	Amp	M0516
Rab6b	LexA BD	pLexA	Amp	M0440
Rab6b DN	LexA BD	pLexA	Amp	M0573
Rab6b DA	LexA BD	pLexA	Amp	M0518
Rab6c	LexA BD	pLexA	Amp	M0441
Rab6c DN	LexA BD	pLexA	Amp	M0574
Rab6c DA	LexA BD	pLexA	Amp	M0519
Rab7a	LexA BD	pLexA	Amp	M0442
Rab7a DN	LexA BD	pLexA	Amp	M0575
Rab7a DA	LexA BD	pLexA	Amp	M0520
Rab7b	LexA BD	pLexA	Amp	M0443
Rab7b DN	LexA BD	pLexA	Amp	M0576
Rab7b DA	LexA BD	pLexA	Amp	M0521
Rab8a	LexA BD	pLexA	Amp	M0444
Rab8a DN	LexA BD	pLexA	Amp	M0577
Rab8a DA	LexA BD	pLexA	Amp	M0522
Rab8b	LexA BD	pLexA	Amp	M0445
Rab8b DN	LexA BD	pLexA	Amp	M0523
Rab8b DA	LexA BD	pLexA	Amp	M0523
Rab9a	LexA BD	pLexA	Amp	M0446
Rab9a DN	LexA BD	pLexA	Amp	M0579
Rab9a DA	LexA BD	pLexA	Amp	M0524
Rab10	LexA BD	pLexA	Amp	M0448
Rab10 DN	LexA BD	pLexA	Amp	xH0342
Rab10 DA	LexA BD	pLexA	Amp	M0526
Rab11a	LexA BD	pLexA	Amp	M0449
Rab11a DN	LexA BD	pLexA	Amp	M0582

Rab11a DA	LexA BD	pLexA	Amp	M0527
Rab11b	LexA BD	pLexA	Amp	M0450
Rab11b DN	LexA BD	pLexA	Amp	M0583
Rab11b DA	LexA BD	pLexA	Amp	M0528
Rab13	LexA BD	pLexA	Amp	M0451
Rab13 DN	LexA BD	pLexA	Amp	M0584
Rab13 DA	LexA BD	pLexA	Amp	M0529
Rab14	LexA BD	pLexA	Amp	M0452
Rab14 DN	LexA BD	pLexA	Amp	M0585
Rab14 DA	LexA BD	pLexA	Amp	M0530
Rab15	LexA BD	pLexA	Amp	M0453
Rab15 DN	LexA BD	pLexA	Amp	M0586
Rab15 DA	LexA BD	pLexA	Amp	M0531
Rab17	LexA BD	pLexA	Amp	M0454
Rab17 DN	LexA BD	pLexA	Amp	M0587
Rab17 DA	LexA BD	pLexA	Amp	M0532
Rab18	LexA BD	pLexA	Amp	M0455
Rab18 DN	LexA BD	pLexA	Amp	M0588
Rab18 DA	LexA BD	pLexA	Amp	M0533
Rab20	LexA BD	pLexA	Amp	M0456
Rab20 DN	LexA BD	pLexA	Amp	M0479
Rab20 DA	LexA BD	pLexA	Amp	M0534
Rab23	LexA BD	pLexA	Amp	M0458
Rab23 DN	LexA BD	pLexA	Amp	M0481
Rab23 DA	LexA BD	pLexA	Amp	M0536
Rab25	LexA BD	pLexA	Amp	M0460
Rab25 DN	LexA BD	pLexA	Amp	M0483
Rab25 DA	LexA BD	pLexA	Amp	M0538
Rab27a	LexA BD	pLexA	Amp	M0461
Rab27a DN	LexA BD	pLexA	Amp	M0484
Rab27a DA	LexA BD	pLexA	Amp	M0539
Rab28	LexA BD	pLexA	Amp	M0463
Rab28 DN	LexA BD	pLexA	Amp	M0486
Rab28 DA	LexA BD	pLexA	Amp	M0541
Rab29	LexA BD	pLexA	Amp	M0464
Rab29 DN	LexA BD	pLexA	Amp	M0487
Rab29 DA	LexA BD	pLexA	Amp	M0542
Rab30	LexA BD	pLexA	Amp	M0465
Rab30 DN	LexA BD	pLexA	Amp	M0488
Rab30 DA	LexA BD	pLexA	Amp	M0543
Rab32	LexA BD	pLexA	Amp	M0467
Rab32 DN	LexA BD	pLexA	Amp	M0490
Rab32 DA	LexA BD	pLexA	Amp	M1374
Rab33b	LexA BD	pLexA	Amp	M0468
Rab33b DN	LexA BD	pLexA	Amp	M0492
Rab33b DA	LexA BD	pLexA	Amp	M0547
Rab34	LexA BD	pLexA	Amp	M0469
Rab34 DN	LexA BD	pLexA	Amp	M0493
Rab34 DA	LexA BD	pLexA	Amp	M0548
Rab35	LexA BD	pLexA	Amp	M0470
Rab35 DN	LexA BD	pLexA	Amp	M0494
Rab35 DA	LexA BD	pLexA	Amp	M0549
Rab36	LexA BD	pLexA	Amp	M0471
Rab36 DN	LexA BD	pLexA	Amp	M0495
Rab36 DA	LexA BD	pLexA	Amp	M0550
Rab37	LexA BD	pLexA	Amp	M0472
Rab37 DN	LexA BD	pLexA	Amp	M0496
Rab37 DA	LexA BD	pLexA	Amp	M0551
Rab38	LexA BD	pLexA	Amp	M0466

Rab38 DN	LexA BD	pLexA	Amp	M0497
Rab38 DA	LexA BD	pLexA	Amp	M0552
Rab39a	LexA BD	pLexA	Amp	M0474
Rab39a DN	LexA BD	pLexA	Amp	M0498
Rab39a DA	LexA BD	pLexA	Amp	M0553
Rab39b	LexA BD	pLexA	Amp	M0475
Rab39b DN	LexA BD	pLexA	Amp	M0499
Rab39b DA	LexA BD	pLexA	Amp	M0554
Rab40a	LexA BD	pLexA	Amp	M0476
Rab40a DN	LexA BD	pLexA	Amp	M0500
Rab40a DA	LexA BD	pLexA	Amp	M0555
Rab40b	LexA BD	pLexA	Amp	M0477
Rab40b DN	LexA BD	pLexA	Amp	M0501
Rab40b DA	LexA BD	pLexA	Amp	M0556
Rab40c	LexA BD	pLexA	Amp	M0478
Rab40c DN	LexA BD	pLexA	Amp	M0502
Rab40c DA	LexA BD	pLexA	Amp	M0557
$SopD_{wt}$	GAL4 AD_{N-term}	pGAD	Amp	M2297
$SopD_{N219A}$	GAL4 AD_{N-term}	pGAD	Amp	M2298
$SopD_{R312A}$	GAL4 AD_{N-term}	pGAD	Amp	M2479
$pGAD_{empty}$	GAL4 AD		Amp	M0688
$pLexA_{empty}$	LexA BD		Amp	M0330
Varp	GAL4 AD_{C-term}	pGADc	Amp	M2302

Site-directed mutagenesis

Q5® Site-Directed Mutagenesis Kit (KLD, New England Biolabs) was used for the generation of all mutants used for this study according to a provided protocol by the manufacturer. Primers for site-directed mutagenesis were designed automatically on NEBaseChanger online platform (http://nebasechanger.neb.com/).

Transformation of chemically competent *E. coli*

The competence of a microorganism describes its ability to uptake foreign DNA. Typically, 50-100 µl cell suspension was mixed with 100-500 ng plasmid DNA, incubated for 10 min on ice, and after a heat shock for 30 s at 42°C kept on ice for another 5 min. Subsequently, 1 mL of prewarmed (37°C) SOC medium was added to the transformed cells, and the culture was incubated at 37°C for 1 h while shaking. Afterward, bacterial cultures were pelleted (2 min, 375 g), resuspended in 250 µl sterile H_2O, and streak onto suitable selection agar plates. Single colonies were visible overnight after incubation at 37°C.

Plasmid preparation

In order to multiply correct plasmids, they were transformed into Mach1 *E.coli* strain and streak on the agar plates supplemented with corresponding antibiotics. Overnight grown single colonies were transferred into liquid LB-medium (10 ml for Miniprep or 50 ml for Midiprep) supplemented with appropriate antibiotics and grown overnight at 37°C while shaking. Overnight grown cultures were collected by centrifugation (3000 g, 20 min, 4°C). Resulted cell pellets were processed by PureYield™ Plasmid Mini- or Midiprep System (Promega) according to a provided

protocol by the manufacturer. Concentrations of yielded plasmids were measured on NanoDropTM 2000 (Thermo Scientific) and they were stored at -20°C.

Agarose gel electrophoresis

Due to the negative charge of the nucleic acids, DNA fragments migrate to the anode in agarose gel matrix. Since the net charge is proportional to the length of an oligonucleotide, it is possible to separate DNA fragments according to their molecular weight. Typically, 1% (w/v) agarose gels were prepared with TAE buffer and ran in electrophoresis chambers filled with TAE buffer at 100 V for 30-60 min. The DNA was stained with Stain G (Serva) diluted 1:50000 and used for gel preparation. Visualization was performed on a transilluminator equipped with a blue or UV spectrum light source. The 1kb-Ladder (NEB) was used as a size standard. For further DNA purification from the agarose gel or from liquid reaction preparations, the commercially available Monarch Gel Extraction Kit (NEB) was used according to a provided protocol by the manufacturer. The DNA was eluted in 10 µL nuclease-free ddH$_2$O.

Yeast two-hybrid assay

For the big screen yeast mating procedure was selected and applied as follows: pLexA-Rab plasmids (bait) encoding for full-length Rab proteins were transformed with MAT-a yeast strain Y187 and plated on selection dropout medium lacking tryptophan (SD-W) [279]. 700 µL of stationary yeast culture was collected at 375 g for 2 min and resuspended by vortexing in 100 µL sterile one-step buffer (0.2 M lithium acetate, 40% PEG 3350, and 100 mM DTT)[280]. Subsequently, 500 ng of respective plasmid DNA was added to the cells and incubated at room temperature for 15 min followed by heat shock for 30 min at 45 °C. MAT-α S. cerevisiae L40ΔGal4 strain was transformed the same way with the pGAD-HA-SopD plasmid (prey) encoding for wild-type SopD and grown on SD-L plates (lacking leucine) at 30°C for 3–4 days. Afterward, single colonies of a prey and a bait clone were grown separately in 300 µl YAPD media overnight at 30°C and 180 rpm. Subsequently, 250 µl of an appropriate selection medium were inoculated with 50 µl of overnight grown cultures and incubated at 30°C overnight while shaking. 50µL of bait and prey culture were added sequentially to 100 µL YAPD media in a 96-well plate (Sarstedt) and incubated for 22–24 h at 30 °C and 180 rpm. 5 µL of resuspended cells were spotted on SD-LW plates as mating control and SD-LWH (lacking histidine) for phenotypic readout. Plates were analyzed after 3–4 days of incubation at 30 °C. 3-Amino-1,2,4-triazole (2.5 mM, 3-AT, Sigma Aldrich), an inhibitor of the histidine biosynthesis, was added to SD-LWH agar probing the interaction stability. For the validation of revealed interaction hits, MAT-α S. cerevisiae L40ΔGal4 strain was co-transformed with 1 µg pGAD-HA-SopD plasmid and corresponding pLexA-Rab plasmid respectively like described before, plated on selection plates lacking leucine and tryptophan (SD-LW) and grown at 30°C for 3 days. Subsequently, grown yeast were resuspended in sterile water, diluted to OD$_{600}$

= 0.4 and 5 µl of the diluted cultures were spotted on selection plates SD-LW, SD-LWH, and SD-LWH with 2.5 mM 3-AT. After 3-4 days at 30°C plates were analyzed.

6.4 Biochemical methods [h]

Protein expression

For recombinant production of proteins, the *E. coli* BL21-Codon Plus (DE3) strain (for the Rab/Ras proteins and the effectors fusion proteins) or BL21-Codon Plus (DE3)-RIL strain (for GtgE variants, SopD and SopD2) were transformed with 100-500 ng of the respective plasmid and grown overnight in 20 ml of lysogeny broth (LB) medium containing 125 µg/mL ampicillin (and 34 µg/mL chloramphenicol for BL21-Codon Plus (DE3)-RIL cells) at 37°C and 180 rpm (Innova 44 shaking incubator, New Brunswick). The expression cultures (1 L of LB medium or ^{15}N supplemented M9 minimal medium for isotope labeling) containing corresponding antibiotics were inoculated with 20 ml of the overnight cultures and grown under the same conditions. At OD_{600} = 0.5-0.8, protein expression was induced by the addition of 1 mM isopropylthiogalactopyranosid (IPTG, final) for Rab variants and effectors as well as 0.5 mM IPTG for GtgE, SopD, and SopD2, followed by overnight incubation at 22°C and 180 rpm. GDI was expressed using the baculovirus expression system in *S. frugiperda* cells (Sf9, Thermo Scientific) and was purified as described before [171]. Cdc42, SrtA, and Rab8a were expressed and purified as described recently [215,262,281]. RRSP and FTase were kindly provided by Dr. Wachtel. Cells were harvested by centrifugation at 8500 g and 20°C for 30 min (Sigma 8K, Sigma Centrifuges). After resuspending and washing the pelleted bacteria in phosphate-buffered saline (PBS, 137 mM NaCl, 2.7 mM KCl, 10 mM NaH_2PO_4, 2 mM KH_2PO_4), cells were centrifuged at 3000 g and 4°C for 20 min (5810 R, Eppendorf). The pellets were snap-frozen in liquid nitrogen and stored at -20°C until further use.

Protein purification

Pellets containing GtgE variants, SopD, SopD2, or effectors were resuspended in buffer A (50 mM HEPES, 500 mM NaCl, 1 mM $MgCl_2$, 2 mM β-Mercaptoethanol (ß-ME) at pH 7.5) in a ratio of 10 ml buffer to 1 g pellet. For pellets containing Rab/Ras proteins buffer A was supplemented with 10 µM Guanosine 5′-diphosphate (GDP). A spatula tip of DNAse I (Sigma Aldrich) was added to the suspension and cells were disrupted in a high-pressure fluidizer at 1.8 kbar (Constant Systems Ltd.). Subsequently, 1 mM phenylmethylsulfonyl fluoride (PMSF, final concentration) was added and the crude protein extract was cleared by centrifugation at 20000 rpm and 4°C for 45 min (Avanti J-26 XP with JA25.50 rotor, Beckman Coulter). The crude lysate containing VARP-ANK1 was supplemented with 1 mM 4-(2-Aminoethyl)benzenesulfonyl fluoride (AEBSF; Sigma Aldrich, final concentration) and 5% of glycerol (v/v) before clearing the lysate.

---

[h] The text in this section was modified and reprinted with permission from Savitskiy *et al*, 2020 [248]. Copyright (2020) Elsevier.

For the purification of all proteins via fused His_6-affinity tag, the cleared protein extract was applied to an immobilized metal affinity chromatography (IMAC) using a 5 mL Nuvia column chelating Ni^{2+}-ions (Bio-Rad Laboratories) that was equilibrated with buffer A beforehand. For all chromatography purifications, the NGC QuestTM 10 medium-pressure liquid chromatography (MPLC) system (Bio-Rad) was used. The cleared lysate was loaded onto the column and washed with 6-8 column volumes (CV) 8% buffer B (buffer A supplemented with 500 mM imidazole). Subsequently, a 20 CV gradient of 8-100% buffer B was applied, where target proteins eluted between 18-35% buffer B. Relevant fractions were analyzed by sodium dodecyl sulfate-polyacrylamide gel electrophoresis (SDS-PAGE) and pure protein fractions were pooled. Subsequently, the proteins were dialyzed against 5 L dialysis buffer (20 mM HEPES, 100 mM NaCl, 2 mM ß-ME at pH 7.5) overnight at 4°C. During dialysis, the target proteins were incubated with 1 mg TEV-protease (containing a His_7-affinity tag, in house preparation) per 40 mg target protein in order to quantitatively cleave the fused His_6-affinity and MBP solubility tag. To purify the proteins of interest from the protease and the cleaved tags, reverse IMAC was applied, either collecting the target protein in the flow-through (GtgE, SopD, SopD2, and effectors) or 5% buffer B elution fraction (Rab/Ras proteins).

For further purification size exclusion chromatography using a 16/600 Superdex 75 pg column (GE Healthcare) was performed. The column was equilibrated with gel filtration buffer (20 mM HEPES, 50 mM NaCl, 1 mM $MgCl_2$, 10 µM GDP, 2 mM DTT at pH 7.5 for Rab/Ras proteins, and the same buffer system without GDP for other proteins). Fractions containing pure and monodisperse protein of interest were identified by SDS-PAGE, concentrated to 5-30 mg/mL using Amicon Ultra 15 ml centrifugal filters (Merck Millipore), flash-frozen in liquid nitrogen, and stored at -80°C.

Rab32 farnesylation

Rab32 was incubated with FTase (in house preparation as described before [282]) in the presence of farnesyl pyrophosphate (FPP, Sigma Aldrich) for 2 h at 30°C and 300 rpm (Rab32:FTase:FPP molar ratio 2:1:12) in the reaction buffer (20 mM HEPES, 50 mM NaCl, 1 mM $MgCl_2$, 0.5 mM $ZnCl_2$, 10 µM GDP, 2 mM DTT at pH 7.5). Farnesylation was confirmed via intact protein mass spectrometry on an LCMS system.

Rab32 proteolysis by GtgE

For quantitative modification, Rab32:GDP was submitted to GtgE-mediated proteolysis at 25°C for 2 h (GtgE:Rab32 molar ratio 1:200) in a gel filtration buffer (20 mM HEPES, 50 mM NaCl, 1 mM $MgCl_2$, 10 µM GDP, 2 mM DTT at pH 7.5). Cleaved Rab32 variants used in spFRET measurements were generated as described recently [215]. Proteolysis completion was monitored via SDS-PAGE.

SrtA-mediated protein ligation [i]

Immobilization of proteins was performed with 1.875 mg of functionalized MNPs at a total volume of 200 µL. MNPs were gently shaken in the presence of 25 µM SrtA 5M and 150 µM GtgE in Ligation Buffer (20 mM HEPES pH 7.4, 100 mM NaCl, 5 mM $CaCl_2$, 1 mM $MgCl_2$, 1 mM TCEP) for 1 h at 37°C. Subsequently, the beads were washed eight times with Buffer C (20 mM Hepes pH 7.4, 1 mM TCEP) supplemented with (I) 100 mM NaCl, (II) 500 mM NaCl and 10 mM EGTA, (III) 1 mM $CaCl_2$, (IV) 1 mM $CaCl_2$ and 1 mM peptide 2 (SGGSSGGGSSG**LPETG**G), (V) 1 mM $CaCl_2$ and 4-(hydroxymercuri)benzoic acid sodium salt as SrtA inhibitor (#55540, Sigma-Aldrich), (VI+VII) 500 mM NaCl and 10 mM EGTA, or (VIII) 100 mM NaCl. MNPs coupled to enzymes were used immediately for subsequent analysis.

---

[i] The text for this section was reprinted with permission from Fauser *et al*, 2020 [215]. Copyright (2020) American Chemical Society.

6.5 Chemical methods [j]

Functionalization of MNPs (Peptide 1)

For functionalization of MNPs with peptide 1 (Fmoc-N′-GGGGSGGGSGGG-C′, purchased from GenScript), 1 equivalent of peptide 1, 2 equivalents of 1-bis(dimethylamino)methylene]-1H-1,2,3-triazolo[4,5-b]pyridinium-3-oxide hexafluorophosphate (HATU) (Sigma-Aldrich) and 2 equivalents of N,N-diisopropylethylenamine (Sigma-Aldrich) were dissolved in a total volume of 0.5 mL N,N-dimethylformamide (DMF) (Sigma-Aldrich). The total concentration of peptide 1 was adjusted to 1.2 mM. After 5 min, the reaction mixture was added to 3.125 mg silane coated ferric oxide core (mean diameter 0.5 µm) Amine Magnetic Beads (Raybiotech Inc., #801–113–2) and was gently shaken for 1 h at room temperature. Subsequently, the reaction mixture was withdrawn, and functionalized MNPs were submitted twice to 1 mL 20% piperidine (Sigma-Aldrich) for deprotection. After 10 min at room temperature, 20% piperidine was removed and functionalized MNPs washed several times in DMF and subsequently stored in PBS at 4 °C. Since no agglomeration was observed during the coupling procedure, we avoided the use of stabilizing agents.

---

[j] The text for this section was reprinted with permission from Fauser *et al*, 2020 [215]. Copyright (2020) American Chemical Society.

6.6 Analytical methods [k]

Bradford assay

Bradford assay (Thermo Scientific) was used according to a provided protocol by the manufacturer to determine protein concentrations.

GTPase nucleotide loading

The inactive Rab32:GDP variants were prepared by incubation of the crude protein extract with purified, tag-free SopD2 (50 nM) directly after cell disruption for 30 min at room temperature before the first IMAC was performed. The GTP or GppNHp exchange was performed in SEC buffer by supplementing the buffer with 5 mM EDTA and a 40-fold excess of the desired nucleotide to a small GTPase and incubated at room temperature for 2 h. Nucleotide exchange was stopped by adding 5 mM $MgCl_2$ (final concentration) to the protein solution and separation of the GTPase from an excess of nucleotide was performed using a NAP5 desalting column equilibrated with SEC buffer containing 10 μM GDP or 1 μM GppNHp respectively. Protein containing eluate was confirmed with NanoDrop™ 2000 (Thermo Scientific), flash-frozen in liquid nitrogen, and stored at -80°C. Nucleotide loading efficiency was verified by ion-pairing reversed-phase high-performance chromatography (RP-HPLC). To this end, protein samples (40 μM, 22 μL) were heat precipitated at 95°C for 5 min and centrifuged for 5 min at 21000 g. The supernatant was subjected to chromatographic separation on Shimadzu UFPLC (Prominence series) equipped with a C18 column (Prontosil C18, F184PS050, Bischoff Chromatography) using 50 mM potassium phosphate buffer pH 6.6, 10 mM tetra-n-butylammonium bromide, 12 % acetonitrile (v/v). Nucleotides were detected at 254 nm and resulting peaks were integrated and normalized to the total amount of nucleotides detected set to 100 %. The retention time of each nucleotide was determined with the respective nucleotide standard in a separate run. The same procedure was applied to other GTPases used in this work.

GTPase hydrolysis assay

After proteins were loaded with GTP, the nucleotide loading efficiency was verified by ion-pairing RP-HPLC (see GTPase nucleotide loading). Subsequently, Rab proteins (50 μM) were incubated for 30 min at room temperature in the absence or presence of catalytic amounts of SopD or SopD2 (1 μM). The reaction was stopped by heat (95°C for 5 min), the reaction mixtures were cleared by centrifugation (21000 g, 5 min, 4°C) and supernatants were submitted to nucleotide analysis on the ion-pairing RP-HPLC (see GTPase nucleotide loading). Resulting peaks of eluted nucleotides

---

[k] The text in this section was modified and reprinted with permission from Savitskiy *et al*, 2020 [248]. Copyright (2020) Elsevier.

were integrated and normalized to the data provided by corresponding single Rab proteins. The same procedure was applied for the kinetic studies of SopD and SopD2, but with lower enzyme amounts (85-500 nM, see Figure 27) and multiple incubation time points (0.5 – 120 min).

Protein complex formation on analytical size exclusion chromatography

For the complex formation of Rab32 with VARP-ANK1, GDI, and LRRK2$_{10-661}$ or HRas with RalGDS and RalGDS$_{N54R}$ or Rab8a with SopD a Superdex 75 10/300 GL (GE Healthcare) was attached to a UFPLC system (Prominence series, Shimadzu). For complex formation with VARP, the respective Rab32 preparation was incubated with VARP-ANK1 in a 1:1 molar ratio (50 µM) at 15°C for 1 hour. The same procedure was applied to other GTPase and effectors. For GDI binding studies, Rab32 was additionally farnesylated before the incubation with GDI for complex formation (1:1 molar ratio, 50 µM). Subsequently, 50 µl were chromatographically separated on an aSEC and fractionated to 0.5 ml fractions. The gel filtration buffer (20 mM HEPES at pH 7.5, 50 mM NaCl, 1 mM MgCl$_2$, 2 mM DTT, 10 µM GDP or 1 µM GppNHp respectively; the GDP containing buffer was supplemented with 2 mM AlCl$_3$ and 20 mM NaF for Rab8a:SopD aSEC runs) was used as a mobile phase for protein separation at 0.5 ml/min flow rate. Proteins were detected at 280 nm. The individual runs of single proteins served as a reference. Vitamin B$_{12}$ was used as an internal standard.

Native polyacrylamide gel electrophoresis (PAGE)

For native PAGE all samples were prepared in a non-reducing non-denaturing sample buffer (50 mM Tris (pH 6.8), 0.01 % (w/v) bromophenol blue, 25 % (v/v) glycerol) which allows maintaining the secondary structure and native charge density of the proteins of interest. The gels were prepared as described in Table M14 and 10-20 µl of samples (max. 1 µg of protein) were loaded on the gel and run for 4 h at 50 mA. Silver staining was used to visualize the protein bands.

Table M14 | Composition of a 6 % native polyacrylamide gel

Reagent	Volume
40 % Acrylamid:Bisacrylamide (29:1)	2 ml
4 x Tris glycine buffer (100 mM Tris base, 800 mM glycine, pH 8.5)	2.5 ml
ddH$_2$O	5.4 ml
10% APS	100 µl
TEMED	9 µl

Silver staining

Silver staining was performed according to the steps in Table M15.

Table M15 | Silver staining procedure for two gels

Step and buffer composition	Time
Fixation 60 ml 50% acetone (v/v) 1.5 ml 50% Trichloroacetic Acid 25 µl Formaldehyde (v/v) in ddH2O	5 min
Wash with ddH$_2$O	3 x 5 s
Pretreatment 1 60 ml 50% acetone (v/v)	5 min
Pretreatment 2 60 ml ddH$_2$O 100 µl 10% (w/v) Na$_2$S$_2$O$_3$ x 5H$_2$O	1 min
Wash with ddH$_2$O	3 x 5 s
Staining 60 ml ddH$_2$O 800 µl 20 % (w/v) AgNO$_3$ 600 µl 35 % Formaldehyde (v/v) in ddH$_2$O	8 min
Wash with ddH$_2$O	3 x 5 s
Development 60 ml ddH$_2$O 2.0 Na$_2$CO$_3$ 25 µl 35 % Formaldehyde (v/v) in ddH2O 25 µl 10 % (w/v) Na$_2$S$_2$O$_3$ x 5H$_2$O	30-60 s
Stopping 10 % Acetic acid (v/v) in ddH$_2$O	30-60 s
Wash with ddH$_2$O	3 x 5 s

SDS-PAGE

Proteins were separated using homemade 15 % acrylamide gels (Table M16) with Color Prestained Protein Standard (Broad Range (11–245 kDa), NEB). Gels used for GtgE kinetic measurements were loaded with 5 µg protein per line and were densitometrically analyzed via Image Lab Software (Bio-Rad) and normalized to MBP signal followed by exponential fit (OriginLab, 2019b, v9.65).

Table M16 | Composition of 15% SDS-PAGE gels. The amounts stated below are calculated for 4 gels with 1mm sickness.

Stacking gel	
Stacking gel buffer (4x)	1.5 ml
Acrylamide/Bis-acrylamide (30%)	1 ml
H$_2$O	3.5 ml
APS (10%)	48 µl
TEMED	6 µl

Resolving gel	
Resolving gel buffer (4x)	5 ml
Acrylamide/Bis-acrylamide (30%)	10 ml
H$_2$O	5 ml
APS (10%)	100 µl
TEMED	10 µl

Single-pair FRET measurements [l]

For the spFRET measurements, the Rab32 mutants were diluted to concentrations in the range of 20–100 pM in buffer containing 20 mM HEPES, 50 mM NaCl, 1 mM MgCl$_2$, and 10 µM GDP at pH 7.5. Measurements were carried out on a homebuilt [283] three-color dual-polarization confocal microscope with pulsed-interleaved excitation [284,285] and multi-parameter fluorescence detection [286] using only two of the laser lines (LDH-D-C-485, LDH-D-C-640, PicoQuant). The laser power measured before the objective was 100 µW for blue excitation and 70 µW for red excitation. Bursts of single molecules diffusing through the confocal volume of the microscope were measured for at least 3 h. The obtained data were analyzed with PAM [287], a Matlab-based software. Bursts with a minimum of 100 photons were selected and the ALEX-2CDE filter [288] was used to further narrow down the burst selection to only double-labeled proteins. Single-dye populations were used to calculate crosstalk and direct excitation. The γ-factor was calculated by linear interpolation of 1/S vs. E of a control measurement of a DNA sample containing two different FRET populations, since the protein measurements mainly showed only one population. Distances were determined using the photon distribution analysis [289] with a Förster radius of 52 Å, which was adjusted from the manufacturer's value based on an index of refraction of n = 1.4 and the decreased lifetime and thus the quantum yield of Alexa488.

---

[l] spFRET experiments were conducted by Vanessa Trauschke in collaboration with Prof. Don C. Lamb, LMU.

Molecular dynamics simulations [m]

The crystal structure of Rab32 in complex with GppCp and the effector VARP (PDB:4CYM [114]) served as the starting structure for the molecular dynamics simulations. VARP atoms were removed and the carbon atom between the β- and ɣ-phosphate was replaced with oxygen to replicate GTP. Furthermore, an Mg^{2+} ion was inserted in a position such that it had contact with both the β- and ɣ-phosphate. The gamma phosphate was removed to form the GDP-bound variants of Rab32. The Amber ff14sb force field [290] was used for the protein, while additional parameters for GDP and GTP were taken from the Amber parameter database [291]. The peptide bond between G59 and V60 was removed to form the proteolyzed variants of Rab32. Sodium and chloride ions were added to reach a salt concentration of 0.1 M. The complex was set at the center of a truncated octahedron box large enough to have a minimum distance of 10 Å from the edges and filled with water molecules that were modeled using OPC 4-point rigid model [292]. The solvated box was then energy minimized (5000 steps), followed by 25 ps of heating and 50 ps of density equilibration, followed by a simulation using an NPT ensemble at 300 K. During these phases, the protein's heavy atoms, the nucleotide, and the magnesium ions were restrained at their initial positions using a harmonic potential with a decreasing force constant starting at 5.0 $kcal.mol^{-1}Å^{-2}$ and ending with 1.0 $kcal.mol^{-1}Å^{-2}$. Production simulations were performed without any restraints. The pmemd version of the Amber 16 software package was used employing the hydrogen mass repartitioning feature of the Parmed tool, which allows a simulation time step of 4fs [293]. Long-range interactions were included using the particle mesh Ewald (PME) method combined with periodic boundary conditions and a 9 Å cut-off for real space non-bonded interactions. Trajectories were processed and analyzed using the CPPTRAJ program. Figures were generated using the PyMol software package [294].

NMR [n]

The uniformly ^{15}N-labeled NMR samples of Rab32 and KRas were at 100 µM protein concentration in buffer (20 mM HEPES pH 7.5, 50 mM NaCl, 1 mM $MgCl_2$, 2 mM DTT, 10 µM GDP) with 10% D_2O for a lock signal. NMR experiments were recorded at 298 K on a 600-MHz Bruker Avance NMR spectrometers with cryogenic triple resonance gradient probes. NMR spectra were processed by TOPSPIN3.5 (Bruker), then analyzed using NMRFAM-SPARKY [295].

Circular dichroism

Measurements of CD spectra were carried out on a JASCO 715 CD spectrometer equipped with a Peltier-temperature controller. Spectra were measured at 20 µM protein concentration in a

---

[m] MD simulations were performed by Danial P. J. Dehkordi in collaboration with Prof. Martin Zacharias, TUM.
[n] NMR data were collected and analyzed by Dr. Hyun-Seo Kang in collaboration with Prof. Michael Sattler, TUM.

quartz cuvette with 1 mm path length (Hellma) in 1 mM HEPES pH 7.5, 2.5 mM NaCl, 50 µM MgCl$_2$, 0.5 µM GDP or GppNHp. The temperature was increased by 30°C/h and molar ellipticity was measured at 220 nm. Data were normalized by setting the plateau signal of the thermally unfolded protein to 1.0 and fitted to a Boltzmann function.

Fluorescence spectroscopy

For determination of the nucleotide dissociation kinetics of Rab32 and Rab32$_{cleaved}$, appropriate GTPase was loaded with GDP or GppNHp (non-hydrolyzable GTP analog) bearing a mant fluorescent moiety. The mant-GDP or mant-GppNHp nucleotide dissociation was monitored via the release of the fluorescent nucleotide resulting in a decrease of the fluorescent signal using a fluorescence spectrometer Fluoromax-4 (Horiba Jobin Yvon) with the following parameters: λ_{exc}: 360 nm, λ_{em}: 440 nm, excitation slit: 1 nm, emission slit: 5 nm. Measurements were conducted at 25°C in 20 mM HEPES, 50 mM NaCl, 1 mM MgCl$_2$, 1 mM ß-ME at pH 7.5 with 500 nM Rab32. Nucleotide exchange was started by the addition of an excess of the corresponding mant-free nucleotide (20x) to the Rab32 in the cuvette (Hellma). Full dissociation was achieved by the addition of 5 mM EDTA into the cuvette to maximize the nucleotide release.

Mass spectrometry

All samples for mass spectrometry (MS) analysis were diluted in water to a final protein concentration of 0.1 mg/ml and 1 µl was applied to an ESI-ion trap mass spectrometer (LCQ fleet, Thermo Scientific) coupled to a UHPLC system (Ultimate 3000, Thermo Scientific) equipped with a ProSwift™ RP-4H column (1×50 mm, Thermo Scientific) at a flow rate of 0.2 ml/min. The proteins eluted with a linear gradient of 5–50% acetonitrile (0.1% formic acid) in 6 min. The total ion chromatogram raw data were analyzed with the Xcalibur Software v.3.1 (Thermo Scientific) and deconvoluted using MagTran v.1.02 [296].

Quantification of immobilized GtgE

After the coupling of GFP-enzyme fusion GtgE construct to MNPs, 190 µg TEV protease was added to 1.875 mg MNPs (corresponds to at least 2.5-fold molar excess of TEV) to ensure quantitative cleavage. In control experiments with soluble GFP-fusion constructs, less TEV (molar ratio of 1:1) was used. MNPs and soluble substrate were incubated overnight at 4 °C. Dilution of soluble proteolyzed substrate was used to generate a standard curve for GFP fluorescence. GFP fluorescence of the MNP supernatant was measured and quantified in TECAN Spark microplate reader (Tecan) at λ_{ex} = 475 nm and λ_{em} = 520 nm. The concentration of enzymes was assessed by Bradford assay.

Calculations of kinetic efficiencies

For the determination of nucleotide dissociation (k_{off}) measured by fluorescence spectroscopy, reaction curves were fitted to a one-phase exponential decay function with time constant parameter according to equation 1 using the software OriginPro (OriginLab, 2019b, v9.65).

$$F(t) = F_0 + F_A \cdot e^{-t \times k_{off}} \qquad \text{equation (1)}$$

with F(t): fluorescence intensity, F_0: minimum fluorescence intensity, F_A: total fluorescence amplitude (i.e. $F_{max} - F_0$, with F_{max}: maximum fluorescence intensity), k_{off}: dissociation constant.

For the determination of catalytic efficiencies (k_{cat}/K_M) of GTP hydrolysis verified by reversed-phase high-performance liquid chromatography (RP-HPLC), reaction curves were fitted to a single exponential function according to equation 2 using the software OriginPro 2019b (OriginLab, v9.65). The resulting rate constants(k_{obs}) was divided by the concentration of the used enzyme to gain k_{cat}/K_M values.

$$F(t) = F_0 + F_A \cdot e^{-k_{obs} \times t} \qquad \text{equation (2)}$$

with F(t): GTP amount, F_0: minimum GTP amount, F_A: total amplitude of GTP amount (i.e. $F_{max} - F_0$, with F_{max}: maximum GTP amount) and the k_{obs} is the observed rate constant. Statistical significance was validated by paired Student's t-test in GraphPad Prism (Version 4.0).

7. LICENSES AND PERMISSIONS

Figure 5 and **Figure 6** were adapted and modified with permission from Stenmark, 2009 [6]. Copyright (2020) Springer Nature Limited. License number 4933921463334.

SPRINGER NATURE

Rab GTPases as coordinators of vesicle traffic

Author: Harald Stenmark
Publication: Nature Reviews Molecular Cell Biology
Publisher: Springer Nature
Date: Jul 15, 2009

Copyright © 2009, Springer Nature

Quick Price Estimate

This service provides permission for reuse only.
If you do not have a copy of the article you are using, you may copy and paste the content and reuse according to the terms of your agreement. Please be advised that obtaining the content you license is a separate transaction not involving RightsLink.

⚑ This reuse request is free of charge although you are required to obtain a license through RightsLink and comply with the license terms and conditions. You will not be charged for this order. Please select the Continue button and place an order for this reuse.

⚑ Adaptations/modifications - Springer Nature allows adaptation of figures for style and formatting purposes under this license under the condition that this does not alter the meaning of the content.

I would like to... ⑦	reuse in a dissertation/thesis	Circulation/distribution ⑦	1 - 29
I am a/an... ⑦	academic/university or research institute	Are you the author of this Springer Nature content? ⑦	no
My format is... ⑦	print and electronic	I will be translating... ⑦	no
I would like to use... ⑦	figures/tables/illustrations	My currency is...	EUR - €
Number of figures/tables ⑦	2	Quick Price	0.00 EUR
High-res required ⑦	no		

QUICK PRICE **CONTINUE**

Terms and Conditions

SPRINGER NATURE LICENSE
TERMS AND CONDITIONS

Oct 21, 2020

This Agreement between Mr. Sergey Savitskiy ("You") and Springer Nature ("Springer Nature") consists of your license details and the terms and conditions provided by Springer Nature and Copyright Clearance Center.

License Number	4933921463334
License date	Oct 21, 2020
Licensed Content Publisher	Springer Nature
Licensed Content Publication	Nature Reviews Molecular Cell Biology
Licensed Content Title	Rab GTPases as coordinators of vesicle traffic
Licensed Content Author	Harald Stenmark
Licensed Content Date	Jul 15, 2009
Type of Use	Thesis/Dissertation
Requestor type	academic/university or research institute
Format	print and electronic
Portion	figures/tables/illustrations
Number of figures/tables/illustrations	2
High-res required	no
Will you be translating?	no

7. LICENSES AND PERMISSIONS

Circulation/distribution	1 - 29
Author of this Springer Nature content	no
Title	Manipulation of small GTPases by bacterial proteases and GTPase activating proteins
Institution name	TU Munich
Expected presentation date	Dec 2020
Portions	Figures 2 and 3
Requestor Location	Mr. Sergey Savitskiy Martinistr. 52 N45 IBS Hamburg, 20251 Germany Attn: Mr. Sergey Savitskiy
Total	0.00 EUR

Terms and Conditions

Springer Nature Customer Service Centre GmbH
Terms and Conditions

This agreement sets out the terms and conditions of the licence (the **Licence**) between you and **Springer Nature Customer Service Centre GmbH** (the **Licensor**). By clicking 'accept' and completing the transaction for the material (**Licensed Material**), you also confirm your acceptance of these terms and conditions.

1. Grant of License

1. 1. The Licensor grants you a personal, non-exclusive, non-transferable, world-wide licence to reproduce the Licensed Material for the purpose specified in your order only. Licences are granted for the specific use requested in the order and for no other use, subject to the conditions below.

1. 2. The Licensor warrants that it has, to the best of its knowledge, the rights to license reuse of the Licensed Material. However, you should ensure that the material you are requesting is original to the Licensor and does not carry the copyright of another entity (as credited in the published version).

1. 3. If the credit line on any part of the material you have requested indicates that it was reprinted or adapted with permission from another source, then you should also seek permission from that source to reuse the material.

2. Scope of Licence

2. 1. You may only use the Licensed Content in the manner and to the extent permitted by these Ts&Cs and any applicable laws.

2. 2. A separate licence may be required for any additional use of the Licensed Material, e.g. where a licence has been purchased for print only use, separate permission must be obtained for electronic re-use. Similarly, a licence is only valid in the language selected and does not apply for editions in other languages unless additional translation rights have been granted separately in the licence. Any content owned by third parties are expressly excluded from the licence.

2. 3. Similarly, rights for additional components such as custom editions and derivatives require additional permission and may be subject to an additional fee. Please apply to Journalpermissions@springernature.com/bookpermissions@springernature.com for these rights.

2. 4. Where permission has been granted **free of charge** for material in print, permission may also be granted for any electronic version of that work, provided that the material is incidental to your work as a whole and that the electronic version is essentially equivalent to, or substitutes for, the print version.

2. 5. An alternative scope of licence may apply to signatories of the STM Permissions Guidelines, as amended from time to time.

3. Duration of Licence

3. 1. A licence for is valid from the date of purchase ('Licence Date') at the end of the relevant period in the below table:

Scope of Licence	Duration of Licence
Post on a website	12 months
Presentations	12 months
Books and journals	Lifetime of the edition in the language purchased

4. Acknowledgement

4. 1. The Licensor's permission must be acknowledged next to the Licenced Material in print. In electronic form, this acknowledgement must be visible at the same time as the figures/tables/illustrations or abstract, and must be hyperlinked to the journal/book's homepage. Our required acknowledgement format is in the Appendix below.

5. Restrictions on use

5. 1. Use of the Licensed Material may be permitted for incidental promotional use and minor editing privileges e.g. minor adaptations of single figures, changes of format, colour and/or style where the adaptation is credited as set out in Appendix 1 below. Any

100

7. LICENSES AND PERMISSIONS

other changes including but not limited to, cropping, adapting, omitting material that affect the meaning, intention or moral rights of the author are strictly prohibited.

5. 2. You must not use any Licensed Material as part of any design or trademark.

5. 3. Licensed Material may be used in Open Access Publications (OAP) before publication by Springer Nature, but any Licensed Material must be removed from OAP sites prior to final publication.

6. Ownership of Rights

6. 1. Licensed Material remains the property of either Licensor or the relevant third party and any rights not explicitly granted herein are expressly reserved.

7. Warranty

IN NO EVENT SHALL LICENSOR BE LIABLE TO YOU OR ANY OTHER PARTY OR ANY OTHER PERSON OR FOR ANY SPECIAL, CONSEQUENTIAL, INCIDENTAL OR INDIRECT DAMAGES, HOWEVER CAUSED, ARISING OUT OF OR IN CONNECTION WITH THE DOWNLOADING, VIEWING OR USE OF THE MATERIALS REGARDLESS OF THE FORM OF ACTION, WHETHER FOR BREACH OF CONTRACT, BREACH OF WARRANTY, TORT, NEGLIGENCE, INFRINGEMENT OR OTHERWISE (INCLUDING, WITHOUT LIMITATION, DAMAGES BASED ON LOSS OF PROFITS, DATA, FILES, USE, BUSINESS OPPORTUNITY OR CLAIMS OF THIRD PARTIES), AND
WHETHER OR NOT THE PARTY HAS BEEN ADVISED OF THE POSSIBILITY OF SUCH DAMAGES. THIS LIMITATION SHALL APPLY NOTWITHSTANDING ANY FAILURE OF ESSENTIAL PURPOSE OF ANY LIMITED REMEDY PROVIDED HEREIN.

8. Limitations

8. 1. _BOOKS ONLY:_ Where **'reuse in a dissertation/thesis'** has been selected the following terms apply: Print rights of the final author's accepted manuscript (for clarity, NOT the published version) for up to 100 copies, electronic rights for use only on a personal website or institutional repository as defined by the Sherpa guideline (www.sherpa.ac.uk/romeo/).

9. Termination and Cancellation

9. 1. Licences will expire after the period shown in Clause 3 (above).

9. 2. Licensee reserves the right to terminate the Licence in the event that payment is not received in full or if there has been a breach of this agreement by you.

Appendix 1 — Acknowledgements:

101

For Journal Content:
Reprinted by permission from [**the Licensor**]: [**Journal Publisher** (e.g. Nature/Springer/Palgrave)] [**JOURNAL NAME**] [**REFERENCE CITATION** (Article name, Author(s) Name), [**COPYRIGHT**] (year of publication)

For **Advance Online Publication papers:**
Reprinted by permission from [**the Licensor**]: [**Journal Publisher** (e.g. Nature/Springer/Palgrave)] [**JOURNAL NAME**] [**REFERENCE CITATION** (Article name, Author(s) Name), [**COPYRIGHT**] (year of publication), advance online publication, day month year (doi: 10.1038/sj.[JOURNAL ACRONYM].)

For Adaptations/Translations:
Adapted/Translated by permission from [**the Licensor**]: [**Journal Publisher** (e.g. Nature/Springer/Palgrave)] [**JOURNAL NAME**] [**REFERENCE CITATION** (Article name, Author(s) Name), [**COPYRIGHT**] (year of publication)

<u>Note: For any republication from the British Journal of Cancer, the following credit line style applies:</u>

Reprinted/adapted/translated by permission from [**the Licensor**]: on behalf of Cancer Research UK: : [**Journal Publisher** (e.g. Nature/Springer/Palgrave)] [**JOURNAL NAME**] [**REFERENCE CITATION** (Article name, Author(s) Name), [**COPYRIGHT**] (year of publication)

For **Advance Online Publication** papers:
Reprinted by permission from The [**the Licensor**]: on behalf of Cancer Research UK: [**Journal Publisher** (e.g. Nature/Springer/Palgrave)] [**JOURNAL NAME**] [**REFERENCE CITATION** (Article name, Author(s) Name), [**COPYRIGHT**] (year of publication), advance online publication, day month year (doi: 10.1038/sj.[JOURNAL ACRONYM])

For Book content:
Reprinted/adapted by permission from [**the Licensor**]: [**Book Publisher** (e.g. Palgrave Macmillan, Springer etc) [**Book Title**] by [**Book author(s)**] [**COPYRIGHT**] (year of publication)

Other Conditions:

Version 1.2

Questions? customercare@copyright.com or +1-855-239-3415 (toll free in the US) or +1-978-646-2777.

Figure 15, **Figure 16**, **Figure 17**, **Table 5**, and text passages for the introduction, results, and methods were reprinted, modified, and adapted with permission from Fauser et al, 2020 [215]. Copyright (2020) American Chemical Society.

Figure 18, **Figure 19**, **Figure 20**, **Figure 21**, **Figure 22**, **Figure 29**, supplementary figures, and text passages for results, discussion, and methods were reprinted, modified and adapted with permission from Savitskiy et al (2020) [248]. Copyright (2020) Elsevier. The manuscript is now under review in iScience.

PERMISSION FOR DATA USE AND PRESENTATION

We, hereby, give Sergey Savitskiy our permission for the use and presentation of data, figures, tables, and texts in his dissertation, which were generated during our mutual collaboration.

Prof. Itzen, Aymelt _____

Prof. Lamb, Don C. _____

Prof. Sattler, Michael _____

Prof. Zacharias, Martin _____

Dr. Gülen, Burak _____

Dr. Kang, Hyun-Seo _____

Dr. Wachtel, Rudolf _____

Dehkordi, Danial P. J. _____

Fauser, Joel _____

Fottner, Maximilian _____

Trauschke, Vanessa _____

Oktober 2020

8. REFERENCES

1. Janoueix-Lerosey, I., Jollivet, F., Camonis, J., Marche, P. N. & Goud, B. (1995). Two-hybrid system screen with the small GTP-binding protein Rab6. Identification of a novel mouse GDP dissociation inhibitor isoform and two other potential partners of Rab6. *The Journal of biological chemistry* **270**, 14801–14808.

2. Lindsay, A. J., Jollivet, F., Horgan, C. P., Khan, A. R., Raposo, G., McCaffrey, M. W. *et al. (*2013). Identification and characterization of multiple novel Rab-myosin Va interactions. *Molecular biology of the cell* **24**, 3420–3434.

3. Müller, M. P. & Goody, R. S. (2018). Molecular control of Rab activity by GEFs, GAPs and GDI. *Small GTPases* **9**, 5–21.

4. Downward, J. (1997). Cell cycle: Routine role for Ras. *Current Biology* **7**, R258-R260.

5. Takai, Y., Sasaki, T. & Matozaki, T. (2001). Small GTP-binding proteins. *Physiological reviews* **81**, 153–208.

6. Stenmark, H. (2009). Rab GTPases as coordinators of vesicle traffic. *Nature reviews. Molecular cell biology* **10**, 513–525.

7. Wennerberg, K., Rossman, K. L. & Der, C. J. (2005). The Ras superfamily at a glance. *Journal of cell science* **118**, 843–846.

8. Zhen, Y. & Stenmark, H. (2015). Cellular functions of Rab GTPases at a glance. *Journal of cell science* **128**, 3171–3176.

9. Touchot, N., Chardin, P. & Tavitian, A. (1987). Four additional members of the ras gene superfamily isolated by an oligonucleotide strategy: molecular cloning of YPT-related cDNAs from a rat brain library. *Proceedings of the National Academy of Sciences of the United States of America* **84**, 8210–8214.

10. Brumell, J. H. & Scidmore, M. A. (2007). Manipulation of rab GTPase function by intracellular bacterial pathogens. *Microbiology and molecular biology reviews* **71**, 636–652.

11. Sherwood, R. K. & Roy, C. R. (2013). A Rab-centric perspective of bacterial pathogen-occupied vacuoles. *Cell host & microbe* **14**, 256–268.

12. Silva, M. T. (2012). Classical labeling of bacterial pathogens according to their lifestyle in the host: inconsistencies and alternatives. *Frontiers in microbiology* **3**, 71.

13. Stein, M.-P., Müller, M. P. & Wandinger-Ness, A. (2012). Bacterial pathogens commandeer Rab GTPases to establish intracellular niches. *Traffic (Copenhagen, Denmark)* **13**, 1565–1588.

14. Krengel, U., Scheffzek, K., Scherer, A., Kabsch, W., Wittinghofer, A. & Pai, E. F. (1994). Struktur und Guanosintriphosphat-Hydrolysemechanismus des c-terminal verkuerzten menschlichen Krebsproteins p21-H-Ras.

15. Verstraeten, N., Fauvart, M., Versées, W. & Michiels, J. (2011). The universally conserved prokaryotic GTPases. *Microbiology and molecular biology reviews* **75**, 507-42, second and third pages of table of contents.

16. Wittinghofer, A. & Vetter, I. R. (2011). Structure-function relationships of the G domain, a canonical switch motif. *Annual review of biochemistry* **80**, 943–971.

17. Khan, A. R. & Ménétrey, J. (2013). Structural biology of Arf and Rab GTPases' effector recruitment and specificity. *Structure (London, England: 1993)* **21**, 1284–1297.

18. Feltham, J. L., Dötsch, V., Raza, S., Manor, D., Cerione, R. A., Sutcliffe, M. J. *et al. (*1997). Definition of the switch surface in the solution structure of Cdc42Hs. *Biochemistry* **36**, 8755–8766.

19. Milburn, M. V., Tong, L., deVos, A. M., Brünger, A., Yamaizumi, Z., Nishimura, S. *et al. (*1990). Molecular switch for signal transduction: structural differences between active and inactive forms of protooncogenic ras proteins. *Science (New York, N.Y.)* **247**, 939–945.

20. Constantinescu, A.-T., Rak, A., Alexandrov, K., Esters, H., Goody, R. S. & Scheidig, A. J. (2002). Rab-Subfamily-Specific Regions of Ypt7p Are Structurally Different from Other RabGTPases. *Structure* **10**, 569–579.

21. Pai, E. F., Krengel, U., Petsko, G. A., Goody, R. S., Kabsch, W. & Wittinghofer, A. (1990). Refined crystal structure of the triphosphate conformation of H-ras p21 at 1.35 A resolution: implications for the mechanism of GTP hydrolysis. *The EMBO journal* **9**, 2351–2359.

22. Eathiraj, S., Pan, X., Ritacco, C. & Lambright, D. G. (2005). Structural basis of family-wide Rab GTPase recognition by rabenosyn-5. *Nature* **436**, 415–419.

23. Cherfils, J. & Zeghouf, M. (2013). Regulation of small GTPases by GEFs, GAPs, and GDIs. *Physiological reviews* **93**, 269–309.

24. Barr, F. & Lambright, D. G. (2010). Rab GEFs and GAPs. *Current opinion in cell biology* **22**, 461–470.

25. Traut, T. W. (1994). Physiological concentrations of purines and pyrimidines. *Molecular and cellular biochemistry* **140**, 1–22.

26. Pan, X., Eathiraj, S., Munson, M. & Lambright, D. G. (2006). TBC-domain GAPs for Rab GTPases accelerate GTP hydrolysis by a dual-finger mechanism. *Nature* **442**, 303–306.

27. Jin, Y., Molt, R. W. & Blackburn, G. M. (2017). Metal Fluorides: Tools for Structural and Computational Analysis of Phosphoryl Transfer Enzymes. *Topics in current chemistry (Cham)* **375**, 36.

28. Blümer, J., Rey, J., Dehmelt, L., Mazel, T., Wu, Y.-W., Bastiaens, P. *et al. (*2013). RabGEFs are a major determinant for specific Rab membrane targeting. *The Journal of cell biology* **200**, 287–300.

29. Gomes, A. Q., Ali, B. R., Ramalho, J. S., Godfrey, R. F., Barral, D. C., Hume, A. N. *et al. (*2003). Membrane targeting of Rab GTPases is influenced by the prenylation motif. *Molecular biology of the cell* **14**, 1882–1899.

30. Collins, R. N. (2003). "Getting It On"—GDI Displacement and Small GTPase Membrane Recruitment. *Molecular cell* **12**, 1064–1066.

31. Ignatev, A., Kravchenko, S., Rak, A., Goody, R. S. & Pylypenko, O. (2008). A structural model of the GDP dissociation inhibitor rab membrane extraction mechanism. *The Journal of biological chemistry* **283**, 18377–18384.

32. Ueda, T., Kikuchi, A., Ohga, N., Yamamoto, J. & Takai, Y. (1990). Purification and characterization from bovine brain cytosol of a novel regulatory protein inhibiting the dissociation of GDP from and the subsequent binding of GTP to rhoB p20, a ras p21-like GTP-binding protein. *The Journal of biological chemistry* **265**, 9373–9380.

33. Wu, Y.-W., Tan, K.-T., Waldmann, H., Goody, R. S. & Alexandrov, K. (2007). Interaction analysis of prenylated Rab GTPase with Rab escort protein and GDP dissociation inhibitor explains the need for both regulators. *Proceedings of the National Academy of Sciences of the United States of America* **104**, 12294–12299.

34. Coleman, M. L., Marshall, C. J. & Olson, M. F. (2004). RAS and RHO GTPases in G1-phase cell-cycle regulation. *Nat Rev Mol Cell Biol* **5**, 355–366.

35. Ahearn, I. M., Haigis, K., Bar-Sagi, D. & Philips, M. R. (2011). Regulating the regulator: post-translational modification of RAS. *Nat Rev Mol Cell Biol* **13**, 39–51.

36. Neel, N. F., Martin, T. D., Stratford, J. K., Zand, T. P., Reiner, D. J. & Der, C. J. (2011). The RalGEF-Ral Effector Signaling Network: The Road Less Traveled for Anti-Ras Drug Discovery. *Genes & Cancer* **2**, 275–287.

37. Sasaki, A. T., Chun, C., Takeda, K. & Firtel, R. A. (2004). Localized Ras signaling at the leading edge regulates PI3K, cell polarity, and directional cell movement. *The Journal of cell biology* **167**, 505–518.

38. Oeckinghaus, A. & Ghosh, S. (2009). The NF-kappaB family of transcription factors and its regulation. *Cold Spring Harbor perspectives in biology* **1**, a000034.

39. Fernández-Medarde, A. & Santos, E. (2011). Ras in cancer and developmental diseases. *Genes & Cancer* **2**, 344–358.

40. Prior, I. A., Lewis, P. D. & Mattos, C. (2012). A comprehensive survey of Ras mutations in cancer. *Cancer Research* **72**, 2457–2467.

41. Hobbs, G. A., Der, C. J. & Rossman, K. L. (2016). RAS isoforms and mutations in cancer at a glance. *Journal of cell science* **129**, 1287–1292.

42. Lin, D. T. S., Davis, N. G. & Conibear, E. (2017). Targeting the Ras palmitoylation/depalmitoylation cycle in cancer. *Biochemical Society transactions* **45**, 913–921.

43. Barbieri, E., Di Fiore, P. P. & Sigismund, S. (2016). Endocytic control of signaling at the plasma membrane. *Current opinion in cell biology* **39**, 21–27.

44. Sigismund, S., Confalonieri, S., Ciliberto, A., Polo, S., Scita, G. & Di Fiore, P. P. (2012). Endocytosis and signaling: cell logistics shape the eukaryotic cell plan. *Physiological reviews* **92**, 273–366.

45. Buratta, S., Tancini, B., Sagini, K., Delo, F., Chiaradia, E., Urbanelli, L. *et al. (*2020). Lysosomal Exocytosis, Exosome Release and Secretory Autophagy: The Autophagic- and Endo-Lysosomal Systems Go Extracellular. *International journal of molecular sciences* **21**.

46. Stahl, B., Chou, J. H., Li, C., Südhof, T. C. & Jahn, R. (1996). Rab3 reversibly recruits rabphilin to synaptic vesicles by a mechanism analogous to raf recruitment by ras. *The EMBO journal* **15**, 1799–1809.

47. Vieira, O. V. (2018). Rab3a and Rab10 are regulators of lysosome exocytosis and plasma membrane repair. *Small GTPases* **9**, 349–351.

48. Agola, J. O., Jim, P. A., Ward, H. H., Basuray, S. & Wandinger-Ness, A. (2011). Rab GTPases as regulators of endocytosis, targets of disease and therapeutic opportunities. *Clinical genetics* **80**, 305–318.

49. Bonifacino, J. S. & Glick, B. S. (2004). The Mechanisms of Vesicle Budding and Fusion. *Cell* **116**, 153–166.

50. Hehnly, H. & Stamnes, M. (2007). Regulating cytoskeleton-based vesicle motility. *FEBS letters* **581**, 2112–2118.

51. Alexandrov, K., Simon, I., Yurchenko, V., Iakovenko, A., Rostkova, E., Scheidig, A. J. *et al. (*1999). Characterization of the ternary complex between Rab7, REP-1 and Rab geranylgeranyl transferase. *European journal of biochemistry* **265**, 160–170.

52. Guo, Z., Wu, Y.-W., Das, D., Delon, C., Cramer, J., Yu, S. *et al. (*2008). Structures of RabGGTase-substrate/product complexes provide insights into the evolution of protein prenylation. *The EMBO journal* **27**, 2444–2456.

53. Sivars, U., Aivazian, D. & Pfeffer, S. R. (2003). Yip3 catalyses the dissociation of endosomal Rab-GDI complexes. *Nature* **425**, 856–859.

54. Dirac-Svejstrup, A. B., Sumizawa, T. & Pfeffer, S. R. (1997). Identification of a GDI displacement factor that releases endosomal Rab GTPases from Rab-GDI. *The EMBO journal* **16**, 465–472. https://www.embopress.org/doi/10.1093/emboj/16.3.465.

55. Schoebel, S., Oesterlin, L. K., Blankenfeldt, W., Goody, R. S. & Itzen, A. (2009). RabGDI displacement by DrrA from Legionella is a consequence of its guanine nucleotide exchange activity. *Molecular cell* **36**, 1060–1072.

56. Padfield, P. J., Balch, W. E. & Jamieson, J. D. (1992). A synthetic peptide of the rab3a effector domain stimulates amylase release from permeabilized pancreatic acini. *Proceedings of the National Academy of Sciences of the United States of America* **89**, 1656–1660.

57. Sakane, A., Manabe, S., Ishizaki, H., Tanaka-Okamoto, M., Kiyokage, E., Toida, K. *et al. (*2006). Rab3 GTPase-activating protein regulates synaptic transmission and plasticity through the inactivation of Rab3. *Proceedings of the National Academy of Sciences of the United States of America* **103**, 10029–10034.

58. Anand, S., Khan, M. A., Khushman, M.'d., Dasgupta, S., Singh, S. & Singh, A. P. (2020). Comprehensive Analysis of Expression, Clinicopathological Association and Potential Prognostic Significance of RABs in Pancreatic Cancer. *International journal of molecular sciences* **21**.

59. Guadagno, N. A. & Progida, C. (2019). Rab GTPases: Switching to Human Diseases. *Cells* **8**.

60. Kiral, F. R., Kohrs, F. E., Jin, E. J. & Hiesinger, P. R. (2018). Rab GTPases and Membrane Trafficking in Neurodegeneration. *Current Biology* **28**, R471-R486.

61. Seabra, M. C., Mules, E. H. & Hume, A. N. (2002). Rab GTPases, intracellular traffic and disease. *Trends in Molecular Medicine* **8**, 23–30.

62. Settembre, C., Fraldi, A., Medina, D. L. & Ballabio, A. (2013). Signals from the lysosome: a control centre for cellular clearance and energy metabolism. *Nature reviews. Molecular cell biology* **14**, 283–296.

63. Gopal Krishnan, P. D., Golden, E., Woodward, E. A., Pavlos, N. J. & Blancafort, P. (2020). Rab GTPases: Emerging Oncogenes and Tumor Suppressive Regulators for the Editing of Survival Pathways in Cancer. *Cancers* **12**.

64. Wheeler, D. B., Zoncu, R., Root, D. E., Sabatini, D. M. & Sawyers, C. L. (2015). Identification of an oncogenic RAB protein. *Science (New York, N.Y.)* **350**, 211–217.

65. Armstrong, J., Thompson, N., Squire, J. H., Smith, J., Hayes, B. & Solari, R. (1996). Identification of a novel member of the Rab8 family from the rat basophilic leukaemia cell line, RBL.2H3. *Journal of cell science* **109 (Pt 6)**, 1265–1274.

66. Jaldin-Fincati, J. R., Pavarotti, M., Frendo-Cumbo, S., Bilan, P. J. & Klip, A. (2017). Update on GLUT4 Vesicle Traffic: A Cornerstone of Insulin Action. *Trends in endocrinology and metabolism: TEM* **28**, 597–611.

67. Klip, A., McGraw, T. E. & James, D. E. (2019). Thirty sweet years of GLUT4. *The Journal of biological chemistry* **294**, 11369–11381.

68. Sato, T., Mushiake, S., Kato, Y., Sato, K., Sato, M., Takeda, N. *et al. (*2007). The Rab8 GTPase regulates apical protein localization in intestinal cells. *Nature* **448**, 366–369.

69. Bangs, F. & Anderson, K. V. (2017). Primary Cilia and Mammalian Hedgehog Signaling. *Cold Spring Harbor perspectives in biology* **9**.

70. Lu, Q., Insinna, C., Ott, C., Stauffer, J., Pintado, P. A., Rahajeng, J. *et al. (*2015). Early steps in primary cilium assembly require EHD1/EHD3-dependent ciliary vesicle formation. *Nature cell biology* **17**, 228–240.

71. Nachury, M. V., Loktev, A. V., Zhang, Q., Westlake, C. J., Peränen, J., Merdes, A. *et al. (*2007). A core complex of BBS proteins cooperates with the GTPase Rab8 to promote ciliary membrane biogenesis. *Cell* **129**, 1201–1213.

72. Zhu, S.-L., Luo, M.-Q., Peng, W.-X., Li, Q.-X., Feng, Z.-Y., Li, Z.-X. *et al. (*2015). Sonic hedgehog signalling pathway regulates apoptosis through Smo protein in human umbilical vein endothelial cells. *Rheumatology (Oxford, England)* **54**, 1093–1102.

73. Corbier, C. & Sellier, C. (2017). C9ORF72 is a GDP/GTP exchange factor for Rab8 and Rab39 and regulates autophagy. *Small GTPases* **8**, 181–186.

74. Roland, J. T., Kenworthy, A. K., Peranen, J., Caplan, S. & Goldenring, J. R. (2007). Myosin Vb interacts with Rab8a on a tubular network containing EHD1 and EHD3. *Molecular biology of the cell* **18**, 2828–2837.

75. Eguchi, T., Kuwahara, T., Sakurai, M., Komori, T., Fujimoto, T., Ito, G. *et al. (*2018). LRRK2 and its substrate Rab GTPases are sequentially targeted onto stressed lysosomes and maintain their homeostasis. *Proceedings of the National Academy of Sciences of the United States of America* **115**, E9115-E9124.

76. Lee, H., Flynn, R., Sharma, I., Haberman, E., Carling, P. J., Nicholls, F. J. *et al. (*2020). LRRK2 Is Recruited to Phagosomes and Co-recruits RAB8 and RAB10 in Human Pluripotent Stem Cell-Derived Macrophages. *Stem cell reports* **14**, 940–955.

77. Alessi, D. R. & Sammler, E. (2018). LRRK2 kinase in Parkinson's disease. *Science (New York, N.Y.)* **360**, 36–37.

78. Rivero-Ríos, P., Romo-Lozano, M., Madero-Pérez, J., Thomas, A. P., Biosa, A., Greggio, E. *et al. (*2019). The G2019S variant of leucine-rich repeat kinase 2 (LRRK2) alters endolysosomal trafficking by impairing the function of the GTPase RAB8A. *The Journal of biological chemistry* **294**, 4738–4758.

79. Lara Ordónez, A. J., Fernández, B., Fdez, E., Romo-Lozano, M., Madero-Pérez, J., Lobbestael, E. *et al. (*2019). RAB8, RAB10 and RILPL1 contribute to both LRRK2 kinase-mediated centrosomal cohesion and ciliogenesis deficits. *Human molecular genetics* **28**, 3552–3568.

80. Waschbüsch, D., Purlyte, E., Pal, P., McGrath, E., Alessi, D. R. & Khan, A. R. (2020). Structural Basis for Rab8a Recruitment of RILPL2 via LRRK2 Phosphorylation of Switch 2. *Structure (London, England: 1993)* **28**, 406-417.e6.

81. Reuter, T., Vorwerk, S., Liss, V., Chao, T.-C., Hensel, M. & Hansmeier, N. (2020). Proteomic Analysis of Salmonella-modified Membranes Reveals Adaptations to Macrophage Hosts. *Molecular & cellular proteomics* **19**, 900–912.

82. Anand, I. S., Choi, W. & Isberg, R. R. (2020). Components of the endocytic and recycling trafficking pathways interfere with the integrity of the Legionella-containing vacuole. *Cellular microbiology* **22**, e13151.

83. Kehl, A., Göser, V., Reuter, T., Liss, V., Franke, M., John, C. *et al. (*2020). A trafficome-wide RNAi screen reveals deployment of early and late secretory host proteins and the entire late endo-/lysosomal vesicle fusion machinery by intracellular Salmonella. *PLoS pathogens* **16**, e1008220.

84. Ohbayashi, N., Fukuda, M. & Kanaho, Y. (2017). Rab32 subfamily small GTPases: pleiotropic Rabs in endosomal trafficking. *Journal of biochemistry* **162**, 65–71.

85. Shimizu, F., Katagiri, T., Suzuki, M., Watanabe, T. K., Okuno, S., Kuga, Y. *et al. (*1997). Cloning and chromosome assignment to 1q32 of a human cDNA (RAB7L1) encoding a small GTP-binding protein, a member of the RAS superfamily. *Cytogenetics and cell genetics* **77**, 261–263.

86. Massmann, S., Schürmann, A. & Joost, H.-G. (1997). Cloning of two splicing variants of the novel Ras-related GTPase Rab29 which is predominately expressed in kidney. *Biochimica et Biophysica Acta (BBA) - Gene Structure and Expression* **1352**, 48–55.

87. Helip-Wooley, A. & Thoene, J. G. (2004). Sucrose-induced vacuolation results in increased expression of cholesterol biosynthesis and lysosomal genes. *Experimental cell research* **292**, 89–100.

88. Wang, S., Ma, Z., Xu, X., Wang, Z., Sun, L., Zhou, Y. *et al. (*2014). A role of Rab29 in the integrity of the trans-Golgi network and retrograde trafficking of mannose-6-phosphate receptor. *PloS one* **9**, e96242.

89. Santpere, G. & Ferrer, I. (2009). LRRK2 and neurodegeneration. *Acta neuropathologica* **117**, 227–246.

90. MacLeod, D. A., Rhinn, H., Kuwahara, T., Zolin, A., Di Paolo, G., McCabe, B. D. *et al. (*2013). RAB7L1 interacts with LRRK2 to modify intraneuronal protein sorting and Parkinson's disease risk. *Neuron* **77**, 425–439.

91. McGrath, E., Waschbüsch, D., Baker, B. M. & Khan, A. R. (2019). LRRK2 binds to the Rab32 subfamily in a GTP-dependent manner via its armadillo domain. *Small GTPases*, 1–14.

92. Purlyte, E., Dhekne, H. S., Sarhan, A. R., Gomez, R., Lis, P., Wightman, M. *et al. (*2018). Rab29 activation of the Parkinson's disease-associated LRRK2 kinase. *The EMBO journal* **37**, 1–18.

93. Kuwahara, T., Inoue, K., D'Agati, V. D., Fujimoto, T., Eguchi, T., Saha, S. *et al. (*2016). LRRK2 and RAB7L1 coordinately regulate axonal morphology and lysosome integrity in diverse cellular contexts. *Scientific reports* **6**, 29945.

94. Madero-Pérez, J., Fdez, E., Fernández, B., Lara Ordóñez, A. J., Blanca Ramírez, M., Gómez-Suaga, P. *et al. (*2018). Parkinson disease-associated mutations in LRRK2 cause centrosomal defects via Rab8a phosphorylation. *Molecular neurodegeneration* **13**, 3.

95. Madero-Pérez, J., Fernández, B., Lara Ordóñez, A. J., Fdez, E., Lobbestael, E., Baekelandt, V. *et al. (*2018). RAB7L1-Mediated Relocalization of LRRK2 to the Golgi Complex Causes Centrosomal Deficits via RAB8A. *Frontiers in molecular neuroscience* **11**, 417.

96. Berger, K. L., Cooper, J. D., Heaton, N. S., Yoon, R., Oakland, T. E., Jordan, T. X. *et al. (*2009). Roles for endocytic trafficking and phosphatidylinositol 4-kinase III alpha in hepatitis C virus

replication. *Proceedings of the National Academy of Sciences of the United States of America* **106**, 7577–7582.

97. Aoki, Y., Manzano, R., Lee, Y., Dafinca, R., Aoki, M., Douglas, A. G. L. *et al. (*2017). C9orf72 and RAB7L1 regulate vesicle trafficking in amyotrophic lateral sclerosis and frontotemporal dementia. *Brain: a journal of neurology* **140**, 887–897.

98. Onnis, A., Finetti, F., Patrussi, L., Gottardo, M., Cassioli, C., Spanò, S. *et al. (*2015). The small GTPase Rab29 is a common regulator of immune synapse assembly and ciliogenesis. *Cell death and differentiation* **22**, 1687–1699.

99. Spanò, S., Liu, X. & Galán, J. E. (2011). Proteolytic targeting of Rab29 by an effector protein distinguishes the intracellular compartments of human-adapted and broad-host Salmonella. *Proceedings of the National Academy of Sciences of the United States of America* **108**, 18418–18423.

100. Coppola, U., Annona, G., D'Aniello, S. & Ristoratore, F. (2016). Rab32 and Rab38 genes in chordate pigmentation: an evolutionary perspective. *BMC evolutionary biology* **16**, 26.

101. Aguilar, A., Weber, J., Boscher, J., Freund, M., Ziessel, C., Eckly, A. *et al. (*2019). Combined deficiency of RAB32 and RAB38 in the mouse mimics Hermansky-Pudlak syndrome and critically impairs thrombosis. *Blood advances* **3**, 2368–2380.

102. Bao, X., Faris, A. E., Jang, E. K. & Haslam, R. J. (2002). Molecular cloning, bacterial expression and properties of Rab31 and Rab32. *European journal of biochemistry* **269**, 259–271.

103. Osanai, K., Takahashi, K., Nakamura, K., Takahashi, M., Ishigaki, M., Sakuma, T. *et al. (*2005). Expression and characterization of Rab38, a new member of the Rab small G protein family. *Biological chemistry* **386**, 143–153.

104. Bultema, J. J., Boyle, J. A., Malenke, P. B., Martin, F. E., Dell'Angelica, E. C., Cheney, R. E. *et al. (*2014). Myosin vc interacts with Rab32 and Rab38 proteins and works in the biogenesis and secretion of melanosomes. *The Journal of biological chemistry* **289**, 33513–33528.

105. Loftus, S. K., Larson, D. M., Baxter, L. L., Antonellis, A., Chen, Y., Wu, X. *et al. (*2002). Mutation of melanosome protein RAB38 in chocolate mice. *Proceedings of the National Academy of Sciences of the United States of America* **99**, 4471–4476.

106. Marubashi, S., Shimada, H., Fukuda, M. & Ohbayashi, N. (2016). RUTBC1 Functions as a GTPase-activating Protein for Rab32/38 and Regulates Melanogenic Enzyme Trafficking in Melanocytes. *The Journal of biological chemistry* **291**, 1427–1440.

107. Wasmeier, C., Romao, M., Plowright, L., Bennett, D. C., Raposo, G. & Seabra, M. C. (2006). Rab38 and Rab32 control post-Golgi trafficking of melanogenic enzymes. *The Journal of cell biology* **175**, 271–281.

108. Bultema, J. J., Ambrosio, A. L., Burek, C. L. & Di Pietro, S. M. (2012). BLOC-2, AP-3, and AP-1 proteins function in concert with Rab38 and Rab32 proteins to mediate protein trafficking to lysosome-related organelles. *The Journal of biological chemistry* **287**, 19550–19563.

109. Di Pietro, S. M., Falcón-Pérez, J. M. & Dell'Angelica, E. C. (2004). Characterization of BLOC-2, a complex containing the Hermansky-Pudlak syndrome proteins HPS3, HPS5 and HPS6. *Traffic (Copenhagen, Denmark)* **5**, 276–283.

110. El-Chemaly, S. & Young, L. R. (2016). Hermansky-Pudlak Syndrome. *Clinics in chest medicine* **37**, 505–511.

111. Gerondopoulos, A., Langemeyer, L., Liang, J.-R., Linford, A. & Barr, F. A. (2012). BLOC-3 mutated in Hermansky-Pudlak syndrome is a Rab32/38 guanine nucleotide exchange factor. *Current Biology* **22**, 2135–2139.

112. Martina, J. A., Moriyama, K. & Bonifacino, J. S. (2003). BLOC-3, a protein complex containing the Hermansky-Pudlak syndrome gene products HPS1 and HPS4. *The Journal of biological chemistry* **278**, 29376–29384.

113. Nottingham, R. M., Ganley, I. G., Barr, F. A., Lambright, D. G. & Pfeffer, S. R. (2011). RUTBC1 protein, a Rab9A effector that activates GTP hydrolysis by Rab32 and Rab33B proteins. *The Journal of biological chemistry* **286**, 33213–33222.

114.   Hesketh, G. G., Pérez-Dorado, I., Jackson, L. P., Wartosch, L., Schäfer, I. B., Gray, S. R. *et al.* (2014). VARP is recruited on to endosomes by direct interaction with retromer, where together they function in export to the cell surface. *Developmental cell* **29**, 591–606.

115.   Tamura, K., Ohbayashi, N., Maruta, Y., Kanno, E., Itoh, T. & Fukuda, M. (2009). Varp is a novel Rab32/38-binding protein that regulates Tyrp1 trafficking in melanocytes. *Molecular biology of the cell* **20**, 2900–2908.

116.   Wang, F., Zhang, H., Zhang, X., Wang, Y., Ren, F., Zhang, X. *et al.* (2008). Varp interacts with Rab38 and functions as its potential effector. *Biochemical and Biophysical Research Communications* **372**, 162–167.

117.   Fukuda, M. (2016). Multiple Roles of VARP in Endosomal Trafficking: Rabs, Retromer Components and R-SNARE VAMP7 Meet on VARP. *Traffic (Copenhagen, Denmark)* **17**, 709–719.

118.   Waschbüsch, D., Hübel, N., Ossendorf, E., Lobbestael, E., Baekelandt, V., Lindsay, A. J. *et al.* (2019). Rab32 interacts with SNX6 and affects retromer-dependent Golgi trafficking. *PloS one* **14**, e0208889.

119.   Alto, N. M., Soderling, J. & Scott, J. D. (2002). Rab32 is an A-kinase anchoring protein and participates in mitochondrial dynamics. *The Journal of cell biology* **158**, 659–668.

120.   Bui, M., Gilady, S. Y., Fitzsimmons, R. E. B., Benson, M. D., Lynes, E. M., Gesson, K. *et al.* (2010). Rab32 modulates apoptosis onset and mitochondria-associated membrane (MAM) properties. *The Journal of biological chemistry* **285**, 31590–31602.

121.   Drizyte-Miller, K., Chen, J., Cao, H., Schott, M. B. & McNiven, M. A. (2020). The small GTPase Rab32 resides on lysosomes to regulate mTORC1 signaling. *Journal of cell science*.

122.   Ao, X., Zou, L. & Wu, Y. (2014). Regulation of autophagy by the Rab GTPase network. *Cell death and differentiation* **21**, 348–358.

123.   Hu, Z.-Q., Rao, C.-L., Tang, M.-L., Zhang, Y., Lu, X.-X., Chen, J.-G. *et al.* (2019). Rab32 GTPase, as a direct target of miR-30b/c, controls the intracellular survival of Burkholderia pseudomallei by regulating phagosome maturation. *PLoS pathogens* **15**, e1007879.

124.   Li, Y., Wang, Y., Zou, L., Tang, X., Yang, Y., Ma, L. *et al.* (2016). Analysis of the Rab GTPase Interactome in Dendritic Cells Reveals Anti-microbial Functions of the Rab32 Complex in Bacterial Containment. *Immunity* **44**, 422–437.

125.   Seto, S., Tsujimura, K. & Koide, Y. (2011). Rab GTPases regulating phagosome maturation are differentially recruited to mycobacterial phagosomes. *Traffic (Copenhagen, Denmark)* **12**, 407–420.

126.   Chen, M., Sun, H., Boot, M., Shao, L., Chang, S.-J., Wang, W. *et al.* (2020). Itaconate is an effector of a Rab GTPase cell-autonomous host defense pathway against Salmonella. *Science (New York, N.Y.)* **369**, 450–455.

127.   Fisher, S. L. & Phillips, A. J. (2018). Targeted protein degradation and the enzymology of degraders. *Current opinion in chemical biology* **44**, 47–55.

128.   Han, Z.-J., Feng, Y.-H., Gu, B.-H., Li, Y.-M. & Chen, H. (2018). The post-translational modification, SUMOylation, and cancer (Review). *International journal of oncology* **52**, 1081–1094.

129.   Ivanovic-Burmazovic, I. & Filipovic, M. R. (2019). Saying NO to H2S: A Story of HNO, HSNO, and SSNO. *Inorganic chemistry* **58**, 4039–4051.

130.   Salazar-Roa, M. & Malumbres, M. (2017). Fueling the Cell Division Cycle. *Trends in cell biology* **27**, 69–81.

131.   Grassi, L. & Cabrele, C. (2019). Susceptibility of protein therapeutics to spontaneous chemical modifications by oxidation, cyclization, and elimination reactions. *Amino acids* **51**, 1409–1431.

132.   Salomon, D. & Orth, K. (2013). What pathogens have taught us about posttranslational modifications. *Cell host & microbe* **14**, 269–279.

133.   Kosciuk, T., Price, I. R., Zhang, X., Zhu, C., Johnson, K. N., Zhang, S. *et al. (*2020). NMT1 and NMT2 are lysine myristoyltransferases regulating the ARF6 GTPase cycle. *Nature communications* **11**, 1067.

134.   Hodge, R. G. & Ridley, A. J. (2016). Regulating Rho GTPases and their regulators. *Nat Rev Mol Cell Biol* **17**, 496–510.

135.   Guilluy, C., Rolli-Derkinderen, M., Tharaux, P.-L., Melino, G., Pacaud, P. & Loirand, G. (2007). Transglutaminase-dependent RhoA activation and depletion by serotonin in vascular smooth muscle cells. *The Journal of biological chemistry* **282**, 2918–2928.

136.   Paulmann, N., Grohmann, M., Voigt, J.-P., Bert, B., Vowinckel, J., Bader, M. *et al. (*2009). Intracellular serotonin modulates insulin secretion from pancreatic beta-cells by protein serotonylation. *PLoS biology* **7**, e1000229.

137.   Williams, J. G., Pappu, K. & Campbell, S. L. (2003). Structural and biochemical studies of p21Ras S-nitrosylation and nitric oxide-mediated guanine nucleotide exchange. *Proceedings of the National Academy of Sciences of the United States of America* **100**, 6376–6381.

138.   Ree, R., Varland, S. & Arnesen, T. (2018). Spotlight on protein N-terminal acetylation. *Experimental & molecular medicine* **50**, 1–13.

139.   Castillo-Lluva, S., Tatham, M. H., Jones, R. C., Jaffray, E. G., Edmondson, R. D., Hay, R. T. *et al. (*2010). SUMOylation of the GTPase Rac1 is required for optimal cell migration. *Nature cell biology* **12**, 1078–1085.

140.   Lai, Y.-C., Kondapalli, C., Lehneck, R., Procter, J. B., Dill, B. D., Woodroof, H. I. *et al. (*2015). Phosphoproteomic screening identifies Rab GTPases as novel downstream targets of PINK1. *The EMBO journal* **34**, 2840–2861.

141.   Levin, R. S., Hertz, N. T., Burlingame, A. L., Shokat, K. M. & Mukherjee, S. (2016). Innate immunity kinase TAK1 phosphorylates Rab1 on a hotspot for posttranslational modifications by host and pathogen. *Proceedings of the National Academy of Sciences of the United States of America* **113**, E4776-83.

142.   Olson, M. F. (2018). Rho GTPases, their post-translational modifications, disease-associated mutations and pharmacological inhibitors. *Small GTPases* **9**, 203–215.

143.   Lachance, V., Degrandmaison, J., Marois, S., Robitaille, M., Génier, S., Nadeau, S. *et al. (*2014). Ubiquitylation and activation of a Rab GTPase is promoted by a β_2AR-HACE1 complex. *Journal of cell science* **127**, 111–123.

144.   Yano, H., Kobayashi, I., Onodera, Y., Luton, F., Franco, M., Mazaki, Y. *et al. (*2008). Fbx8 makes Arf6 refractory to function via ubiquitination. *Molecular biology of the cell* **19**, 822–832.

145.   Orchard, R. C. & Alto, N. M. (2012). Mimicking GEFs: a common theme for bacterial pathogens. *Cellular microbiology* **14**, 10–18.

146.   Spanò, S., Gao, X., Hannemann, S., Lara-Tejero, M. & Galán, J. E. (2016). A Bacterial Pathogen Targets a Host Rab-Family GTPase Defense Pathway with a GAP. *Cell host & microbe* **19**, 216–226.

147.   Navarro, L., Koller, A., Nordfelth, R., Wolf-Watz, H., Taylor, S. & Dixon, J. E. (2007). Identification of a molecular target for the Yersinia protein kinase A. *Molecular cell* **26**, 465–477.

148.   Bhogaraju, S., Kalayil, S., Liu, Y., Bonn, F., Colby, T., Matic, I. *et al. (*2016). Phosphoribosylation of Ubiquitin Promotes Serine Ubiquitination and Impairs Conventional Ubiquitination. *Cell* **167**, 1636-1649.

149.   Qiu, J., Sheedlo, M. J., Yu, K., Tan, Y., Nakayasu, E. S., Das, C. *et al. (*2016). Ubiquitination independent of E1 and E2 enzymes by bacterial effectors. *Nature* **533**, 120–124.

150.   Horiguchi, Y., Inoue, N., Masuda, M., Kashimoto, T., Katahira, J., Sugimoto, N. *et al. (*1997). Bordetella bronchiseptica dermonecrotizing toxin induces reorganization of actin stress fibers through deamidation of Gln-63 of the GTP-binding protein Rho. *Proceedings of the National Academy of Sciences of the United States of America* **94**, 11623–11626.

151.   Jank, T., Bogdanović, X., Wirth, C., Haaf, E., Spoerner, M., Böhmer, K. E. *et al. (*2013). A bacterial toxin catalyzing tyrosine glycosylation of Rho and deamidation of Gq and Gi proteins. *Nature structural & molecular biology* **20**, 1273–1280.

152.   Orth, J. H. C., Fester, I., Siegert, P., Weise, M., Lanner, U., Kamitani, S. *et al. (*2013). Substrate specificity of Pasteurella multocida toxin for α subunits of heterotrimeric G proteins. *The FASEB journal* **27**, 832–842.

153.   Zhou, Y., Huang, C., Yin, L., Wan, M., Wang, X., Li, L. *et al. (*2017). Nε-Fatty acylation of Rho GTPases by a MARTX toxin effector. *Science (New York, N.Y.)* **358**, 528–531.

154.   Mukherjee, S., Liu, X., Arasaki, K., McDonough, J., Galán, J. E. & Roy, C. R. (2011). Modulation of Rab GTPase function by a protein phosphocholine transferase. *Nature* **477**, 103–106.

155.   Aktories, K., Rösener, S., Blaschke, U. & Chhatwal, G. S. (1988). Botulinum ADP-ribosyltransferase C3. Purification of the enzyme and characterization of the ADP-ribosylation reaction in platelet membranes. *European journal of biochemistry* **172**, 445–450.

156.   Genth, H., Schmidt, M., Gerhard, R., Aktories, K. & Just, I. (2003). Activation of phospholipase D1 by ADP-ribosylated RhoA. *Biochemical and Biophysical Research Communications* **302**, 127–132.

157.   Meng, K., Zhuang, X., Peng, T., Hu, S., Yang, J., Wang, Z. *et al. (*2020). Arginine GlcNAcylation of Rab small GTPases by the pathogen Salmonella Typhimurium. *Communications biology* **3**, 287.

158.   Luong, P., Kinch, L. N., Brautigam, C. A., Grishin, N. V., Tomchick, D. R. & Orth, K. (2010). Kinetic and structural insights into the mechanism of AMPylation by VopS Fic domain. *The Journal of biological chemistry* **285**, 20155–20163.

159.   Mattoo, S., Durrant, E., Chen, M. J., Xiao, J., Lazar, C. S., Manning, G. *et al. (*2011). Comparative analysis of Histophilus somni immunoglobulin-binding protein A (IbpA) with other fic domain-containing enzymes reveals differences in substrate and nucleotide specificities. *The Journal of biological chemistry* **286**, 32834–32842.

160.   Müller, M. P., Peters, H., Blümer, J., Blankenfeldt, W., Goody, R. S. & Itzen, A. (2010). The Legionella effector protein DrrA AMPylates the membrane traffic regulator Rab1b. *Science (New York, N.Y.)* **329**, 946–949.

161.   Biancucci, M., Minasov, G., Banerjee, A., Herrera, A., Woida, P. J., Kieffer, M. B. *et al. (*2018). The bacterial Ras/Rap1 site-specific endopeptidase RRSP cleaves Ras through an atypical mechanism to disrupt Ras-ERK signaling. *Science signaling* **11**, eaat8335.

162.   Shao, F., Merritt, P. M., Bao, Z., Innes, R. W. & Dixon, J. E. (2002). A Yersinia Effector and a Pseudomonas Avirulence Protein Define a Family of Cysteine Proteases Functioning in Bacterial Pathogenesis. *Cell* **109**, 575–588.

163.   Wachtel, R. (2018). Biochemische und strukturelle Einsichten der proteolytischen Modifikation kleiner GTPasen durch bakterielle Effektoren aus Salmonella enterica und Vibrio vulnificus, Universitätsbibliothek der TU München, München.

164.   Wachtel, R., Bräuning, B., Mader, S. L., Ecker, F., Kaila, V. R. I., Groll, M. *et al. (*2018). The protease GtgE from Salmonella exclusively targets inactive Rab GTPases. *Nature communications* **9**, 44.

165.   Barthelmes, K., Ramcke, E., Kang, H.-S., Sattler, M. & Itzen, A. (2020). Conformational control of small GTPases by AMPylation. *Proceedings of the National Academy of Sciences of the United States of America* **117**, 5772–5781.

166.   Worby, C. A., Mattoo, S., Kruger, R. P., Corbeil, L. B., Koller, A., Mendez, J. C. *et al. (*2009). The fic domain: regulation of cell signaling by adenylylation. *Molecular cell* **34**, 93–103.

167.   Yarbrough, M. L., Li, Y., Kinch, L. N., Grishin, N. V., Ball, H. L. & Orth, K. (2009). AMPylation of Rho GTPases by Vibrio VopS disrupts effector binding and downstream signaling. *Science (New York, N.Y.)* **323**, 269–272.

168.   Aktories, K. (2015). Rho-modifying bacterial protein toxins. *Pathogens and disease* **73**, ftv091.

113

169. Ost, G. S., Wirth, C., Bogdanović, X., Kao, W.-C., Schorch, B., Aktories, P. J. K. *et al. (*2020). Inverse control of Rab proteins by Yersinia ADP-ribosyltransferase and glycosyltransferase related to clostridial glucosylating toxins. *Science advances* **6**, eaaz2094.

170. von Eichel-Streiber, C., Boquet, P., Sauerborn, M. & Thelestam, M. (1996). Large clostridial cytotoxins — a family of glycosyltransferases modifying small GTP-binding proteins. *Trends in microbiology* **4**, 375–382.

171. Oesterlin, L. K., Goody, R. S. & Itzen, A. (2012). Posttranslational modifications of Rab proteins cause effective displacement of GDP dissociation inhibitor. *Proceedings of the National Academy of Sciences of the United States of America* **109**, 5621–5626.

172. Spanò, S. & Galán, J. E. (2012). A Rab32-dependent pathway contributes to Salmonella typhi host restriction. *Science (New York, N.Y.)* **338**, 960–963.

173. Hurley, D., McCusker, M. P., Fanning, S. & Martins, M. (2014). Salmonella-host interactions - modulation of the host innate immune system. *Frontiers in Immunology* **5**, 481.

174. Fàbrega, A. & Vila, J. (2013). Salmonella enterica serovar Typhimurium skills to succeed in the host: virulence and regulation. *Clinical microbiology reviews* **26**, 308–341.

175. Guibourdenche, M., Roggentin, P., Mikoleit, M., Fields, P. I., Bockemühl, J., Grimont, P. A. D. *et al. (*2010). Supplement 2003-2007 (No. 47) to the White-Kauffmann-Le Minor scheme. *Research in microbiology* **161**, 26–29.

176. Suar, M., Jantsch, J., Hapfelmeier, S., Kremer, M., Stallmach, T., Barrow, P. A. *et al. (*2006). Virulence of Broad- and Narrow-Host-Range Salmonella enterica Serovars in the Streptomycin-Pretreated Mouse Model. *IAI* **74**, 632–644.

177. Castanheira, S. & García-Del Portillo, F. (2017). Salmonella Populations inside Host Cells. *Frontiers in cellular and infection microbiology* **7**, 432.

178. Chaudhuri, D., Roy Chowdhury, A., Biswas, B. & Chakravortty, D. (2018). Salmonella Typhimurium Infection Leads to Colonization of the Mouse Brain and Is Not Completely Cured With Antibiotics. *Frontiers in microbiology* **9**, 1632.

179. Eckmann, L. & Kagnoff, M. F. (2001). Cytokines in host defense against Salmonella. *Microbes and infection* **3**, 1191–1200.

180. Mastroeni, P. & Grant, A. J. (2011). Spread of Salmonella enterica in the body during systemic infection: unravelling host and pathogen determinants. *Expert reviews in molecular medicine* **13**, e12.

181. Ryu, C. B., Lee, M. L., Namgoong, E. K., Kee, S. Y., Lee, W. G. & Woo, J. H. (1995). Bacteremia with nontyphi Salmonella and therapeutic implication. *The Korean Journal of Internal Medicine* **10**, 146–149.

182. Hiyoshi, H., Tiffany, C. R., Bronner, D. N. & Bäumler, A. J. (2018). Typhoidal Salmonella serovars: ecological opportunity and the evolution of a new pathovar. *FEMS microbiology reviews* **42**, 527–541.

183. Spanò, S. (2016). Mechanisms of Salmonella Typhi Host Restriction. *Advances in experimental medicine and biology* **915**, 283–294.

184. Roth, G. A., Abate, D., Abate, K. H., Abay, S. M., Abbafati, C., Abbasi, N. *et al. (*2018). Global, regional, and national age-sex-specific mortality for 282 causes of death in 195 countries and territories, 1980–2017: a systematic analysis for the Global Burden of Disease Study 2017. *The Lancet* **392**, 1736–1788.

185. Lou, L., Zhang, P., Piao, R. & Wang, Y. (2019). Salmonella Pathogenicity Island 1 (SPI-1) and Its Complex Regulatory Network. *Frontiers in cellular and infection microbiology* **9**, 270.

186. Galán, J. E. (2001). Salmonella interactions with host cells: type III secretion at work. *Annual review of cell and developmental biology* **17**, 53–86.

187. Spiering, D. & Hodgson, L. (2011). Dynamics of the Rho-family small GTPases in actin regulation and motility. *Cell adhesion & migration* **5**, 170–180.

188. Mallo, G. V., Espina, M., Smith, A. C., Terebiznik, M. R., Alemán, A., Finlay, B. B. *et al. (*2008). SopB promotes phosphatidylinositol 3-phosphate formation on Salmonella vacuoles by recruiting Rab5 and Vps34. *The Journal of cell biology* **182**, 741–752.

189. Bakowski, M. A., Braun, V., Lam, G. Y., Yeung, T., Heo, W. D., Meyer, T. *et al. (*2010). The phosphoinositide phosphatase SopB manipulates membrane surface charge and trafficking of the Salmonella-containing vacuole. *Cell host & microbe* **7**, 453–462.

190. Malik-Kale, P., Jolly, C. E., Lathrop, S., Winfree, S., Luterbach, C. & Steele-Mortimer, O. (2011). Salmonella - at home in the host cell. *Frontiers in microbiology* **2**, 125.

191. Jennings, E., Thurston, T. L. M. & Holden, D. W. (2017). Salmonella SPI-2 Type III Secretion System Effectors: Molecular Mechanisms And Physiological Consequences. *Cell host & microbe* **22**, 217–231.

192. Liss, V., Swart, A. L., Kehl, A., Hermanns, N., Zhang, Y., Chikkaballi, D. *et al. (*2017). Salmonella enterica Remodels the Host Cell Endosomal System for Efficient Intravacuolar Nutrition. *Cell host & microbe* **21**, 390–402.

193. Ho, T. D., Figueroa-Bossi, N., Wang, M., Uzzau, S., Bossi, L. & Slauch, J. M. (2002). Identification of GtgE, a novel virulence factor encoded on the Gifsy-2 bacteriophage of Salmonella enterica serovar Typhimurium. *Journal of bacteriology* **184**, 5234–5239.

194. Jiang, X., Rossanese, O. W., Brown, N. F., Kujat-Choy, S., Galán, J. E., Finlay, B. B. *et al. (*2004). The related effector proteins SopD and SopD2 from Salmonella enterica serovar Typhimurium contribute to virulence during systemic infection of mice. *Molecular microbiology* **54**, 1186–1198.

195. Brumell, J. H., Kujat-Choy, S., Brown, N. F., Vallance, B. A., Knodler, L. A. & Finlay, B. B. (2003). SopD2 is a novel type III secreted effector of Salmonella typhimurium that targets late endocytic compartments upon delivery into host cells. *Traffic (Copenhagen, Denmark)* **4**, 36–48.

196. Jones, M. A., Wood, M. W., Mullan, P. B., Watson, P. R., Wallis, T. S. & Galyov, E. E. (1998). Secreted effector proteins of Salmonella dublin act in concert to induce enteritis. *IAI* **66**, 5799–5804.

197. Zhang, S., Santos, R. L., Tsolis, R. M., Stender, S., Hardt, W.-D., Bäumler, A. J. *et al. (*2002). The Salmonella enterica serotype typhimurium effector proteins SipA, SopA, SopB, SopD, and SopE2 act in concert to induce diarrhea in calves. *Infection and immunity* **70**, 3843–3855.

198. Knuff-Janzen, K., Tupin, A., Yurist-Doutsch, S., Rowland, J. L. & Finlay, B. B. (2020). Multiple Salmonella-pathogenicity island 2 effectors are required to facilitate bacterial establishment of its intracellular niche and virulence. *PLoS one* **15**, e0235020.

199. Schroeder, N., Henry, T., Chastellier, C. de, Zhao, W., Guilhon, A.-A., Gorvel, J.-P. *et al. (*2010). The virulence protein SopD2 regulates membrane dynamics of Salmonella-containing vacuoles. *PLoS pathogens* **6**, e1001002.

200. D'Costa, V. M., Braun, V., Landekic, M., Shi, R., Proteau, A., McDonald, L. *et al. (*2015). Salmonella Disrupts Host Endocytic Trafficking by SopD2-Mediated Inhibition of Rab7. *Cell reports* **12**, 1508–1518.

201. Teo, W. X., Yang, Z., Kerr, M. C., Luo, L., Guo, Z., Alexandrov, K. *et al. (*2017). Salmonella effector SopD2 interferes with Rab34 function. *Cell biology international* **41**, 433–446.

202. Oliver, J. D. (2015). The Biology of Vibrio vulnificus. *Microbiology spectrum* **3**, VE-0001-2014.

203. Haftel, A. & Sharman, T. (2020). StatPearls. Vibrio Vulnificus, Treasure Island (FL).

204. Jones, M. K. & Oliver, J. D. (2009). Vibrio vulnificus: disease and pathogenesis. *IAI* **77**, 1723–1733.

205. Gavin, H. E., Beubier, N. T. & Satchell, K. J. F. (2017). The Effector Domain Region of the Vibrio vulnificus MARTX Toxin Confers Biphasic Epithelial Barrier Disruption and Is Essential for Systemic Spread from the Intestine. *PLoS pathogens* **13**, e1006119.

115

206.   Murciano, C., Lee, C.-T., Fernández-Bravo, A., Hsieh, T.-H., Fouz, B., Hor, L.-I. *et al. (*2017). MARTX Toxin in the Zoonotic Serovar of Vibrio vulnificus Triggers an Early Cytokine Storm in Mice. *Frontiers in cellular and infection microbiology* **7**, 332.

207.   Jeong, H.-G. & Satchell, K. J. F. (2012). Additive function of Vibrio vulnificus MARTX(Vv) and VvhA cytolysins promotes rapid growth and epithelial tissue necrosis during intestinal infection. *PLoS pathogens* **8**, e1002581.

208.   Wiles, T. J. & Mulvey, M. A. (2013). The RTX pore-forming toxin α-hemolysin of uropathogenic Escherichia coli: progress and perspectives. *Future microbiology* **8**, 73–84.

209.   Gavin, H. E. & Satchell, K. J. F. (2015). MARTX toxins as effector delivery platforms. *Pathogens and disease* **73**, ftv092.

210.   Sheahan, K.-L., Cordero, C. L. & Satchell, K. J. F. (2007). Autoprocessing of the Vibrio cholerae RTX toxin by the cysteine protease domain. *The EMBO journal* **26**, 2552–2561.

211.   Satchell, K. J. F. (2007). MARTX, multifunctional autoprocessing repeats-in-toxin toxins. *IAI* **75**, 5079–5084.

212.   Antic, I., Biancucci, M. & Satchell, K. J. F. (2014). Cytotoxicity of the Vibrio vulnificus MARTX toxin effector DUF5 is linked to the C2A subdomain. *Proteins* **82**, 2643–2656.

213.   Jang, S. Y., Hwang, J., Kim, B. S., Lee, E.-Y., Oh, B.-H. & Kim, M. H. (2018). Structural basis of inactivation of Ras and Rap1 small GTPases by Ras/Rap1-specific endopeptidase from the sepsis-causing pathogen Vibrio vulnificus. *The Journal of biological chemistry* **293**, 18110–18122.

214.   Antic, I., Biancucci, M., Zhu, Y., Gius, D. R. & Satchell, K. J. F. (2015). Site-specific processing of Ras and Rap1 Switch I by a MARTX toxin effector domain. *Nature communications* **6**, 7396.

215.   Fauser, J., Savitskiy, S., Fottner, M., Trauschke, V. & Gulen, B. (2020). Sortase-Mediated Quantifiable Enzyme Immobilization on Magnetic Nanoparticles. *Bioconjugate chemistry* **31**, 1883–1892.

216.   Berrade, L., Garcia, A. E. & Camarero, J. A. (2011). Protein microarrays: novel developments and applications. *Pharmaceutical research* **28**, 1480–1499.

217.   Britton, J., Dyer, R. P., Majumdar, S., Raston, C. L. & Weiss, G. A. (2017). Ten-Minute Protein Purification and Surface Tethering for Continuous-Flow Biocatalysis. *Angew. Chem.* **129**, 2336–2341.

218.   Yang, H.-W., Hua, M.-Y., Liu, H.-L., Huang, C.-Y. & Wei, K.-C. (2012). Potential of magnetic nanoparticles for targeted drug delivery. *Nanotechnology, science and applications* **5**, 73–86.

219.   Muley, A. B., Mulchandani, K. H. & Singhal, R. S., eds (2020). Enzyme nanoarchitectures built with carbon nanotubes, Elsevier Academic Press, (Kumar, C. V., Ed.) pp 39–76, Methods in Enzymology Series 630.

220.   Xu, J., Sun, J., Wang, Y., Sheng, J., Wang, F. & Sun, M. (2014). Application of iron magnetic nanoparticles in protein immobilization. *Molecules (Basel, Switzerland)* **19**, 11465–11486.

221.   Meldal, M. & Schoffelen, S. (2016). Recent advances in covalent, site-specific protein immobilization. *F1000Research* **5**.

222.   Rosen, C. B. & Francis, M. B. (2017). Targeting the N terminus for site-selective protein modification. *Nature chemical biology* **13**, 697–705.

223.   Raliski, B. K., Howard, C. A. & Young, D. D. (2014). Site-specific protein immobilization using unnatural amino acids. *Bioconjugate chemistry* **25**, 1916–1920.

224.   Singh, R. K., Tiwari, M. K., Singh, R. & Lee, J.-K. (2013). From protein engineering to immobilization: promising strategies for the upgrade of industrial enzymes. *International journal of molecular sciences* **14**, 1232–1277.

225.   Fontana, A., Spolaore, B., Mero, A. & Veronese, F. M. (2008). Site-specific modification and PEGylation of pharmaceutical proteins mediated by transglutaminase. *Advanced Drug Delivery Reviews* **60**, 13–28.

226.   Mao, H., Hart, S. A., Schink, A. & Pollok, B. A. (2004). Sortase-mediated protein ligation: a new method for protein engineering. *Journal of the American Chemical Society* **126**, 2670–2671.

227.   Popp, M. W., Antos, J. M., Grotenbreg, G. M., Spooner, E. & Ploegh, H. L. (2007). Sortagging: a versatile method for protein labeling. *Nature chemical biology* **3**, 707–708.

228.   Tanaka, T., Kamiya, N. & Nagamune, T. (2005). N-terminal glycine-specific protein conjugation catalyzed by microbial transglutaminase. *FEBS letters* **579**, 2092–2096.

229.   Mazmanian, S. K., Liu, G., Ton-That, H. & Schneewind, O. (1999). Staphylococcus aureus sortase, an enzyme that anchors surface proteins to the cell wall. *Science (New York, N.Y.)* **285**, 760–763.

230.   Navarre, W. W. & Schneewind, O. (1994). Proteolytic cleavage and cell wall anchoring at the LPXTG motif of surface proteins in gram-positive bacteria. *Molecular microbiology* **14**, 115–121.

231.   Chen, I., Dorr, B. M. & Liu, D. R. (2011). A general strategy for the evolution of bond-forming enzymes using yeast display. *Proceedings of the National Academy of Sciences of the United States of America* **108**, 11399–11404.

232.   Dorr, B. M., Ham, H. O., An, C., Chaikof, E. L. & Liu, D. R. (2014). Reprogramming the specificity of sortase enzymes. *Proceedings of the National Academy of Sciences of the United States of America* **111**, 13343–13348.

233.   Hirakawa, H., Ishikawa, S. & Nagamune, T. (2012). Design of Ca2+-independent Staphylococcus aureus sortase A mutants. *Biotechnology and bioengineering* **109**, 2955–2961.

234.   Chen, Q., Sun, Q., Molino, N. M., Wang, S.-W., Boder, E. T. & Chen, W. (2015). Sortase A-mediated multi-functionalization of protein nanoparticles. *Chemical communications (Cambridge, England)* **51**, 12107–12110.

235.   Glasgow, J. E., Salit, M. L. & Cochran, J. R. (2016). In Vivo Site-Specific Protein Tagging with Diverse Amines Using an Engineered Sortase Variant. *Journal of the American Chemical Society* **138**, 7496–7499.

236.   Uth, C., Zielonka, S., Hörner, S., Rasche, N., Plog, A., Orelma, H. *et al. (*2014). A chemoenzymatic approach to protein immobilization onto crystalline cellulose nanoscaffolds. *Angewandte Chemie (International ed. in English)* **53**, 12618–12623.

237.   Zou, Z., Gau, E., El-Awaad, I., Jakob, F., Pich, A. & Schwaneberg, U. (2019). Selective Functionalization of Microgels with Enzymes by Sortagging. *Bioconjugate chemistry* **30**, 2859–2869.

238.   Freiburger, L., Sonntag, M., Hennig, J., Li, J., Zou, P. & Sattler, M. (2015). Efficient segmental isotope labeling of multi-domain proteins using Sortase A. *Journal of biomolecular NMR* **63**, 1–8.

239.   Fottner, M., Brunner, A.-D., Bittl, V., Horn-Ghetko, D., Jussupow, A., Kaila, V. R. I. *et al. (*2019). Site-specific ubiquitylation and SUMOylation using genetic-code expansion and sortase. *Nature chemical biology* **15**, 276–284.

240.   Jacobitz, A. W., Kattke, M. D., Wereszczynski, J. & Clubb, R. T. (2017). Sortase Transpeptidases: Structural Biology and Catalytic Mechanism. *Advances in protein chemistry and structural biology* **109**, 223–264.

241.   Cheng, G., Xing, J., Pi, Z., Liu, S., Liu, Z. & Song, F. (2019). α-Glucosidase immobilization on functionalized Fe3O4 magnetic nanoparticles for screening of enzyme inhibitors. *Chinese Chemical Letters* **30**, 656–659.

242.   Thanh, B. T., van Sau, N., Ju, H., Bashir, M. J. K., Jun, H. K., Phan, T. B. *et al. (*2019). Immobilization of Protein A on Monodisperse Magnetic Nanoparticles for Biomedical Applications. Journal of Nanomaterials, 2019, 1-9. *Journal of Nanomaterials* **2019**, 1–9.

243.   Chen, X., Zaro, J. L. & Shen, W.-C. (2013). Fusion protein linkers: property, design and functionality. *Advanced Drug Delivery Reviews* **65**, 1357–1369.

244.   Pishesha, N., Ingram, J. R. & Ploegh, H. L. (2018). Sortase A: A Model for Transpeptidation and Its Biological Applications. *Annual review of cell and developmental biology* **34**, 163–188.

245.   Corr, S. A., Rakovich, Y. P. & Gun'ko, Y. K. (2008). Multifunctional Magnetic-fluorescent Nanocomposites for Biomedical Applications. *Nanoscale Res Lett* **3**, 87–104.

246.   Ton-That, H., Mazmanian, S. K., Faull, K. F. & Schneewind, O. (2000). Anchoring of surface proteins to the cell wall of Staphylococcus aureus. Sortase catalyzed in vitro transpeptidation reaction using LPXTG peptide and NH(2)-Gly(3) substrates. *The Journal of biological chemistry* **275**, 9876–9881.

247.   Naik, M. T., Suree, N., Ilangovan, U., Liew, C. K., Thieu, W., Campbell, D. O. *et al. (*2006). Staphylococcus aureus Sortase A transpeptidase. Calcium promotes sorting signal binding by altering the mobility and structure of an active site loop. *The Journal of biological chemistry* **281**, 1817–1826.

248.   Savitskiy, S., Wachtel, R., Pourjafar-Dehkordi, D., Kang, H.-S., Trauschke, V., Lamb, D. C. *et al. (*2020). Proteolysis of Rab32 by Salmonella GtgE induces an inactive GTPase Conformation. *Under review in iScience*.

249.   Pai, E. F., Kabsch, W., Krengel, U., Holmes, K. C., John, J. & Wittinghofer, A. (1989). Structure of the guanine-nucleotide-binding domain of the Ha-ras oncogene product p21 in the triphosphate conformation. *Nature* **341**, 209–214.

250.   Scheidig, A. J., Burmester, C. & Goody, R. S. (1999). The pre-hydrolysis state of p21ras in complex with GTP: new insights into the role of water molecules in the GTP hydrolysis reaction of ras-like proteins. *Structure* **7**, 1311-S2.

251.   Sasaki, T., Kikuchi, A., Araki, S., Hata, Y., Isomura, M., Kuroda, S. *et al. (*1990). Purification and characterization from bovine brain cytosol of a protein that inhibits the dissociation of GDP from and the subsequent binding of GTP to smg p25A, a ras p21-like GTP-binding protein. *The Journal of biological chemistry* **265**, 2333–2337.

252.   Joberty, G., Tavitian, A. & Zahraoui, A. (1993). Isoprenylation of Rab proteins possessing a C-terminal CaaX motif. *FEBS letters* **330**, 323–328.

253.   LeBlanc, S. J., Kulkarni, P. & Weninger, K. R. (2018). Single Molecule FRET: A Powerful Tool to Study Intrinsically Disordered Proteins. *Biomolecules* **8**, 140.

254.   Kalinin, S., Peulen, T., Sindbert, S., Rothwell, P. J., Berger, S., Restle, T. *et al. (*2012). A toolkit and benchmark study for FRET-restrained high-precision structural modeling. *Nature methods* **9**, 1218–1225.

255.   Huang, L., Hofer, F., Martin, G. S. & Kim, S. H. (1998). Structural basis for the interaction of Ras with RalGDS. *Nature structural biology* **5**, 422–426.

256.   Fetics, S. K., Guterres, H., Kearney, B. M., Buhrman, G., Ma, B., Nussinov, R. *et al. (*2015). Allosteric effects of the oncogenic RasQ61L mutant on Raf-RBD. *Structure (London, England : 1993)* **23**, 505–516.

257.   Filchtinski, D., Sharabi, O., Rüppel, A., Vetter, I. R., Herrmann, C. & Shifman, J. M. (2010). What makes Ras an efficient molecular switch: a computational, biophysical, and structural study of Ras-GDP interactions with mutants of Raf. *Journal of molecular biology* **399**, 422–435.

258.   Brückner, A., Polge, C., Lentze, N., Auerbach, D. & Schlattner, U. (2009). Yeast two-hybrid, a powerful tool for systems biology. *International journal of molecular sciences* **10**, 2763–2788.

259.   Wagemans, J. & Lavigne, R. (2015). Identification of protein-protein interactions by standard gal4p-based yeast two-hybrid screening. *Methods in molecular biology (Clifton, N.J.)* **1278**, 409–431.

260.   Gazdag, E.-M., Streller, A., Haneburger, I., Hilbi, H., Vetter, I. R., Goody, R. S. *et al. (*2013). Mechanism of Rab1b deactivation by the Legionella pneumophila GAP LepB. *EMBO reports* **14**, 199–205.

261.   Wong, L. S., Khan, F. & Micklefield, J. (2009). Selective covalent protein immobilization: strategies and applications. *Chemical reviews* **109**, 4025–4053.

262. Gulen, B., Rosselin, M., Fauser, J., Albers, M. F., Pett, C., Krisp, C. *et al. (*2020). Identification of targets of AMPylating Fic enzymes by co-substrate-mediated covalent capture. *Nat. Chem.*

263. Cambria, E., Renggli, K., Ahrens, C. C., Cook, C. D., Kroll, C., Krueger, A. T. *et al. (*2015). Covalent Modification of Synthetic Hydrogels with Bioactive Proteins via Sortase-Mediated Ligation. *Biomacromolecules* **16**, 2316–2326.

264. Schoonen, L., Pille, J., Borrmann, A., Nolte, R. J. M. & van Hest, J. C. M. (2015). Sortase A-Mediated N-Terminal Modification of Cowpea Chlorotic Mottle Virus for Highly Efficient Cargo Loading. *Bioconjugate chemistry* **26**, 2429–2434.

265. Eathiraj, S., Mishra, A., Prekeris, R. & Lambright, D. G. (2006). Structural basis for Rab11-mediated recruitment of FIP3 to recycling endosomes. *Journal of molecular biology* **364**, 121–135.

266. Jagoe, W. N., Lindsay, A. J., Read, R. J., McCoy, A. J., McCaffrey, M. W. & Khan, A. R. (2006). Crystal structure of rab11 in complex with rab11 family interacting protein 2. *Structure (London, England: 1993)* **14**, 1273–1283.

267. Wu, M., Wang, T., Loh, E., Hong, W. & Song, H. (2005). Structural basis for recruitment of RILP by small GTPase Rab7. *The EMBO journal* **24**, 1491–1501.

268. Zhu, G., Zhai, P., Liu, J., Terzyan, S., Li, G. & Zhang, X. C. (2004). Structural basis of Rab5-Rabaptin5 interaction in endocytosis. *Nature structural & molecular biology* **11**, 975–983.

269. Tamura, K., Ohbayashi, N., Ishibashi, K. & Fukuda, M. (2011). Structure-function analysis of VPS9-ankyrin-repeat protein (Varp) in the trafficking of tyrosinase-related protein 1 in melanocytes. *The Journal of biological chemistry* **286**, 7507–7521.

270. Pylypenko, O., Rak, A., Durek, T., Kushnir, S., Dursina, B. E., Thomae, N. H. *et al. (*2006). Structure of doubly prenylated Ypt1:GDI complex and the mechanism of GDI-mediated Rab recycling. *The EMBO journal* **25**, 13–23.

271. Goody, P. R., Heller, K., Oesterlin, L. K., Müller, M. P., Itzen, A. & Goody, R. S. (2012). Reversible phosphocholination of Rab proteins by Legionella pneumophila effector proteins. *The EMBO journal* **31**, 1774–1784.

272. Kiontke, S., Langemeyer, L., Kuhlee, A., Schuback, S., Raunser, S., Ungermann, C. *et al. (*2017). Architecture and mechanism of the late endosomal Rab7-like Ypt7 guanine nucleotide exchange factor complex Mon1-Ccz1. *Nature communications* **8**, 14034.

273. Nordmann, M., Cabrera, M., Perz, A., Bröcker, C., Ostrowicz, C., Engelbrecht-Vandré, S. *et al. (*2010). The Mon1-Ccz1 complex is the GEF of the late endosomal Rab7 homolog Ypt7. *Current Biology* **20**, 1654–1659.

274. Liu, W., Liu, X.'n., Li, Y., Zhao, J., Liu, Z., Hu, Z. *et al. (*2017). LRRK2 promotes the activation of NLRC4 inflammasome during Salmonella Typhimurium infection. *The Journal of experimental medicine* **214**, 3051–3066.

275. Gardet, A., Benita, Y., Li, C., Sands, B. E., Ballester, I., Stevens, C. *et al. (*2010). LRRK2 is involved in the IFN-gamma response and host response to pathogens. *Journal of immunology (Baltimore, Md.: 1950)* **185**, 5577–5585.

276. Lu, S., Jang, H., Gu, S., Zhang, J. & Nussinov, R. (2016). Drugging Ras GTPase: a comprehensive mechanistic and signaling structural view. *Chemical Society reviews* **45**, 4929–4952.

277. Siegert, P., Schmidt, G., Papatheodorou, P., Wieland, T., Aktories, K. & Orth, J. H. C. (2013). Pasteurella multocida toxin prevents osteoblast differentiation by transactivation of the MAP-kinase cascade via the Gα(q/11)--p63RhoGEF--RhoA axis. *PLoS pathogens* **9**, e1003385.

278. Scrima, A., Thomas, C., Deaconescu, D. & Wittinghofer, A. (2008). The Rap-RapGAP complex: GTP hydrolysis without catalytic glutamine and arginine residues. *The EMBO journal* **27**, 1145–1153.

279. Green, M. R. & Sambrook, J. (2012). Molecular cloning. A laboratory manual, 4th ed., Cold Spring Harbor Laboratory Press, Cold Spring Harbor, N.Y.

280. Chen, D. C., Yang, B. C. & Kuo, T. T. (1992). One-step transformation of yeast in stationary phase. *Current genetics* **21**, 83–84.

281. Vieweg, S., Mulholland, K., Bräuning, B., Kachariya, N., Lai, Y.-C., Toth, R. *et al.* (2020). PINK1-dependent phosphorylation of Serine111 within the SF3 motif of Rab GTPases impairs effector interactions and LRRK2-mediated phosphorylation at Threonine72. *The Biochemical journal* **477**, 1651–1668.

282. Hougland, J. L., Gangopadhyay, S. A. & Fierke, C. A. (2012). Expansion of protein farnesyltransferase specificity using "tunable" active site interactions: development of bioengineered prenylation pathways. *The Journal of biological chemistry* **287**, 38090–38100.

283. Barth, A., Voith von Voithenberg, L. & Lamb, D. C. (2019). Quantitative Single-Molecule Three-Color Förster Resonance Energy Transfer by Photon Distribution Analysis. *The journal of physical chemistry. B* **123**, 6901–6916.

284. Müller, B. K., Zaychikov, E., Bräuchle, C. & Lamb, D. C. (2005). Pulsed interleaved excitation. *Biophysical journal* **89**, 3508–3522.

285. Kapanidis, A. N., Lee, N. K., Laurence, T. A., Doose, S., Margeat, E. & Weiss, S. (2004). Fluorescence-aided molecule sorting: analysis of structure and interactions by alternating-laser excitation of single molecules. *Proceedings of the National Academy of Sciences of the United States of America* **101**, 8936–8941.

286. Eggeling, C., Berger, S., Brand, L., Fries, J. R., Schaffer, J., Volkmer, A. *et al.* (2001). Data registration and selective single-molecule analysis using multi-parameter fluorescence detection. *Journal of Biotechnology* **86**, 163–180.

287. Schrimpf, W., Barth, A., Hendrix, J. & Lamb, D. C. (2018). PAM: A Framework for Integrated Analysis of Imaging, Single-Molecule, and Ensemble Fluorescence Data. *Biophysical journal* **114**, 1518–1528.

288. Tomov, T. E., Tsukanov, R., Masoud, R., Liber, M., Plavner, N. & Nir, E. (2012). Disentangling subpopulations in single-molecule FRET and ALEX experiments with photon distribution analysis. *Biophysical journal* **102**, 1163–1173.

289. Antonik, M., Felekyan, S., Gaiduk, A. & Seidel, C. A. M. (2006). Separating structural heterogeneities from stochastic variations in fluorescence resonance energy transfer distributions via photon distribution analysis. *The journal of physical chemistry. B* **110**, 6970–6978.

290. Maier, J. A., Martinez, C., Kasavajhala, K., Wickstrom, L., Hauser, K. E. & Simmerling, C. (2015). ff14SB: Improving the Accuracy of Protein Side Chain and Backbone Parameters from ff99SB. *Journal of chemical theory and computation* **11**, 3696–3713.

291. Meagher, K. L., Redman, L. T. & Carlson, H. A. (2003). Development of polyphosphate parameters for use with the AMBER force field. *Journal of computational chemistry* **24**, 1016–1025.

292. Izadi, S., Anandakrishnan, R. & Onufriev, A. V. (2014). Building Water Models: A Different Approach. *The journal of physical chemistry letters* **5**, 3863–3871.

293. Case, D. A., Betz, R. M., Cerutti, D. S., Cheatham, T.E., III, Darden, T. A., Duke, R. E. *et al.* (2016). AMBER 2016, University of California, San Francisco.

294. Schrödinger (2015), LLC, The PyMOL Molecular Graphics System, Version 2.0.

295. Lee, W., Tonelli, M. & Markley, J. L. (2015). NMRFAM-SPARKY: enhanced software for biomolecular NMR spectroscopy. *Bioinformatics (Oxford, England)* **31**, 1325–1327.

296. Zhang, Z. & Marshall, A. G. (1998). A universal algorithm for fast and automated charge state deconvolution of electrospray mass-to-charge ratio spectra. *Journal of the American Society for Mass Spectrometry* **9**, 225–233.

9. APPENDIX

9.1 Supplementary figures
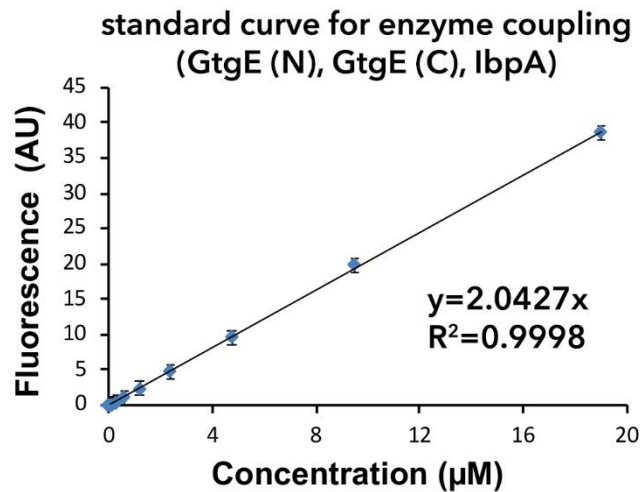
Figure S1 | Standard curve for quantification of the amount of immobilized GtgE. *Fluorescence of TEV-treated GFP-GtgE for C-terminal coupling. Serial dilutions of GFP ranging from 9 nM to 19 μM were measured to produce the standard curve. The values were submitted for a linear fit. The corresponding equations (y), as well as the R2-values, are indicated. Reprinted with permission from Fauser et al, 2020 [215]. Copyright (2020) American Chemical Society.*
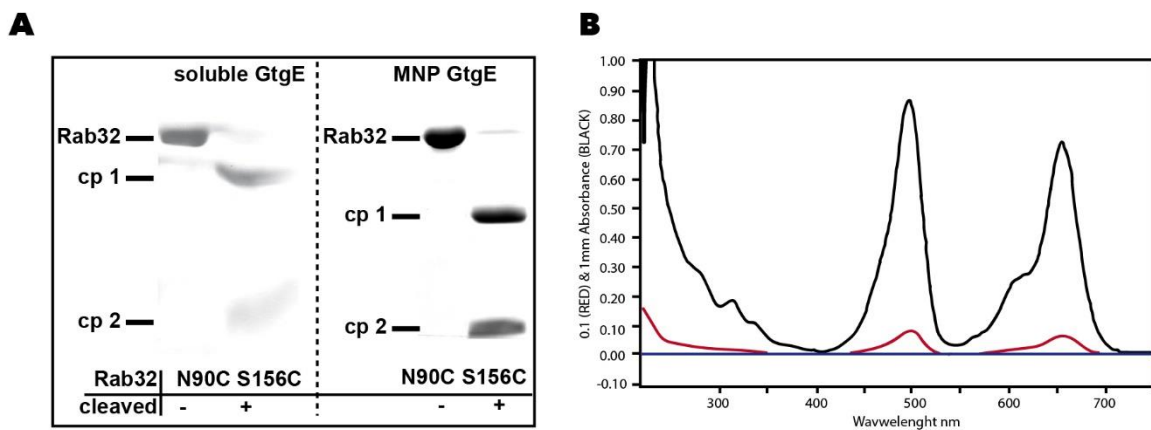
Figure S2 | Production of GtgE treated Rab32 for sp-FRET analysis. (A) *SDS-PAGE indicating quantitative cleavage of Rab32 by both soluble and immobilized GtgE. Bands of Rab32 and its cleavage products 1 (cp 1) and 2 (cp 2) are indicated.* **(B)** *Absorbance spectra of soluble GtgE indicate the labeling of intrinsic Cys residues of GtgE by fluorescent dyes Alexa488-maleimide and Alexa647-maleimide. Red: absorbance spectra at 0.1 mm pathlength. Black: absorbance spectra at 1 mm pathlength. Blue: blank. Reprinted with permission from Fauser et al, 2020 [215]. Copyright (2020) American Chemical Society.*
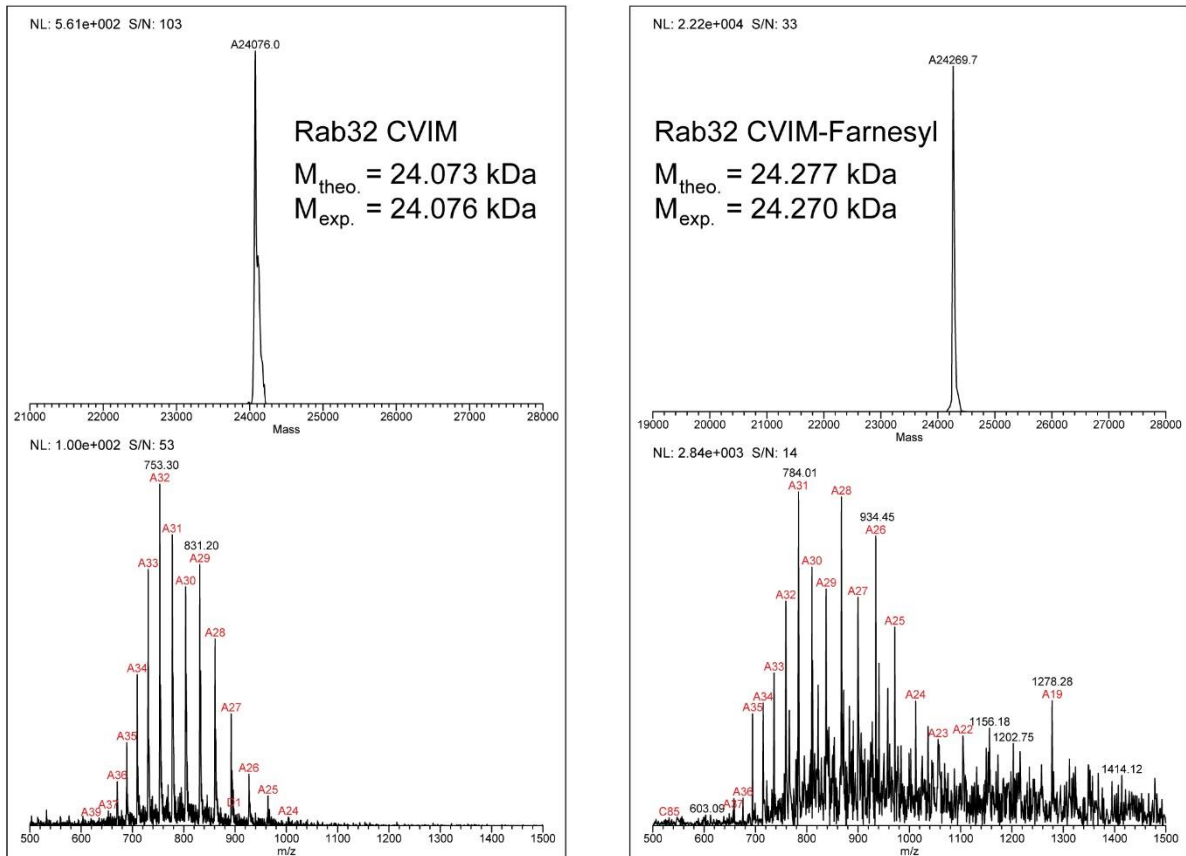
Figure S3 | *Mass spectrometry data of Rab32 CVIM farnesylation with the deconvoluted mass spectra (top) and the m/z spectra (bottom). Left: unmodified Rab32 bearing the CVIM-sequence. Right: farnesylated Rab32 CVIM. Both masses were determined with an offset of 3 Da ($M_{exp.}$) compared to the calculated, theoretical mass ($M_{theo.}$) The measured difference in mass ($\Delta M_{exp.}$ = 194 Da) does not correspond fully to the theoretical Mass difference of an attached farnesyl moiety ($\Delta M_{theo.}$ = 204 Da). The difference of 10 Da is due to the mass resolution limitations of the instrument and m/z-data quality of the farnesylated Rab32 which showed significantly less ionization upon modification. Reprinted with permission from Savitskiy et al, 2020 [248]. Copyright (2020) Elsevier.*
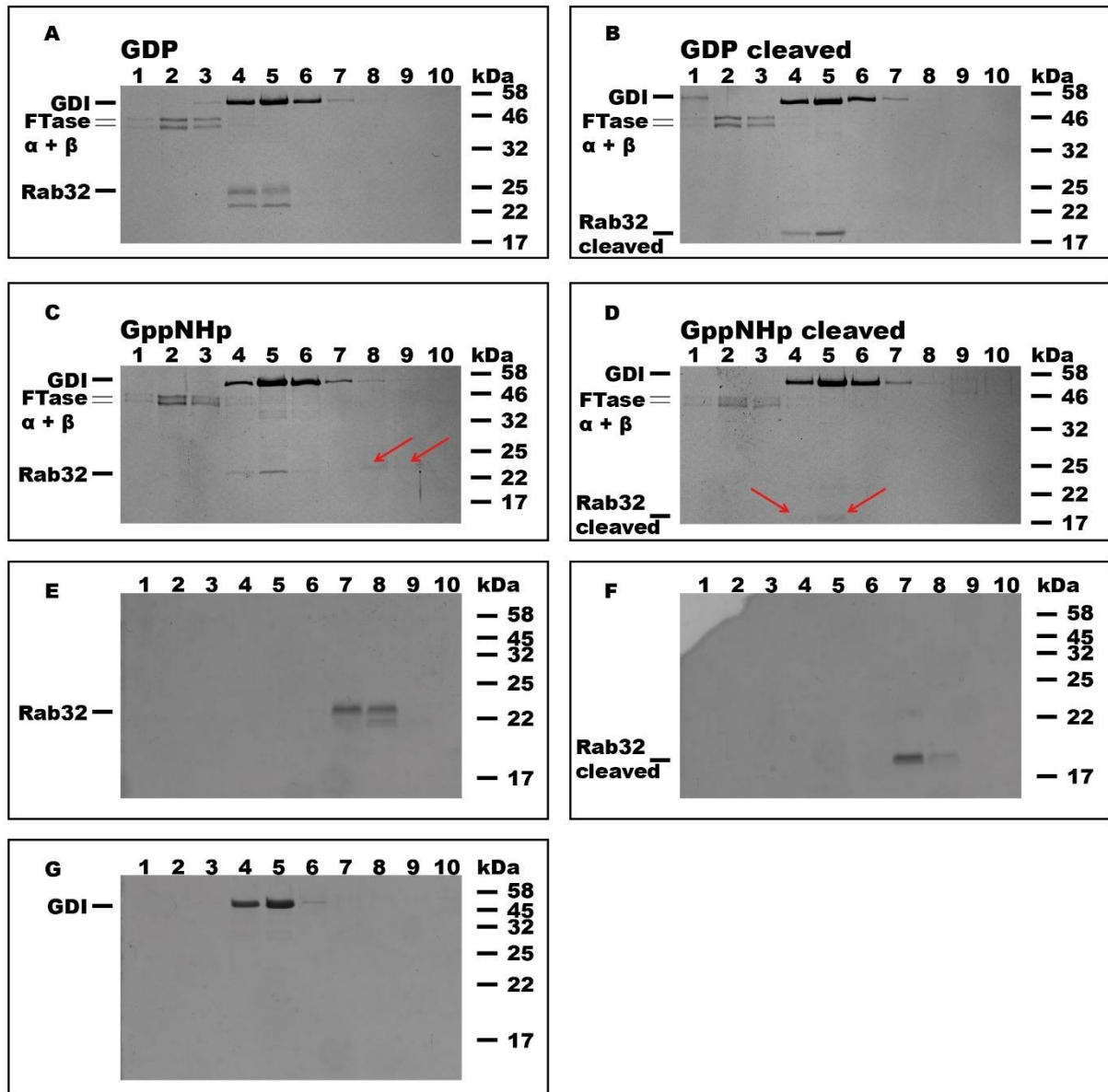
Figure S4 | *Fraction analysis of the Rab32:GDI complex formation on an aSEC. Coomassie-stained SDS-PAGE of fractions from aSEC separations containing farnesylated Rab32 CVIM in the presence of GDI and FTase (compare Figure 19C, D).* **(A)** *Rab32:GDP.* **(B)** *Rab32$_{cleaved}$:GDP.* **(C)** *Rab32:GppNHp.* **(D)** *Rab32$_{cleaved}$:GppNHp. Slightly visible bands are highlighted with arrows. All Rab32 preparations (A-D) are forming a non-covalent complex with GDI indicated by the coelution in fractions 4 and 5. Only Rab32:GppNHp (C) shows a partial complex formation indicated by free Rab32 in fractions 8 and 9.* **(E-G)** *Control runs of single proteins on an analytical SEC. Reprinted with permission from Savitskiy et al, 2020 [248]. Copyright (2020) Elsevier.*
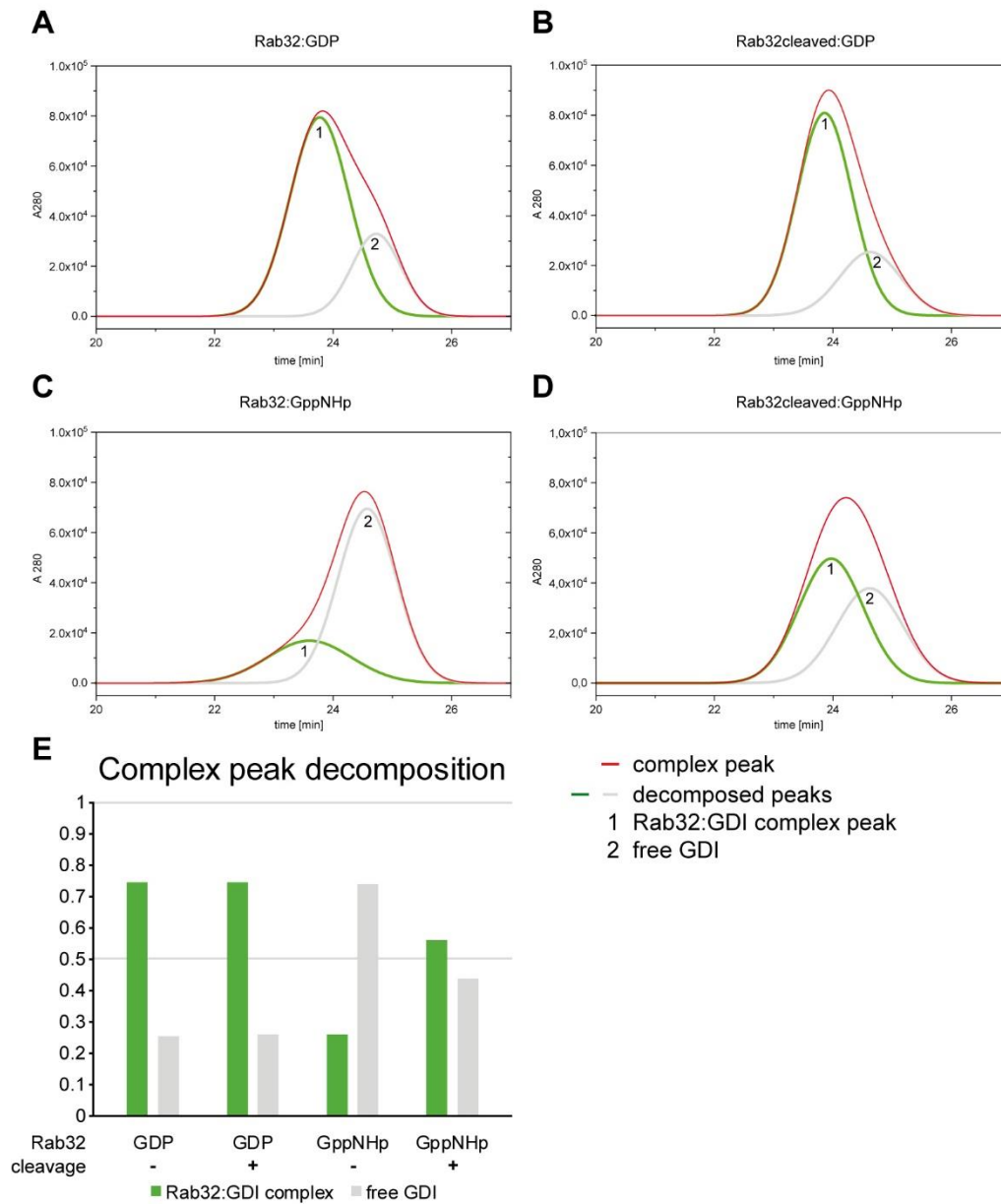
Figure S5 | *Decomposition of eluted complex peaks of Rab32 and GDI: (A) Rab32:GPD:GDI, (B) Rab32cleaved:GDP:GDI, (C) Rab32:GppNHp:GDI, and (D) Rab32cleaved:GppNHp:GDI showing both, the absorption at 280 nm (red chromatogram) as well as the decomposition of the peak into free GDI (2) and the Rab32:GDI complex (1). Peak decomposition was performed using Origin data analysis software (OriginLab 2019b, v9.65) setting the elution time of free GDI in a complex peak to 24.6 min. (E) The populations determined in panels A-D are plotted as a bar chart. Reprinted with permission from Savitskiy et al, 2020 [248]. Copyright (2020) Elsevier.*
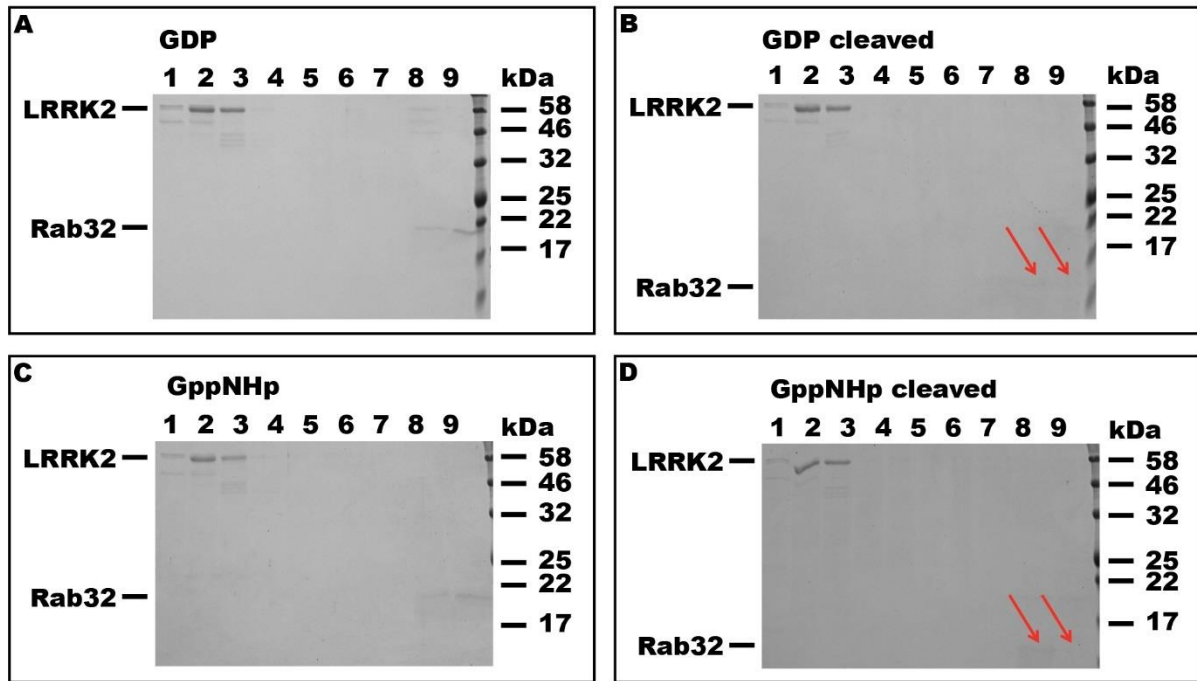
Figure S6 | *Fraction analysis of aSEC runs of LRRK2$_{10-661}$ and Rab32$_{20-201}$ variants (GDP, GppNHp, cleaved, not cleaved). Coomassie-stained SDS-PAGE of fractions from aSEC separations containing Rab32$_{20-201}$.* **(A)** *Rab32:GDP.* **(B)** *Rab32$_{cleaved}$:GDP.* **(C)** *Rab32:GppNHp.* **(D)** *Rab32$_{cleaved}$:GppNHp. Slightly visible bands are highlighted with arrows. None of the preparations (A-D) are forming a non-covalent complex. LRRK2$_{10-661}$ and Rab32$_{20-201}$ are separated by four empty fractions (4-7).*
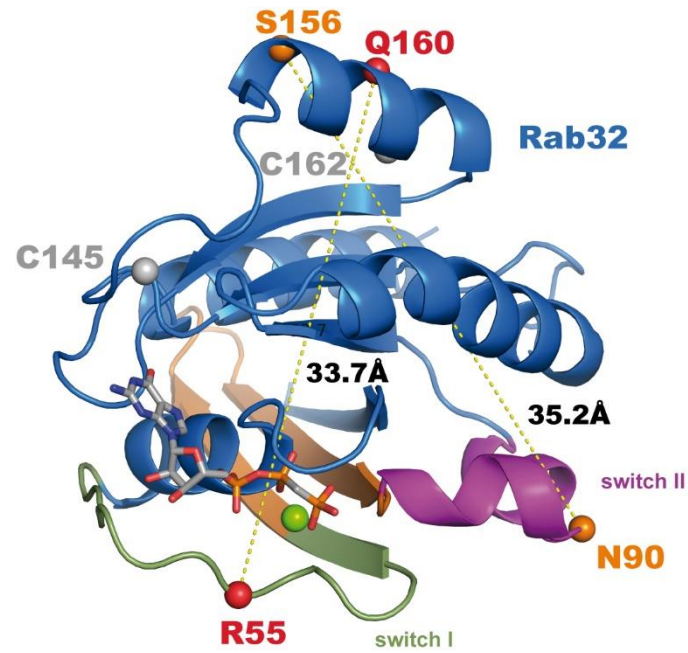
Figure S7 | *Positions of mutated Cys-residues within the Rab32 structure (PDB: 6FF8 [91]). The positions of cysteine mutations and the distances between them are indicated by yellow dotted lines for the two spFRET pairs used (red and orange spheres). Further wild type Cys residues (grey spheres) were mutated to Ser. The positions were labeled stochastically with donor and acceptor molecules. Reprinted with permission from Savitskiy et al, 2020 [248]. Copyright (2020) Elsevier.*
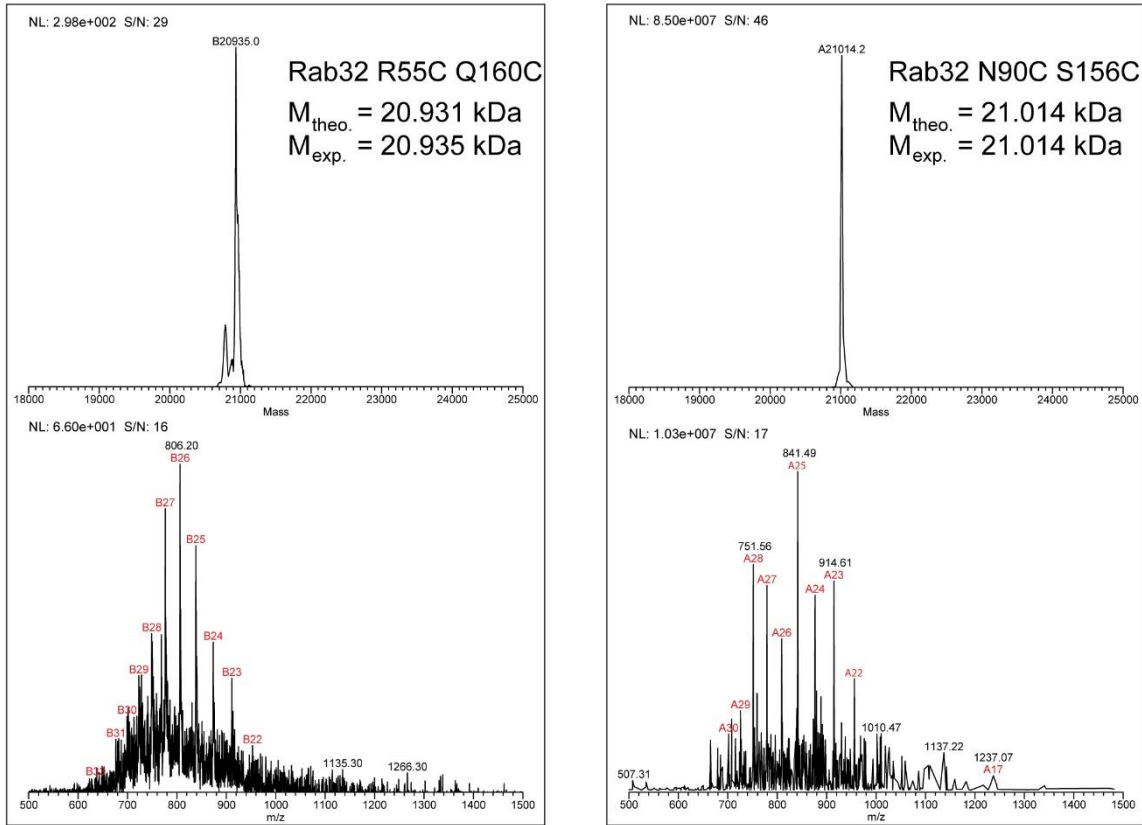
Figure S8 | *Mass spectrometry data of Rab32 cysteine mutants with the deconvoluted mass spectra (top) and the m/z spectra (bottom). Left: Rab32$_{20-201}$ R55C C145S Q160C C162S. Right: Rab32$_{20-201}$ N90C C145S S156C C162S. The determined masses (M$_{exp.}$) are confirming the presence of the correct cysteine mutations for the proteins applied in the spFRET experiments.*
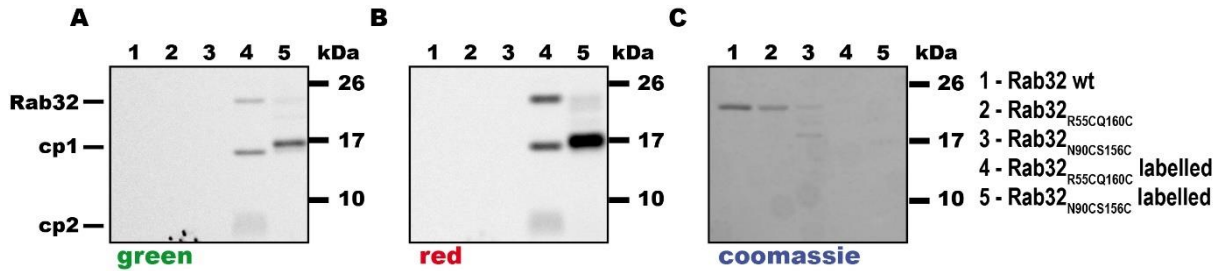
Figure S9 | *In-gel fluorescence of doubly labeled Rab32 mutants. The SDS-PAGE gel was visualized in green **(A)** and red channels **(B)** showing the presence of both fluorescent dyes (Alexa488 and Alexa647) on the Rab32 mutants. Wild type Rab32 and both unlabelled mutants served as a control visualized in Coomassie stain in **C**. Analyzed proteins are indicated. Cp1: cleavage product 1; cp2: cleavage product 2. Reprinted with permission from Savitskiy et al, 2020 [248]. Copyright (2020) Elsevier.*
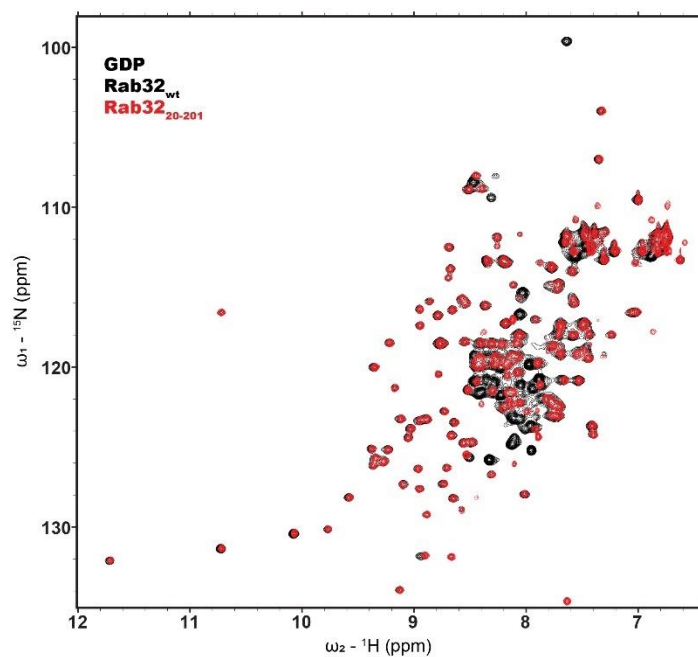
Figure S10 | *1H 15N HSQC spectra of Rab32wt (black) overlaid with a truncated version of Rab32$_{20-201}$ (red) displaying cleared up spectrum in the area around 1H/15N: 8/120 ppm.*
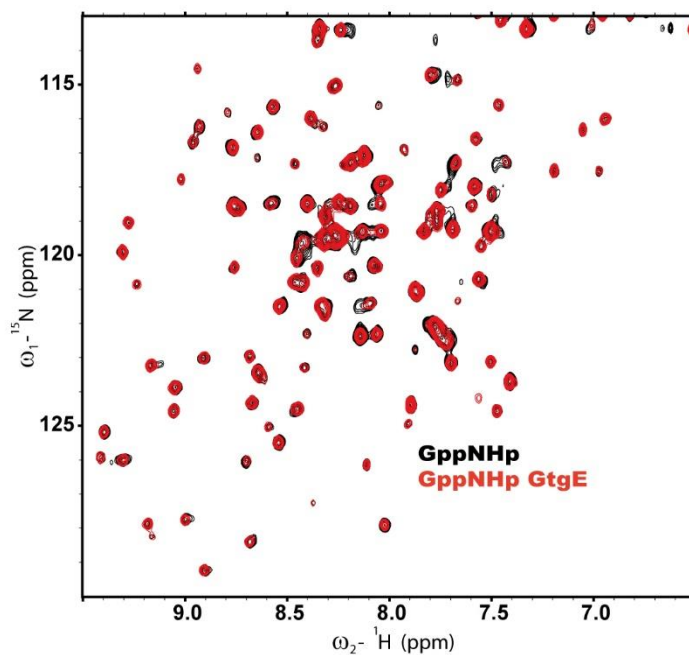
Figure S11 | *1H 15N HSQC spectra of Rab32:GppNHp with GtgE supplementation. Superimposed spectra of Rab32:GppNHp and Rab32:GppNHp in the presence of GtgE protease are very similar. No significant differences in the signals were observed indicating that nucleotide exchange with GppNHp in vitro was already fully completed. Reprinted with permission from Savitskiy et al, 2020 [248]. Copyright (2020) Elsevier.*
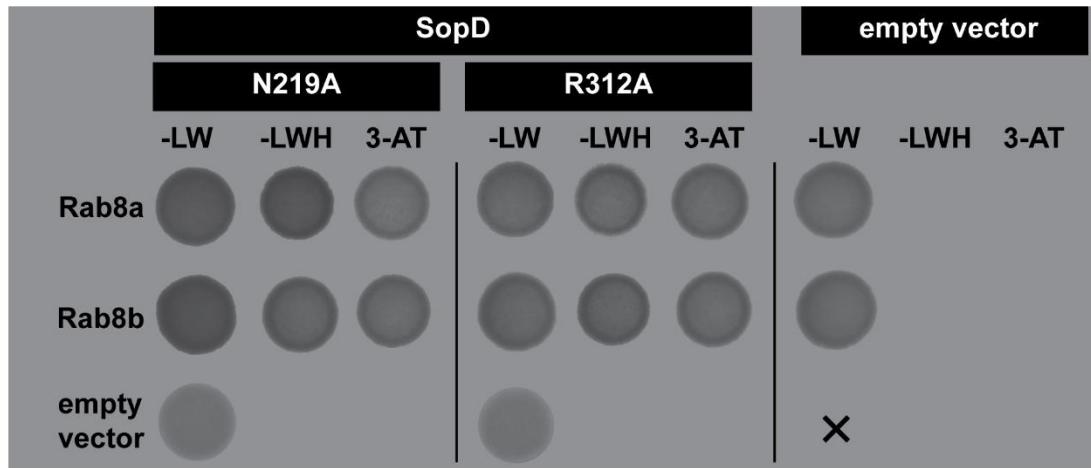
Figure S12 | *Interaction experiment using the Y2H system with Rab8a/b and inactive point mutants of SopD (N219A and R312A). Both point mutants of SopD were able to interact with Rab8 homologs thereby dismissing the crucial importance of these residues for the Rab-GAP interaction.*
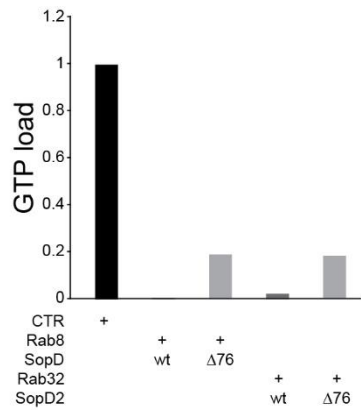
Figure S13 | *Incubation of wild type (wt) SopD and SopD2 with their target proteins Rab8 and Rab32, respectively, resulted in full hydrolysis of GTP within 30 minutes at room temperature. In contrast, incubation of the same targets with N-terminally truncated variants of GAPs (Δ76≙deletion of 76 N-terminal aa) did not show the same GTP hydrolysis. The experimental setup is as described in Figure 26.*

9.2 Supplementary tables

Table S1 | *Anisotropy data of utilized fluorophores in Rab32 spFRET measurements. Residual fluorescence anisotropy r_{inf} and steady-state fluorescence anisotropy r_{ss} of Alexa488 as the donor and Alexa647 as the acceptor are given. Reprinted with permission from Savitskiy et al, 2020 [248]. Copyright (2020) Elsevier.*

	Donor only		Acceptor	
Rab32 mutant	r_{inf}	r_{ss}	r_{inf}	r_{ss}
R55C Q160C	0.070	0.081	0.077	0.10
R55C Q160C cleaved	0.085	0.10	0.20	0.29
N90C S156C	0.081	0.12	0.17	0.21
N90C S156C cleaved	0.11	0.12	0.21	0.28

10. LIST OF FIGURES

132

133

11. LIST OF TABLES

12. ACKNOWLEDGMENTS

13. EIDESSTATTLICHE ERKLÄRUNG

Hiermit versichere ich, dass ich die vorliegende Arbeit selbstständig und nur unter Verwendung der angegebenen Hilfsmittel angefertigt habe. Alle wörtlichen oder inhaltlichen Zitate sind als solche gekennzeichnet und im Literaturverzeichnis aufgeführt. Diese Arbeit wurde noch keiner Prüfungskommission zur Begutachtung vorgelegt.

München, Oktober 2020

Sergey Savitskiy